Turning the tide:
creation of tidal inlet systems
in experimental scale models

MSc research thesis – Final version

Renske Terwisscha van Scheltinga

Studentnumber 3221725
September 2011 - March 2012

Utrecht University; Faculty of Geosciences;
Department of Physical Geography; track morphodynamics of coastal and fluvial systems

Supervisors: Dr. Maarten Kleinhans and Dr. Maarten van der Vegt
Technical support: H. Markies, W. van Dijk, C. Roosendaal and M. van Maarseveen

Abstract

Ever since 120 years people have been trying to create estuaries and tidal inlet systems in experiments, starting with Osborne Reynolds in the 1880's. So far, no group of scientist succeeded creating a physical scale model of a dynamic tidal system. Low-sediment mobility, ebb-dominance and the emergence of unrealistic deep scour holes and large ripples as a result of smooth flow were major problems of earlier experiments. Our objective was to create a tidal inlet system in a laboratory physical scale model by applying a novel method to generate flow, to determine what the possible scale effects are, and whether equilibrium morphology exists, in case of a dynamic state. In our experiments morphology emerged that resembled nature with the existence of an ebb-tidal delta, channel network and inlet channel(s). In contrast to the regular pumping of water, the entire basin (3.8m by 1.2m) was tilted vertically, over the short axis. This novel method of tilting the experimental set-up caused an increased sediment mobility in the ebb- and flood phase because the bed surface slopes in downstream direction, both during flood and ebb phases. This reduced experimental time from weeks to days. Channels formed through backward erosion and started to bifurcate after retreating from the basin margin to form a network of up to four orders. Channels in the back-barrier area were found to migrate cyclically. Resemblance with natural cyclic behaviour such as the number of inlet channels existed and typical ebb- and flood channels separated by sills were present. The use of light-weight grains, an initial sediment basin level considerably higher than mean sea level, a start perturbation and non-erodible barriers were required to create a dynamic tidal inlet system. The parameters most sensitive to the equilibrium morphology were sediment bed level, average water level, inlet width and tidal amplitude. Low average water level with respect to the sediment bed caused long sharply curved channels. These channels had few branches and persisted on the irregularly shaped ebb-tidal delta. Higher average water levels increased channel migration rates, number of branches and a regularly shaped ebb-tidal delta formed. Inlet width and tidal amplitude most importantly affected the shape and extent of the back-barrier basin and ebb-tidal delta, since they determined the strength of the flow. The effect of a rise in water level was that the back-barrier area widened and lengthened, channels deepened and the number of channels increased. The ebb-tidal delta built up in the vertical. In this report possible scale effects, equilibrium state of the system and how the experimental results can be translated to natural systems has been discussed.

Keywords: ebb-tidal delta, tidal channel, back-barrier, morphology, equilibrium, experiment, scale rules, cyclic behaviour

Preface

This research thesis was done as part of the graduation Master of Sciences research at Utrecht University, Faculty of Geosciences; Department of Physical Geography. The research covered a literature study, 35 laboratory experiments, image processing in Matlab and providing a written report. On the 27th of January 2012 this research was orally presented to a number of fellow students and employees of Utrecht University. The research was performed as part of the research group River and delta morphodynamics leaded by Maarten Kleinhans of Utrecht University. The research group shares much experience in morphological experiments. There is not much literature describing experimental research on tidal morphology mainly because of scale issues and other experimental constraints. In this research a new method of generating flow was tested that shortens experimental time considerably and increases sediment mobility. Also recommendations on scale issues were made and tested. The novel experimental method seems promising because experimental results closely resembled natural, dynamic, behaviour. Hopefully the novel method opens up the door to doing more experiments on tidal morphology. There already was significant interest of third parties. A scientific article was recently accepted with results from preparatory experiments of this research:

Kleinhans, M.G., van der Vegt, M., Terwisscha van Scheltinga, R.C., Baar, A.W. and Markies, H., 2012. Turning the tide: experimental creation of tidal channel networks and ebb deltas.

The article will be published in October 2012. The abstract of this research was published at the international conference NCR-days 2011 in Delft: Controlling the Dutch Rivers (NCR: Netherlands Centre for River Studies). The audience awarded me with the award for best research poster presentation (ex aequo). The abstract was also published and orally presented by Wout van Dijk and by Maarten Kleinhans at the conference of European Geosciences Union General Assembly in Austria (April 2012) and at the American Geosciences Union conference in San Francisco (December 2011). The novel method has proven to be promising, even more are the recent results.

Acknowledgements

Summary

A tidal inlet is a narrow channel that connects the open sea with a lagoon. Tidal inlets often occur in barrier island systems and are typified by deltas at each end of the inlets (see front page). The deltas result from the high-velocity, tidal currents that flow through the channels and loose strength when the flow diverts into the sea or lagoon. In the lagoon a back-barrier environment develops with branching channels and tidal flats. The issue of conservation of tidal systems, exposed to the effects of human interference (i.e. land reclamation, dredging, construction of groins and dikes) and climate change is important. Literature describing the hydrodynamics and morphology of ebb-tidal deltas, inlets and channel networks is widely available. The knowledge is largely based on field observations, linear stability analyses and numerical modelling. But the timescale of observations is usually smaller than the timescale of morphological equilibrium. Due to numerical issues models have limited value. Experiments can provide data-rich descriptions of their evolution in fully controlled boundary and initial conditions. But experiments in the field of coastal morphodynamic research are rare mainly because of scale issues and other experimental constraints. Deficits in prior experimental work are the occurrence of low sediment mobility, ebb-dominance, hydraulic smooth boundaries reflected in unrealistic deep scour holes and a static equilibrium because of shear stresses below motion [Kleinhans et al. 2010]. Tilting the experimental set-up will cause increased sediment mobility in the ebb- and flood phase because the bed surface slopes in downstream direction, both during flood and ebb phases. Thus ebb-dominance is counteracted while sediment mobility is increased. Low sediment mobility can also be overcome with the use of light-weight grains. In this thesis it was suggested that scale rules should be more relaxed and that it is more important that the flow remains subcritical and is near uniform. Also the composition of a sediment mixture is essential when relaxing scale rules. It was suggested to use fine sediment that scales with flow depth on the floodplains with a coarse sediment tail to avoid smooth conditions.

The experiments were carried out in a plastic tub of 3.8m x 1.2m x 0.2m. The initial configuration was a sediment basin of about 4cm height that was directly connected to a water basin of about 2.8cm deep. The tide was generated by vertically tilting the set-up, instead of pumping water in and out. The effect of the experimental conditions amplitude of tilting, speed of tilting, inlet width, horizontal water level (MSL), sediment level, sediment bed slope and sediment type on evolution and morphology were investigated. The spatial distribution of bed elevations and tidal water levels within the tilting basin were surveyed through two digital photo cameras. The water was coloured pink such that the colour intensity of the water was an indication of water depth.

In our experiments sediment transport occurred both during the ebb phase as well as during the flood phase. So tilting the set-up to generate flow rather than pumping water in and out worked well to simulate the net effect of tidal flow. Channels formed through backward erosion and started to bifurcate and migrate after retreating from the basin margin. Typical morphology emerged with the existence of an ebb-tidal delta, channel network and inlet channel(s). So the experimental morphology resembled nature. Experiments with poorly sorted sand showed that equilibrium occurred invariably when the sediment in most of the tidal basin was immobile, except near the inlet. Experiments with light-weight grains showed a more dynamic state of channels. Typical ebb- and flood channels separated by sills were present. I also observed abandonment and subsequent filling up of ebb and flood channels with sediment and formation of new channels. In addition bifurcations occurred and a cyclic migration of channels existed in the back-barrier area. Channels in the inlet showed resemblance with natural cyclic behaviour such as the number of inlet channels. In nature constant tidal prism – channel area usually define equilibrium state. The experimental tidal prism and channel area were constant while the ebb-tidal delta and tidal area still expanded. It indicated that the subject of defining equilibrium state is not straightforward. Meanwhile our experiments showed morphological equilibrium state when the back-barrier area remained equally large and the ebb-tidal delta did not expand anymore. This equilibrium state coincided with migration of bars, channels and

shoals and was defined to be a dynamic equilibrium state. The use of light-weight grains, non-erodible barriers, a start perturbation and an initial sediment basin level considerably higher than mean sea level were required initial conditions to produce a dynamic tidal inlet system.

Multiple conditions were investigated in the experiments. The parameters that were most sensitive to the equilibrium morphology were sediment bed level, average water level, inlet width, sediment and tidal amplitude. Low average water level with respect to the sediment bed caused long sharply curved channels, caused by backward erosion. These channels had few branches and persisted on the irregularly shaped ebb-tidal delta. Higher average water levels increased migration rates, number of branches and a regularly shaped ebb-tidal delta formed. Inlet width and tidal amplitude most importantly affected the shape and extent of the back-barrier basin and ebb-tidal delta since they determined strength of flow. The effect to a rise in sea level on equilibrium morphology was a wider and longer back-barrier basin with more channels, a deeper inlet channel and the ebb-tidal delta built up in the vertical.

From applying scale rules it was found that experimental sediment mobility was low while friction was high. But the scaling rules did not incorporate the effect of a tilting sediment bed. The time scale of experimental cyclic behaviour more or less agreed with the scale ratio of time. The scale ratio of time was a function of tidal velocities and basin length. The occurrence of experimental cyclic behaviour associates with all parameters and indicates that experimental sediment mobility was appropriate. It is thus suggested that the net effect of tilting is such that it more or less negates the scale effects predicted from scale rules. Experiments predict an inlet area an order of magnitude higher than the 95-percent confidence limit of extrapolated field data [Mayor-Mora, 1977]. They described that possible scale effect in their experiments was the use of typical size quartz sand which did not scale with prototype barrier sediment conditions. But our results were consistent with founding's of Mayor-Mora [1977] while we scaled sediment by the use of light-weight grains. It is thus suggested that the inlet area versus prism relationship is not a power-relation for the entire range of conditions from experiments to prototype.

The morphology of the experiments compared rather well with observation. Recommendations on folding of the ebb-tidal delta around the inlet and realizing sediment rearrangement were provided. Experimental observations suggest further research on the effect of inlet width on morphology and on inlet dynamics. The experimental set-up also allows investigating estuaries, shore-parallel tidal currents, the effect of wind waves, and more.

Samenvatting voor een leek

Rondom de wereld zijn er verscheidene kusten waarin een smalle geul een binnenzee verbindt met de open zee. Voorbeelden hiervan zijn de Waddenkust van Nederland tot Denemarken, de Amerikaanse zuidelijke oostkust en de Portugese kust. Ook Venetië in Italië ligt in een dergelijke binnenzee. Door deze zeegaten stroomt dagelijks de vloedstroom de binnenzee in en de ebstroom naar buiten. Doordat het zeegat vrij nauw is, versneld de getijstroom wanneer deze het zeegat passeert. Waarna de getijstroom vervolgens uitstroomt in zee, neemt de snelheid van de stroom af en daarmee ook zijn capaciteit om zand te vervoeren. Hierdoor ligt er aan één of beide zijdes van een zeegat vaak een delta. In de binnenzee zelf ligt een geulensysteem waarin de geulen zich blijven vertakken. Hierbij vormen ze indrukwekkende patronen. Tussen de geulen liggen veelal platen die droogvallen tijdens eb. De droogvallende platen en eventuele eilanden hebben in het bijzonder een hoge ecologische waarde voor bodemleven, vogels, vissen en zeehonden. Nu zijn zulke zeegaten met delta's en geulen en platen in de binnenzee dynamische gebieden. Dat houdt in dat de geulen en banken migreren en dat er lokaal erosie of depositie optreedt doordat de ebstroom net even anders stroomt dan de vloedstroom. Deze dynamiek is het waardevolle van zulke getijsystemen en moet daarom behouden blijven. Er is een belangrijke discussie gaande over het behoud van de natuurlijke dynamiek in getijsystemen terwijl de systemen ook beïnvloed zijn en worden door de mens (landwinning, baggeren, aanleggen van dijken, havens ed.) en klimaatverandering. Dit benadrukt de waarde van de resultaten uit dit onderzoek.

Het doel van dit onderzoek was om een getijsysteem te creëren uit een enkel zeegat met vlak achterland waarbij de stroming door het kantelen van de bak gedreven wordt. Vervolgens, bestaat er een evenwichtsmorfologie en hoe ziet deze eruit? Lijkt de experimentele evenwichtsmorfologie op de natuurlijke morfologie van de delta's, zeegat en geulennetwerk? Wat is het effect van bepaalde condities hierop, zijnde: initiële geul, de mate van kanteling, de snelheid van kantelen, de breedte van je zeegat, de waterhoogte in zee, de sediment hoogte, de helling van het sediment bed en het type sediment? Als laatste zijn schaal regels toegepast op de resultaten en vergeleken met natuurlijke systemen. Wat zijn de schaal effecten en welke processen zijn een goede weergave van de natuur?

Er is veel wetenschappelijke literatuur over de waterdynamiek en morfologie van het zeegat, de buiten delta, het geulensysteem en platen. De kennis is vooral afkomstig van observaties en metingen in de natuur, lineaire stabiliteitsvergelijkingen en numerieke modellen. Maar de tijdschalen waarop de morfologie in een soort evenwicht komt zijn vaak langer dan er observaties zijn. Ook hebben numerieke modellen hun eigen beperkingen zoals de complexiteit van sediment transport en is het numeriek lastig om nat- en droogvallen te modelleren. Experimenten echter zouden een volledige beschrijving van het ontstaan van een getijsysteem kunnen nabootsen waarbij de rand condities en initiële condities zelf bepaald worden. Doordat een experiment op kleinere schaal plaatsvindt, is het een versnelde weergave van de realiteit. Maar het probleem is nu dat experimenten zelden gedaan worden om kustmorfologie te onderzoeken. Dit komt vooral door schaalproblemen. Andere beperkingen van eerdere experimenten waren dat de morfologie gevormd was door een ebgedomineerde stroom, er werd weinig sediment verplaatst met de stroom en het type stroming was 'glad' waardoor je diepe gaten krijgt. Het einde van een experiment was meestal als er in de gevormde getijsystemen geen verandering van de bodem meer plaatsvond ondanks dat er water stroomde. In de natuur echter, blijven zulke systemen dynamisch.

In dit onderzoek maken wij gebruik van een compleet nieuwe methode om water te laten stromen die eb en vloed moet nabootsen. Normaalgesproken werd dit gedaan door een golfbeweging te simuleren of water in en uit te pompen. Wij kantelen de bak vanuit één hoekpunt op en neer. Hierdoor gaat water stromen in de richting van de helling waarbij de zandbodem mee helt. Hierdoor is er een lagere stroomsterkte nodig om sediment te eroderen en vervoeren en heb je dus hogere sediment mobiliteit. De sediment mobiliteit wordt ook nog eens verhoogd door gebruik te maken

van hele lichte plastic korrels die gemakkelijk meegevoerd worden. Dan zijn er nog de schaal regels waar aan voldaan moet worden. In de literatuur sectie staat een uitgebreide uitleg waarom deze regels die in eerdere experimenten geformuleerd zijn niet persé opgaan. Het is veel belangrijker dat het type stroming juist is en de stroomsnelheid in verhouding met de waterdiepte. Door grovere korrels te gebruiken zorg je ervoor dat de stroming niet 'glad' is. De experimenten zijn uitgevoerd in een plastic bak van 3.8m bij 1.2 m en 20 cm hoog. Deze bak was opgedeeld in een laag sediment aan de ene kant en water in de rest van de bak. Door de bak te kantelen ging er water in en uit een initieel geultje in het zandbed stromen. De veranderingen van de geul werden zichtbaar gemaakt door middel van camera's aan het plafond die automatisch beelden maakten.

In de experimenten vond er zowel tijdens in- als uitstroom sediment transport plaats. Het kantelen van de bak simuleert dus het effect van eb en vloed. Er ontstond een karakteristieke morfologie met een eb-getijde delta, hoofdgeul(en) in het zeegat en een geulennetwerk in het achterland. De experimentele morfologie was dus vergelijkbaar met die in de natuur. De evenwichtsmorfologie in de experimenten was een systeem waarbij het achterland niet meer groeide en de delta niet meer uitbreidde. In de natuur wordt evenwicht vaak gedefinieerd aan de hand van een verhouding tussen getijvolume en doorstroomoppervlakte van het zeegat. Het experimentele getijvolume en de doorstroomoppervlakte van het zeegat waren al lange tijd redelijk stabiel terwijl de delta nog groeide en het achterland nog uitbreidde. Uit de experimenten blijkt dat het definiëren van een evenwicht wellicht complexer is. Toen het systeem niet meer groeide bleven de geulen wel migreren. De experimentele evenwichtsmorfologie was dus in een dynamische staat. Dit was nog nooit eerder gezien op experimentele schaal. Belangrijke condities om een dynamisch evenwichtssysteem te doen ontstaan waren: lichtgewicht plastic korrels, een zeegat met niet erodeerbare 'eilandkoppen', het sediment bed lag hoger dan de zeestand en een initiële geul. Bij de experimenten met zand vond er na verloop van tijd geen transport meer plaats en was dat dus het evenwicht.

Over het algemeen breidde een geul zich uit door terugschrijdende erosie. Een splitsing vond plaats nadat een geul zich iets had teruggetrokken. Na splitsing vond er zijwaartse migratie plaats. Karakteristieke eb en vloed geulen waren aanwezig met daartussen drempels. Ook werden er geulen verlaten, opgevuld en ontstonden er nieuwe geulen. Migratie van geulen in het achterland gebeurde in een cycliciteit. Ook in het zeegat was er cyclisch gedrag dat ook in de natuur plaatsvindt: het wisselen van het aantal geulen. De morfologie was het meest gevoelig voor de volgende condities: hoogte van het sediment bed, gemiddelde waterhoogte, breedte van het zeegat en de getijamplitude (mate van kanteling). Een zeespiegelstijging leidde tot uitbreiding van het achterland, een dieper zeegat en de eb-getijde delta werd opgehoogd.

Uit de schaal regels bleek dat de mobiliteit van het sediment aan de lage kant was en dat bodemwrijving aan de hoge kant was vergeleken met de natuur. Maar de schaal regels nemen niet het effect mee van het meehellende zandbed tijdens eb en tijdens vloed. Terwijl de tijdschaal van de cycliciteit wel overeenkwam met de schaal verhouding van tijd. De cycliciteit is een gevolg van alle condities en is wellicht een betere maatstaf. De suggestie is dan ook dat de het effect van kantelen dusdanig is dat het ervoor zorgt dat de mobiliteit van het sediment toch juist was. Kortom, aan de schaal regels werd bijna voldaan; de experimentele morfologie en processen daarin leken erg op die in de natuur; een evenwicht werd bereikt waarin geulen en platen dynamisch waren.

Leeswijzer

Deze scriptie is een uitgebreid document. Deze leeswijzer geeft aan welke onderdelen u kunt lezen om een goede eerste indruk te krijgen van de bevindingen en mogelijkheden van dit onderzoek door slechts een selectie te lezen. In dat geval raadt ik u aan om de volgende paragrafen te lezen:

- Chapter 1: Introduction
- Paragraaf 2.4.1
- Paragraaf 2.4.2
- Eerste alinea van 2.5.1
- De figuren en tabellen van hoofdstuk 3
- Eerste alinea van 4.1.1 en figuur 4.1
- Paragraaf 4.2.3
- Sub-hoofdstuk 4.3 selectief lezen
- Sub-hoofdstuk 4.4
- Sub-hoofdstuk 4.5 selectief lezen
- Sub-hoofdstuk 5.2
- Paragraaf 5.2.2
- Paragraaf 5.2.4
- Sub-hoofdstuk 5.5
- Chapter 6: Conclusions

De auteur.

Contents

List of figures

List of tables

Chapter 1: Introduction

A tidal inlet is a narrow channel that connects the open sea with a lagoon. Tidal inlets often occur in barrier island systems and are typified by deltas at one or both ends of the inlets (see front page). The deltas result from deceleration of the high-velocity, tidal currents that flow through the channels and loose strength when the flow diverts into the sea or lagoon. In the lagoon a back-barrier environment develops with branching channels and tidal flats. The back-barrier areas are ecologically important areas for e.g. shellfish aquaculture, fish larvae's and migrating birds. At the same time, the channel system provides natural access to ports [van der Wegen et al. 2008a]. The areas can be densely populated and attractive for recreation which increases the economic value of the systems [van der Vegt 2006]. Literature describing the hydrodynamics and morphology of ebb-tidal deltas, inlets and channel networks is widely available. The knowledge is largely based on field observations, linear stability analyses and numerical modelling. But the timescale of observations is usually smaller than the timescale of morphological equilibrium. Due to numerical issues models have limited value. Experiments can provide data-rich descriptions of their evolution in fully controlled boundary and initial conditions. But experiments in the field of coastal morphodynamic research are rare. The issue of conservation of tidal systems, exposed to the effects of human interference (i.e. land reclamation, dredging, construction of groins and dikes) and climate change is important. Therefore we should improve our understanding on the evolution of a tidal inlet system, the existence of an equilibrium state and the effect of changes in conditions such as sea level rise and land reclamation. Experiments can give new insight on these topics.

Not much is known about the genesis of tidal inlet systems and estuaries because the deposits are usually reworked in nature [Perillo 1995]. Experiments allow describing the evolution of a tidal inlet system from plane bed to equilibrium state. Ever since 120 years people have been trying to create estuaries and tidal inlet systems in experiments, starting with Osborne Reynolds in the 1880's [Reynolds 1887-1891]. So far no group of scientist did succeed creating a physical scale model of a dynamic tidal system. Most importantly, low-sediment mobility, ebb-dominance and the emergence of unrealistic deep scour holes and large ripples have to be avoided. The main objective of this research is to create tidal inlet systems in a laboratory physical scale model by applying a novel method to generate flow. Subsequently, does equilibrium morphology exist and what is the equilibrium morphology of the tidal inlet system? How does it compare to nature? The focus is on morphology and dynamics of the ebb tidal delta, the inlet and the channel networks. We study the sensitivity to the width of the inlet, the tidal conditions, sediment level, initial perturbation and sea-level rise. Third, scaling rules are applied on experimental parameters and those of prototype systems. What are scale effects and which phenomena in experiments represent nature?

Chapter 2: Theoretical review and scope

The theoretical analysis considers literature on morphology of tidal inlet systems and processes governing the morphology from different methods of research. First the reader is introduced to the typical morphology of tidal inlet systems and the principle of sediment transport. Chapter 2.2 considers basic knowledge from observations. The processes governing the morphology of tidal inlet systems are provided. Also quantifications of typical characteristics will be considered and their interrelations. The so called equilibrium state will be defined with a description of simultaneous cyclic behaviour. Then chapter 2.3 covers findings from modelling studies. Modelling studies allowed to test findings from observations. Their results provide better insight in the effect of the character of tidal flow, the relevant effect of waves and their combined action. These two processes most importantly describe the dynamic state of the sediment bed on a range of time and spatial scales. Thereafter chapter 2.4 summarizes prior experimental work, provides findings from prior experiments and most importantly discusses experimental constraints. The last section, chapter 2.5, is on the application of scale rules. First the principle of upscaling is given followed by suggestions on relaxing scale rules. Nevertheless multiple methods of scaling are outlined to allow comparison of results to previous experimental work and allow comparison to nature. Last, chapter 2.6 gives the thesis outline.

2.1   Tidal inlet systems and sediment transport

This section describes typical morphology of tidal inlet systems and estuaries and how they emerged. Also the principles of sediment transport will be explained.

2.1.1 Tidal inlet systems

In many coastlines the tidal water passes through inlets into and from a back-barrier area twice a day and thereby created typical morphology. Figure 2.1 presents four examples of tidal systems with exposed sand bodies. *They are respectively the Dutch Wadden Sea Coast, the Western Scheldt estuary in the southwest of the Netherlands, Cape Hatteras and North Inlet at the Atlantic coast of the United States of America.* The ebb and flood current transport sediment. But the ebb and flood flow not simply reverse the direction at each part of the bed, they may have different flow paths [Reynolds 1887-1891]. So what has been a scouring flow during ebb can be a depositing flow during flood. A typical shape of the sand bodies results from the local change in the character of flow and the flow having to pass through a narrow inlet. Figure 2.2 presents a sketch of a typical tidal inlet system. Typical sand bodies are the inlets in between the barriers, the delta at the seaward and at the landward side of the inlet and the channel network in the back-barrier. The seaward delta is referred to as the ebb-tidal delta while the landward delta is the flood-tidal delta. The region of the ebb-tidal delta is shallow, with depths in the order of several meters. Some parts can be above mean sea level. The delta is folded around the deep ebb-dominated channel [de Swart and Zimmerman 2009]. The channel through the inlet usually consists of a central ebb-dominated channel and one or two flood dominated channels. Between the barriers and the mainland generally a back-barrier environment (estuary or lagoon) is situated. The back-barrier shows a typical branching channel network of several orders with tidal bars, meanders and an intertidal zone of tidal flats and salt marshes [de Swart and Zimmerman 2009]. So many coastlines feature inlets with typical morphology of the system as a result of tidal flow.

The deltas, inlet and back-barrier area consist of different sand deposits preserving historical development. Figure 2.3 shows the sedimentological architecture in the bottom of present tidal inlet systems. The deposits in a back-barrier usually consist of fine sands and mud (striped in figure 2.3). While the deposits near the inlet and of the ebb-tidal delta are usually coarser and consist of medium
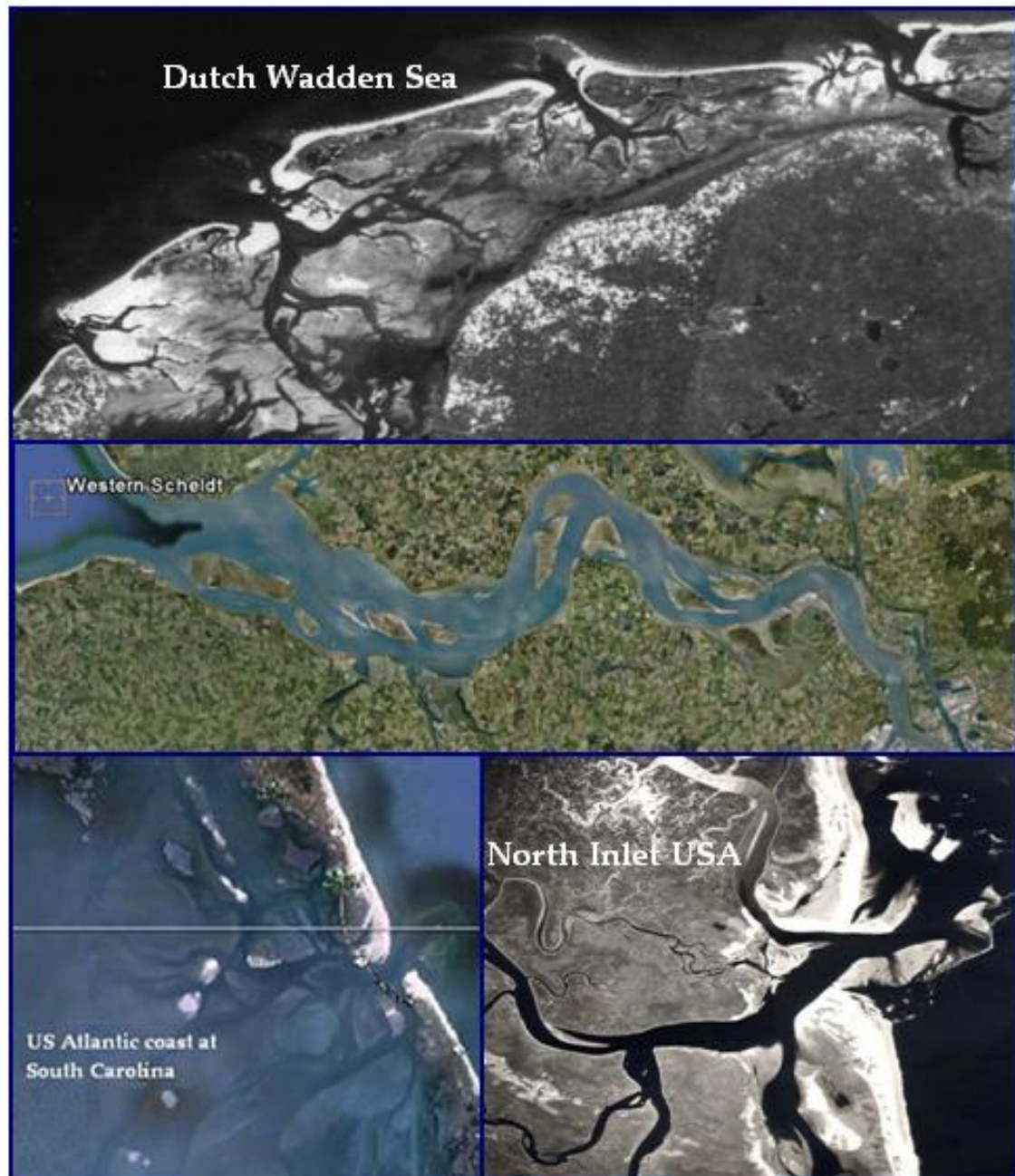
Figure 2.1 Examples of tidal systems with exposed sand bodies.

sand (densely dotted in figure 2.3). The sequence of bottom layers found indicated vertical accretion of thick layers of sediment. At the same time typical deposits of sub-environments are long-stretched and layered top of each indicating migration. The theory is that present barrier island systems migrated landward when sea level rose since the last glaciation [Masselink and Hughes 2003]. Continental shelves which lay dry during the last glaciations became flooded. This caused a complicated process of reworking of sediment, filling in of the topographic lows of the glacial landscape and erosion of topographic heights [de Swart and Zimmerman 2009]. Another phenomenon that can lead to the formation of a tidal inlet system is a breach through a barrier island or the coastline [Stefanon et al. 2009]. Barrier morphology is affected by a number of factors which include sea level, sediment supply, substrate gradient, geological inheritance, wave energy level, tides and wind [Masselink and Hughes 2003]. In terms of barrier evolution and stratigraphy, the two most important factors are sea level and sediment supply. It depends on a combination of these two factors whether the barriers are prograding (figure 2.3 typical stratigraphy), stationary or

retrograding [Masselink and Hughes 2003]. So most tidal inlet systems formed and migrated when sea level rose and their preservation depends on future conditions.

The schematizations in figure 2.2 and figure 2.3 give rise to some contradictions. The figures show a well-developed flood tidal delta and a well-developed ebb tidal delta. While in nature it is usually observed that either the ebb tidal delta or the flood tidal delta is well-developed [de Swart and Zimmerman 2009]. Figure 2.2 presents the direction of the tidal current parallel to the coast which is the case for the Dutch Wadden Sea Coast. Though, the direction of the tide can also be perpendicular to the coast. This is observed for the U.S. Atlantic Coast where ebb-tidal deltas are usually more symmetrical than for the Dutch Wadden Sea Coast. So despite of having general morphology, the morphology of a tidal inlet system strongly depends on local conditions.
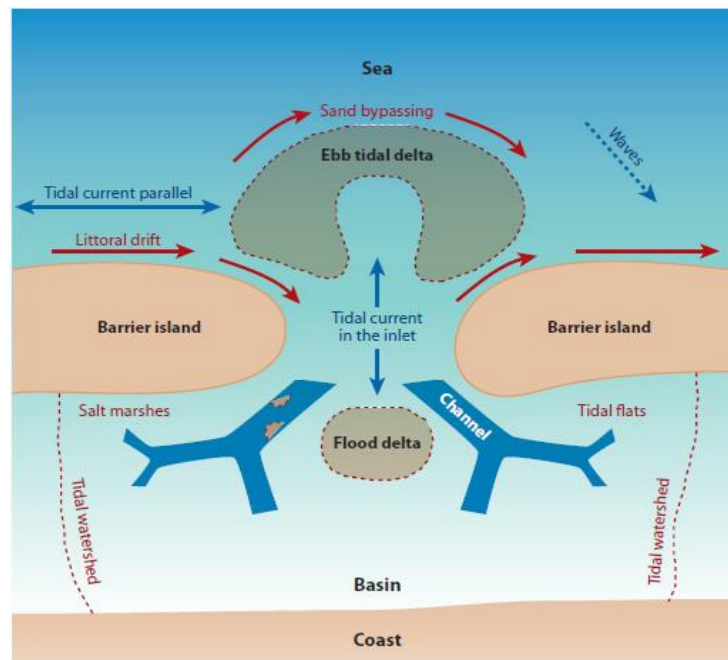
Figure 2.2 Sketch of an idealized tidal inlet system, showing the different geomorphologic elements and the dominant physical processes and phenomena. From De Swart and Zimmerman 2009.
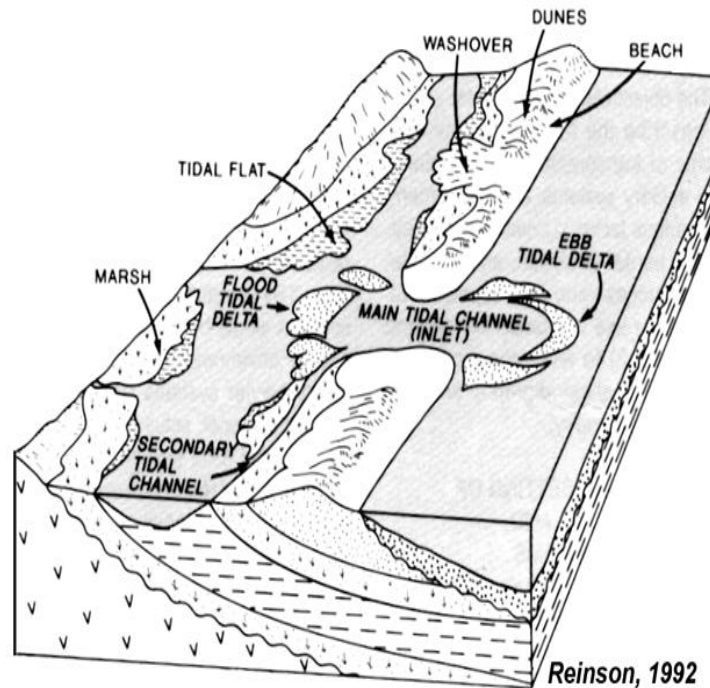
Figure 2.3 Block diagram illustrating the various sub-environments in a barrier island system. Note the stratigraphy which shows the barriers island system to be a prograding system due to sea level rise since the last glaciation. From Masselink and Hughes 2003 (page 244).

2.1.2 Estuaries

As long as freshwater is discharged into the sea in a channeled form, there is a potential for the development of an estuarine environment [Perillo 1995]. An estuary is a partly enclosed sediment body that is fed by river water and has a free connection to the sea so it is influenced by tide. It forms a transition zone between river environments and ocean environments. Estuaries occur in many types wherein geology is often a major control. A certain type of estuary is comparable to a tidal inlet system because they are tide-dominated and also form channel networks and an ebb-tidal delta. Well-known examples are the Westerscheldt in the Netherlands and the Thames in the United Kingdom. So in an estuary the tidal flow interacts with river flow. River discharges in tide dominated estuaries are generally small compared with the tidal prism (< 5%). Perillo [1995] introduces the role of tides to be complex and less well studied than many other aspects. A short and well-written introduction is given here by Wells, edited by Perillo [1995, page 179]:

> *We know that certain basins, such as the North Sea, the Yellow Sea and the Bay of Fundy have especially large tide ranges because of basin geometry. We know that when tides converge in coastal embayment's, such as estuaries, their energy is concentrated and the range increases as tides are forced through smaller cross-sectional areas. We know that as tides move upstream through smaller cross-sectional areas, the tidal currents become progressively more asymmetric in both speed and duration. Commonly estuaries have lengths of the same order as the tidal wavelength. Yet, even when generalizations and simplifying assumptions are made, it is difficult to unravel the role of tides in sedimentation pattern and morphological development because of the difference in source, distribution, and nature of both fine and coarse sediments found within estuaries.*

The general sedimentology of a specific estuary is the consequence of many conditions. One of the most important is the sediment source. The sediment source may be from the river or the adjacent shelf. The sediment is introduced into the estuary by tidal action or a current along the shore. Erosion of inner estuary rocks or pre-estuary sediments and biogenic material may also be significant

[Perillo 1995]. Documentary on geological records of "estuaries" is typically applied to flooded incised valley-fills with brackish trace fossils. In such settings topology and basin geometry have a strong control on morphology during infilling. The question arises to what extent the morphology is controlled by the original topology. Also, Perillo [1995] states that the understanding of coastal-plane estuaries may be biased by estuaries along the east coast of the U.S. and in the Netherlands. Experiments can provide new insight on the effect of topology and basin geometry on morphology.

2.1.3 Sediment transport

A current or drift acts on the bed sediment [Reynolds 1887-1891]. The primary action is not so much to drag the grains along the bottom but to pick them up, hold them in some kind of eddying suspension at certain distance above the bottom and then allow them to settle. As a consequence, there is a layer of water adjacent to the bottom that is loaded with sediment. The thickness of the layer depends on the sediment properties and current velocity. The faster the current and the finer the sediment, the thicker and the denser the loaded layer will be [Reynolds 1887-1891].

The most important modes of transport are bed load and suspended load transport. Bed load moves in the form of sliding and rolling grains. Suspended load is defined "*that part of the total sediment transport which is maintained in suspension by turbulence in the flowing water for considerably periods of time without contact with the bed*" [Van Rijn 1993]. Both transport modes may occur simultaneously and the transition zone cannot be well-defined. Whether sediment is in suspension or transported as bed load is largely determined by the equilibrium between the fluid drag force and the gravity force, expressed in the terminal fall velocity. Small particles have a low fall velocity and are therefore more easily transported as suspended sediment since gravity does not pull them down.

The force that a current exerts on the bed surface is described by the bed shear stress τ_b (N/m^2). The bed shear stress is given:

$$\tau_b = \rho \, g \, u^2/C^2 \tag{2.1}$$

with ρ_w being the water density (kg/m^3), g the gravity acceleration (m/s^2), u the depth-averaged flow velocity (m/s) and C the Chézy coefficient (m$^{0.5}$/s) [Van Rijn 1993]. The Chézy coefficient is a measure for bottom friction. A certain velocity is needed before particles start to move [Van Rijn 1993]. Then, the quantity of the sediment which passes a particular section increases much faster than the velocity [Reynolds 1887-1891]. To initiate and retain motion, a bed shear stress is needed just larger than the critical bed-shear stress, $\tau_{b,cr}$. Shields (1936) did many experiments to determine the initiation of motion for different grain sizes. He determined an empirical dimensionless parameter for bed shear stress, the Shields parameter θ. It describes whether the flow is sufficiently strong to initiate motion [Van Rijn 1993]. This is given by:

$$\theta_{cr} = \tau_{b,cr} / ((\rho_s - \rho_w) \, gd_{50}) \tag{2.2}$$

with $\tau_{b,cr}$ is the critical bed shear stress (N/m^2), ρ_s the sediment density (kg/m^3), ρ_w the water density (kg/m^3), g the gravity acceleration (m/s^2) and d_{50} the median grain size (m). Figure 2.4 shows the classical Shields diagram for a fixed temperature and viscosity. For fine sediment with a boundary Reynolds number below 6 (sediment size of about 8 mm) a relatively high critical Shields stress is needed to initiate motion. Since the gravity action on a smaller particle is smaller which would make it more easy to initiate the motion. Still, a higher mobility parameter is needed to initiate motion. This is due to fine sediment being more 'sticky' (cohesive) and fine particles induce less turbulence. Roughness elements such as grain particles generate eddies which affect the turbulence structure and hence the flow velocities close to the bottom. Roughness elements facilitate initiation of motion [Van Rijn 1993]. In turbulent flow conditions the flow velocities are not constant in space and time. In addition, the particles are random in size, shape and position [Van Rijn 1993]. So the actual transport

of sediment is not necessarily described by a simple formulation. This is resembled in the availability of different deterministic transport formulas that differentiate in the parameters needed to obtain a transport rate (i.e. Meyer-Peter Mueller, Bagnold and Van Rijn). In short, the most important parameters for determining sediment transport are flow velocity, water depth, bottom roughness and sediment size and density. Transport formulations generally determine sediment transport, q_s (m^2/s), from the flow velocity, u (m/s), to the power of 3 to 5 [Van Rijn 1993]. When, at a particular place, the sediment load of the water is less than the full load due to its velocity, it will take up from such place more sediment than is released. The water increases its load at the expense of the bed. The bed is lowered or eroded locally. Conversely, when the water is overloaded by sediment net deposition will take place. Consequently, the bed will raise [Reynolds 1887-1891]. Predominantly, changes in velocity determine deposition and erosion of the bed. The gradual change of the sediment bed does not depend on the rate of deposit and withdrawal, but on the tidally averaged excess of one of these over the other.
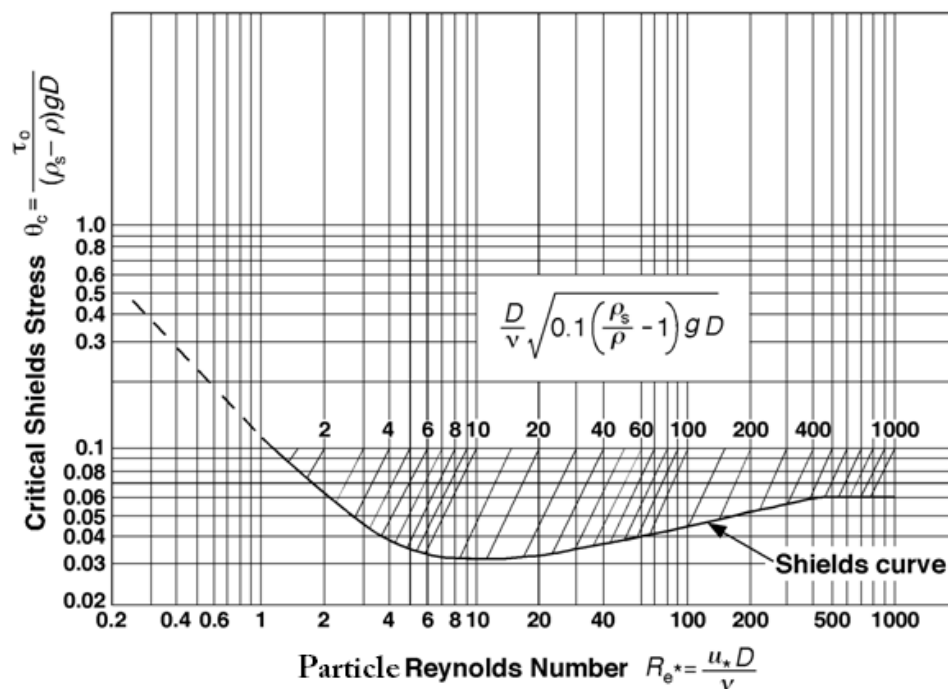
Figure 2.4 Shields diagram describing the initiation of motion for a current over a plane bed from the dimensionless critical Shields parameter and the particle Reynolds number. The numbers in the figure present median sediment size (mm).
Source: http://serc.carleton.edu/NAGTWorkshops/sedimentary/activities/14100.html.

2.2   Observations

This section provides basic knowledge from observations. First a classification scheme introduces the most important processes governing the morphology of tidal inlet systems. Then the development of channels and subsequent channel patterns is described for. Quantifications of typical characteristics of channels such as width-to depth ratios, channel branching numbers and channel areas are considered. Channel areas have interrelations with tidal water volumes and sediment volumes introducing the concept of equilibrium state. The so called equilibrium state will be defined. Thereafter the existing of an equilibrium state is discussed because of its dynamic state and simultaneous cyclic behaviour.

2.2.1 Classification scheme

Hubbard et al. [1979] classified tidal inlet systems based on examples from the south-eastern Atlantic coast of the USA. Three types of inlets are identified and schematized in figure 2.5, being tide-

dominated (A), wave-dominated (B) and transitional (C). In short, tide domination (A) causes deep ebb-tidal channels and flood-tidal deltas to be poorly developed. When the tide is dominant, the extent of the main ebb channel is much larger, up to several times the width of the inlet such as for the inlets near South Carolina and Georgia [Davis Jr. and FitzGerald 2004]. Wave-dominated (B) inlets are characterized by large, lobate flood-tidal deltas building into wide open lagoons. The ebb-tidal delta is small. Wave-induced currents push the ebb-tidal lobe close to the inlet mouth such as for the coast of Florida and North Carolina. Tidal channels are generally shallow (less than 6m) and bifurcate landward and seaward of the inlet. In transitional inlets (C), major sand bodies are typically concentrated in the inlet. The inlets vary widely in morphology and sand body geometry. Hubbard et al. [1979] do not explicitly describe the configuration of the lagoon but the schematization shows that the lagoon mainly consists of shoals and channels. The inlet between the barrier islands is maintained by the separation of landward and seaward transport through the inlet. Other factors than the tidal current and waves exhibit less controls. Their effects are more difficult to quantify. Nevertheless, factors that determine the particular morphology of a tidal inlet system are [Hubbard et al. 1979]:

1) tidal prism
2) inlet cross-sectional area and shape
3) the nature of the back-barrier bay (shape, geometry, size, geology)
4) fresh water input
5) relative changes in sea level
6) sediment supply

The most important parameter governing the shaping process of the typical coastal structures is considered to be tidal prism [Dieckmann et al. 1988]. Tidal prism is defined as *total volume of water that enters and leaves the tidal basin during one tidal cycle*. It is a function of the tidal range and the morphology of the back-barrier. The dimensions of inlets and ebb deltas correspond to the tidal prism [O'Brien 1969 and Domwbrowski and Mehta 1996 in Powell et al. 2006]. When the tidal prism of one basin reduces suddenly by land reclamation, the inlet reduces in size over a few decades [Oost 1995]. Oost [1995] provides time scales in which active existence time is supposed to be studied. He gives an order of magnitude for the tidal system of 1.000 year. The back-barrier channel system, inlet channel and ebb-tidal delta have an active existence time of 10 to 1.000 year. Local differences in factors, recent changes due to human interference and a long existence time makes the subject of equilibrium volumes and system response hard to deduce for natural systems.
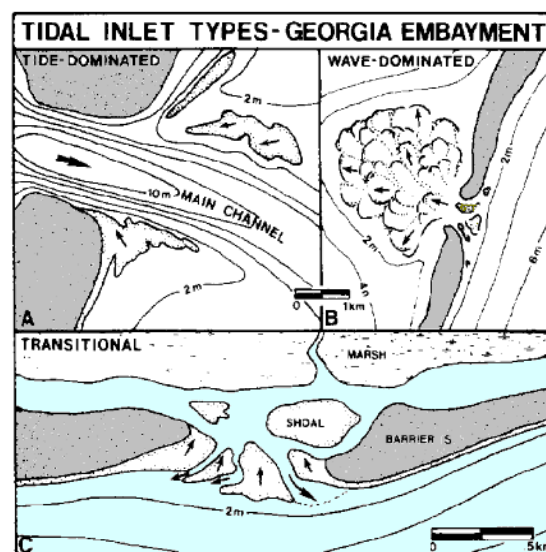
Figure 2.5 Tidal inlet classification [Hubbard et al. 1979].
Arrows show dominant transport direction.

2.2.2 Channel initiation and early development

Channels develop when a small depression in the sheet flow causes the discharge to concentrate. Sediment transport is related to the power of velocity, therefore a small increase in flow velocity due to a depression causes an increase in sediment transport capacity [Van Rijn 1993]. An increasing flow depth leads to a decrease in bed surface area and therefore less bed friction per unit flow volume. Both processes induce a positive feedback mechanism which leads to channel development. The channelization usually extends basin inwards by headward erosion [Kleinhans et al. 2008] because of a larger hydraulic gradient from the tidal flats towards the channel head. Nevertheless the channel cannot become infinitively deep, which introduces the subject of channel character and morphological equilibrium. The definite channel character is controlled by properties such as slope, cohesiveness of the banks, Froude number and channel width and depth. The latter depend on imposed water discharge, grain size and sediment concentration [Hoyal and Sheets 2009]. Also, the channel character/instability controls the avulsion cycles within a system and therefore the development of a channel network. Cleveringa and Oost [1999] describe the origination of channel systems to be regarded as an ebb-driven drainage network, governed by backward erosion.

The back-barrier typically shows a channel network. The channel network drains the area. Rodriguez-Iturbe et al. [1992] found that a tree like drainage network arises from the assumption of an equilibrium configuration with minimum energy dissipation [van der Wegen et al. 2008]. They assume equal energy dissipation per unit area of channel anywhere in the river network. In a tidal system the basin alternately drowns and drains during flood and ebb. The ebb flow has to get going from zero speed at slack water. As a result maximum ebb velocities usually occur at lower water levels than maximum flood velocities. According to Cleveringa and Oost [1999] flooding changes the configuration that arises from draining the basin. So the draining of the basin result in a tree like network while the flooding flow disturbs the process and is likely to change the "equilibrium configuration". Does this behaviour express that the more tree-like the network is, the more dominant the draining flow (ebb) is over the flooding flow? Addressing equilibrium morphology in case of tidal flow is of no ways simple. The complex interaction of hydrodynamic and morphodynamic processes in tidal basins limits the applicability of process-based models [Cleveringa and Oost 1999]. They can be improved using the fractal geometry (section 2.2.5) from behaviour-oriented models such as the dynamical equilibrium morphology [Cleveringa and Oost 1999]. Rinaldo et al. 1999 find well-defined power law relations for larger channels between cross-sectional area, drainage area, tidal prism, channel width, and peak discharge. Comparison to experimental results may provide greater insight in aspects of morphodynamic adjustments and equilibrium morphology.

2.2.3 Marsdiep Inlet

The Dutch tidal inlet Marsdiep between Den Helder and Texel got a passage from the North Sea to the present Wadden Sea in 1170 (Allerheiligenvloed). Data on the water depth of the inlet is collected by A.P. Oost (U.U. and Deltares) and provides information of a evolving tidal inlet system. Figure 2.6 shows an increase in water depth from 1300 to the year 1980 [Oost 2011, the data is confidential because it is not published yet]. From 1385 to 1700 the inlet depth increases linearly. From 1700 the water depth increases less and the trend is variable. This period of time coincides with human interference of the system by land reclamation. Does the variability result from human interference only or can a part of the variability be explained by tidal forcing?
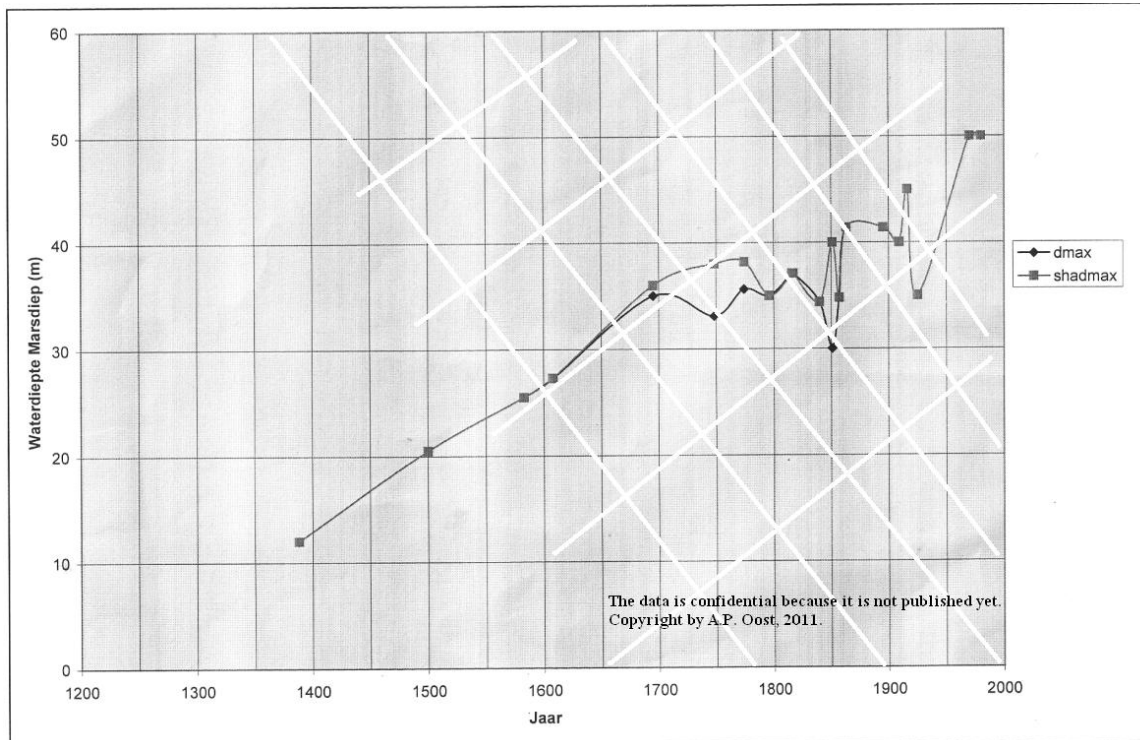
Figure 2.6 Data on the increase of the water depth of the Marsdiep inlet over time (years) at the Dutch Wadden Sea Coast. The data is confidential because it is not published yet. Copyright by A.P. Oost, 2011.

2.2.4 Width to depth ratios of tidal channels

The typical morphology of a tidal basin consists of an inlet with main channels and further inside the basin, the main channels become shallower and undergo a sequence of bifurcations. It results in a complex pattern of channels and tidal flats. Channel meandering is seen for the main channels as well as for the smaller channels of tidal channel networks (figure 2.1). The discharge increases in the seaward direction so both width and depth is expected to increase in the seaward direction. But the width and depth of the channels is also influenced by the critical threshold for erosion and deposition [Fagherazzi and Furbish 2001 in Kleinhans et al. 2008]. The width-depth ratio is often used to determine bar pattern and therefore channel pattern [Kleinhans et al. 2010]. The width to depth ratio is defined as:

$$\beta = W/D \qquad\qquad (2.3)$$

with W being the top width and D the mean depth. The width to depth ratio in tide dominated inlets is usually small [Hubbard et al. 1979]. The inlet channels and larger channels in the Dutch Wadden Sea have a width to depth ratio of about 35 (Vlie and Ameland inlet, calculated from depth maps of 1999 and 2005). The ebb- and flood channels near the tidal divide usually have higher width to depth ratios of about 60-100. Literature describes values from about 5 and higher (up to 150) [Dènaix 1811 in Stefanon et al. 2009]. In rivers the width to depth ratio is usually much higher than 30 [Chang et al. 1979]. The question arises how width to depth ratios of experimental channels compare to observations and what processes and conditions describe dissimilarities.

2.2.5 Hierarchical analysis

The large inlet channel branches into smaller channels, which finally give way to (inter) tidal gullies [Cleveringa and Oost 1999]. In order to describe the branching patterns of channel systems Horton introduced a hierarchical and fractal analysis of channel circumference [Cleveringa and Oost 1999]. Cleveringa and Oost [1999] found by applying Horton's method that tidal-channel systems in the Dutch Wadden Sea have similar branching patterns. The channel systems have the same

23

characteristic as three- to four- times branching networks. Figure 2.7 is an example of what a three- to four-times branching networks involves. The smallest channels are assigned to first order. Two first-order channels merge into a second-order channel, and so on [Cleveringa and Oost 1999]. The branch lengths of these channels decrease logarithmically. Their actual configuration is a result of a self-organising nature with a natural variability. Regarding tidal-channel systems, Cleveringa and Oost [1999] state that the three- to four-times branching network is an equilibrium morphology.

Subsequent, Marani et al. [2003] found that total channel length relates well to watershed area rather than to its tidal prism. This founding is a somewhat counterintuitive result because typical tidal features are generally related to tidal prism [Hubbard et al. 1979 and Cleveringa and Oost 1999]. Marani et al. [2003] analyzed the relevant morphometric features of the observed tidal networks and salt marshes. It allows one to sketch drainage directions, unchanneled flow lengths, and contributing areas to determine any channel cross section. Drainage direction was deduced from the related water surface gradients. For direct comparison to proper experimental result one has to consider that the work of Marani et al. [2003] generally considered channel networks in highly vegetated areas. Still, it is of interest for recent experimental works because it is not straightforward whether tidal channel networks are a remnant of rain water drainage systems and/or tidal flow channelization. If the latter is the case and assuming that vegetation captured the configuration of the network, the channel dimensions and networks of vegetated areas are still representative for unvegetated areas. Likewise Marani et al. [2003] suggest that the concept of inheritance is supported. The salt marsh area might be a proxy of the dynamic forcing responsible for the formation of the network during its history. After colonization by alophytic vegetation the network only undergoes minor changes not altering its basic structure [Marani et al. 2003].
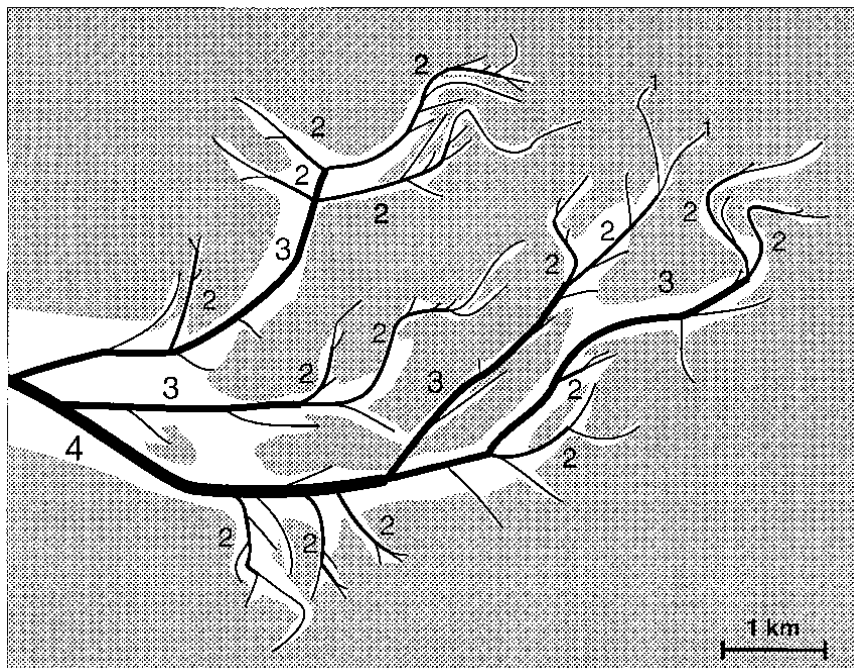
Figure 2.7 Horton's hierarchical analysis. The smallest channels are assigned to the first order. Two first-order channels merge into a second-order channel, and so on. A lower-order channel that joins a higher order channel does not change the order of the latter. From Cleveringa and Oost 1999.

2.2.6 Empirical relationships that define equilibrium

Empirical relationships between tidal prism P, channel area Ac and ebb-tidal delta sand volume ESV exist. The long-term empirical relationships are used to define equilibrium state, assuming stable boundary conditions [Dastgheib et al. 2008]. Such relationships can be useful for predicting adjustment to natural or human induced changes such as land reclamation and partial closure of

basins. Tidal prism is defined as *total volume of water that enters and leaves the tidal basin during one tidal cycle*. It is mainly a function of the tidal range and morphology of the back-barrier basin. The idealized geometry with a representation of parameters is illustrated in figure 2.8.
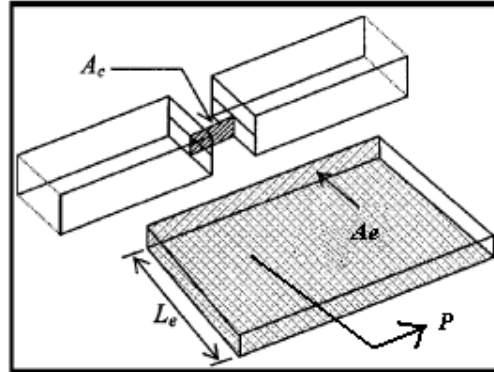
Figure 2.8 Idealized geometry with channel area A_c, tidal prism P (the volume of water that enters and leaves the lagoon during each tidal cycle), Length of estuary L_e and area of estuary entrance A_e. From Powell et al. 2006.

The sand volume of the ebb-tidal delta ESV is related to the tidal prism P (in m^3) by

$$\text{ESV} = c_1 \, P^{\, c_2} \quad\quad\quad\quad (2.4)$$

$$\text{ESV} = 0.0066 \quad P^{\, 1.23} \quad\quad\quad (2.4a) \quad \text{[Walton and Adams 1976 in van der Vegt 2006].}$$

$$\text{ESV} = 3.80 \times 10^{-3} \, P^{\, 1.26} \quad\quad (2.4b) \quad \text{for the Atlantic US Coast [Powell et al. 2006]}$$

The constants c1 = 0.0066 and c2 = 1.23 hold for systems that are in a natural equilibrium state [Walton and Adams 1976 in van der Vegt 2006]. Typical values of the tidal prism are between 106 and 109 m3. Equilibrium exists between cross-sectional channel area A_c (m^2) and tidal prism P (m^3) [O'Brien 1969 in Powell et al. 2006]:

$$A_c = a \, P^{\, m} \quad\quad\quad\quad (2.5)$$

$$A_c = 4.69 \times 10^{-4} \quad P^{\, 0.85} \quad\quad (2.5a) \quad \text{[O'Brien, 1969 in Powell et al. 2006]:}$$

$$A_c = 6.25 \times 10^{-5} \, P^{\, 1.00} \quad\quad (2.5b) \quad \text{Florida's entrances[Powell et al. 2006]}$$

The coefficients *a* and *m* vary from entrance to entrance but from 28 US inlets it was obtained that best-fit values are $a = 4.69 \times 10^{-4}$ and m = 0.85. Powell et al. [2006] applied the empirical relationship on 66 inlets of the Atlantic Coast and Gulf Coast. They found a best fit for *a = 6.25 x 10^{-5}* and *m = 1.* Their results are given in figure 2.9. The islands along the Dutch and German Wadden coast also show an almost linear relation between tidal prism P and the depth of the ebb-dominated channel [Sha 1990 in van der Vegt 2006]. Experiments by Mayor-Mora [1977] predicted an inlet area an order of magnitude higher than the 95-percent confidence limit of extrapolated field data [Mayor-Mora, 1977]. They suggested that the inlet area versus prism relationship may not be an exponential relation for the entire range of conditions from experiments to prototype or that scale effects are important. Mayor-Mora [1977] described that possible scale effect in their experiments was the use of typical size quartz sand which did not scale with prototype barrier sediment conditions. Our experiments do scale sediment and results can thus define if the inlet area versus prism relationship holds for the lower range of conditions of Mayor-Mora [1977].
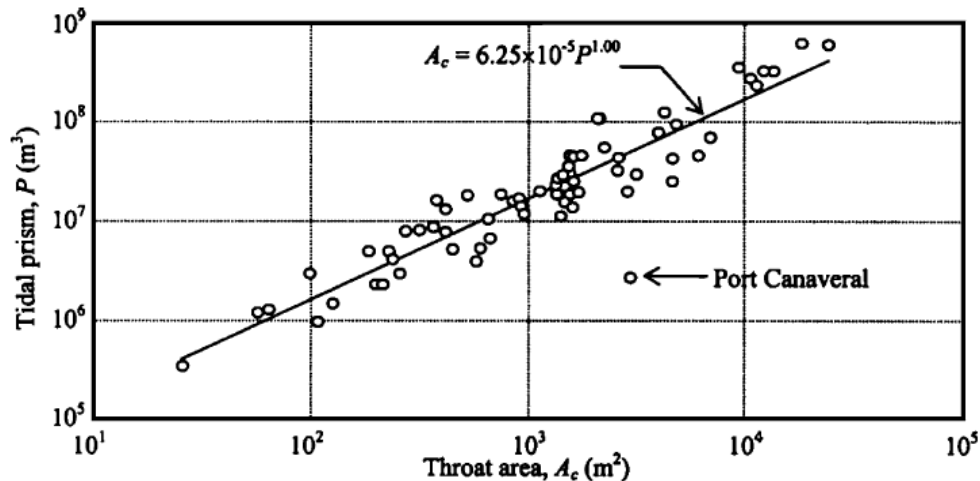
Figure 2.9 Area-prism data for Florida entrances. From Powell et al. 2006.

2.2.7 Dynamic equilibrium state

Morphodynamic equilibrium is often assumed [van der Wegen et al. 2008] based on the relation between ebb-tidal delta volume (ESV) or tidal prism (P) and the inlet area (Ac) (previous section). The concept of ''morphodynamic equilibrium'' refers to a certain natural and steady state of the bathymetry in a tidal system [Van der Wegen et al. 2008]. But the empirical relations do not explain the origin of the equilibrium and its sensitivity to changing conditions [van der Wegen et al. 2008]. The equilibrium state may be dynamic in the sense of regular or cyclic migration of shoals and channels. The dynamic behaviour and adjustment to equilibrium occurs on different spatial scales but timescales interact with each other. It results in a state wherein a process of continuous and dynamic feedback is maintained [De Vriend 1996 in Van der Wegen et al. 2008]. The equilibrium characteristics may be a subject of geological inheritance and the dynamic feedback can be reflected in timescales of centuries to millennia. In contrast, major impacts by humans occurred over decennia to centuries. Observations usually comprise less time than all these processes cover so the subject of dynamic equilibrium state is still under debate. A modelling study by van der Wegen et al. [2008] suggests that when basins evolve towards a state of less morphodynamic activity it is represented by stable characteristic patterns. Also the basin deepens and widens less. A continuous sediment export toward the sea and bar and shoal migration is still observed. Closer analysis of van der Wegen et al. [2008] on the hydrodynamic characteristics over time shows:

- ✓ lower width averaged velocity peaks,
- ✓ similar ebb and flood duration and velocities along the basin,
- ✓ constant time lags between maximum velocities and maximum water levels,
- ✓ a stable relationship of the ratio of the water volume stored on the shoals and the channel volume (Vs/Vc, criterion to determine the flood- and ebb-dominancy of a tidal inlet)
- ✓ A stable relationship of the ratio of the tidal amplitude to mean channel depth (a/h).

These relations can help in determining when an eventual equilibrium may be defined.

2.2.8 Cyclic behaviour

Tidal systems remain dynamic over time. Field studies from a few centuries show that the channels in the Dutch Wadden Sea and in the back-barrier at the coast of South Carolina actively migrate. The channels do so by eroding bars and depositing new bars. Also in the inlets the channels shift continuously and cyclically [Oost 1995 Chapter 3]. The tidal systems have multiple inlets with single, double or triple channels. Also the number of channels show a cyclic behaviour of shifting between the numbers of inlet channels [Oost 1995 Chapter 3]. Ameland inlet (most natural system of the Frisian Islands) is modulating between a one-channel and a two-channel system during a period of

approximately 50 years [De Grimal 1998 in Dissanayake et al. 2008 and Oost 1995]. Also the tidal inlets between the barrier islands shift/migrate continuously and, as far as known from a few centuries, cyclically (Oost 1995 Ch. 3). A summary of cyclic and migrational behaviour is observed in:

- eastward migration of inlets whereby it takes over drainage systems
- Pinkegat: cyclic development of the main channel from one main channel to two or more main channels. In case of one main channel the channel is relatively deep and migrates eastward. Simultaneously the barrier to the west expands. As a result the flood flow acquires more time to reach the back-barrier. Eventually it washes out new channels. A multiple channel inlet system arises. The channels are shallower. They also migrate eastward. The channels that are situated the furthest to the west migrate the fastest. After some decennia the channels fuse or silt up. Eventually one main channel remains.
- Zoutkamperlaag: the ebb-tidal delta shows channel migration from the west to the north and from there to the east. The channel migration on the ebb-tidal delta modifies the location of the tidal current. Thereby it influences the main channels in the inlet. Usually two separate channels arise in the main channel that separate more and more in time. Eventually the western channel is abandoned.
- The back-barrier shows a response to the transition in the number of channel inlets. The high water area becomes smaller in the west due to a change in the tidal signal. At the same time the high water area shifts slightly eastward.
- On the ebb-tidal delta, smaller-scale bars are observed that migrate. The migration is referred to as cyclic bar behaviour and the bars migrate from the inlet and attach to the coast [De Swart et al. 2004 and Ehlers 1988 in Dissanayake et al. 2008]. It indicates that sand is by passed from one barrier island to the next [de Swart and Zimmerman 2009].
- Smaller-scale channels and shoals repetitively form in the region of the ebb-tidal delta and subsequently migrate from one side of the inlet to the other side [van der Vegt 2006]. Typical time scale of this cycle ranges between decades (Ameland Inlet, the Netherlands) to centuries (Texel Inlet, the Netherlands). The long-shore transport is generated by a combination of waves and currents [different researchers in de Swart and Zimmerman, 2009]. The waves generally approach the coast under an oblique angle and thereby generate long-shore currents. A part of the sediment bypasses the ebb-tidal delta and reaches the up drift part of the next island (figure 2.2). Another part of the sediment is transported into the inlet and is either deposited there, imported into the basin or exported back whereby it contributes to the maintenance of the ebb-tidal delta [de Swart and Zimmerman 2009].

In the last decades human interference, by land reclamation and the construction of groins, has been of major influence on the natural behaviour of tidal inlet systems. It is difficult to distinguish between cyclic phenomena and the adjustment of the system due to human interference and to see which process is being dominant. Experiments can provide better insight on cyclic phenomena.

2.3 (2D) Modelling studies

Modelling studies allow testing findings from observations and experiments. First an overview of modelling efforts will be provided. The first section provides insight in the capabilities of morphological models as well as in the shortcomings in results of models on morphological change. The next sections provide insight in the effect of the character of the tidal flow and the effect of wind waves on typical morphology. The ebb-tidal delta, inlet, flood tidal delta, the channel networks and basin geometry are considered separately.

2.3.1 Modelling capabilities

Morphodynamic models have experienced increasing popularity since computer power increased exponentially. Most of the models are 1-dimensional or 2-dimensional but the last decade attempts have been made to develop quasi- and fully three dimensional models [Cayocca 2001] with the

development of the Delft3D model. Normally depth averaged schemes cannot account for undertow, wave asymmetry, density currents or curvature-induced secondary flows [Cayocca 2001]. If models do incorporate these processes, they do so by introducing a formulation that approaches the net effect. The focus of this study is on the ebb-tidal delta, inlet and channel networks which are large-scale features. Consequently the focus is on the long-term morphological development. In contrast, the more advanced Delft3D modelling might be better suited for understanding the complexity of flow and sediment transport on small scales. The 2D-modelling approaches are suited for large-scale and long-term approaches.

Multiple studies were done on the evolution of the ebb-tidal delta and on channel networks by the analysis of conceptual and numerical models [van der Vegt 2006; Dastgheib et al. 2008; Dissanayake et al. 2009]. The objective of the modelling studies was to achieve equilibrium state and realistic morphology. Van der Vegt [2006] simulated the almost linear relation between ebb-tidal sand volume ESV and tidal prism P. It was found that the balance between net (tidally averaged) intersection of sediment transport from the current and waves and between the net sediment transport due to bed slopes maintains the equilibrium. Van der Vegt [2006] could not achieve the folding of the ebb tidal delta around the ebb-dominated channel in his model. Nor could the model accurately resemble the morphology of the ebb-tidal deltas of the USA Atlantic coast and Dutch Wadden coast. Dastgheib et al. [2008] simulated a stable condition of the tidal basin in the Western Dutch Wadden Sea. The stable condition strongly depends on the initial condition of the model as well as on the forcing conditions. Dissanayake et al. [2009] showed that initial basin configuration and tidal signal influence the ebb-tidal delta morphology. The ebb-tidal delta did not achieve an equilibrium state. The model showed unrealistic wide and deep channels. In addition, results strongly depended on sediment transport formulation. So although models of ebb-tidal deltas and models of tidal basins reproduce basic morphology, improvement is needed.

Geleynse et al. [2011] showed by means of a modelling study how sediment characteristics result in different morphology of river deltas. The morphodynamics are dominated by river flow, tidal currents or wind waves (figure 2.10). Meanwhile, a tidal inlet systems is a combination of all this in one single system. The ebb-tidal delta consists of sand and the morphology is determined by tidal currents and wind waves. The flood-tidal delta rather resembles sand-silt conditions. While the channel networks and tidal flats consist of finer sediment and clay. The morphology of the channels is determined by the tidal and possibly river flow while the mud flats are eroded by wind waves [de Swart and Zimmerman 2009]. In most modelling studies the frequent sediment grain size corresponds to a medium beach sand. Cayocca [2001] models the interaction between the inlet and the lagoon. In nature much finer sediment predominates in the lagoon. The morphological changes predicted by the model in the lagoon are expected to be underestimated around the tidal flats [Cayocca 2001]. The development of tidal flats is not modelled while tidal flats considerably affect the tidal flow when flooding and draining a basin. So how to involve the different sediment characteristics and flow dominance in one model? Van der Vegt [2006] describes the problem with different time-scales. Water motion varies on a scale of seconds to days while the morphodynamic evolution happens on a scale years to decades. Other complications are the coupling between the hydrodynamics and the change in bathymetry which mutually affect each other, non-uniform sediment distributions calculations, wetting and drying and including 3D effects. So far, no model simulates the morphodynamic interactions and configuration of a tidal system or estuary on timescales of centuries in a realistic way.
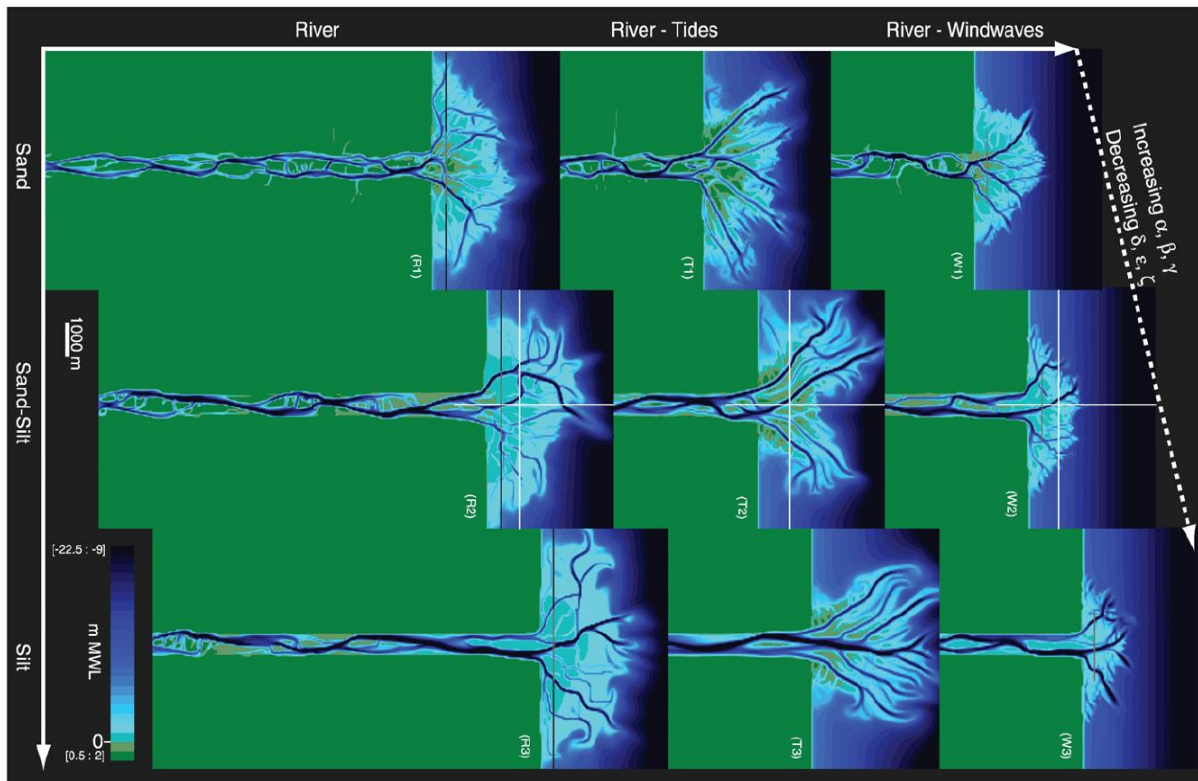
Figure 2.10 Simulated delta morphology for different combinations of hydraulic and sedimentary forcing types after 7.5 simulated years, from Geleynse et al, 2010.

2.3.2 Ebb-tidal delta and inlet

Modelling studies provide knowledge on flow patterns through the inlet. The ebb flow behaves as a free turbulent jet when water flows out of the back-barrier. During flooding, almost radial inflow of water occurs before the water enters the inlet [de Swart and Zimmerman 2009; Valeria et al. 2007; Dissanayake et al. 2009]. Averaged over a tidal cycle it results in a residual current. The residual current in the central channel is in the direction of ebb currents and pushes sediment seaward [different researchers in De Swart and Zimmerman 2009; Dissanayake et al. 2009]. The residual current at the sides of the inlet is in the direction of flood currents. The mean residual tidal flow is organized in cells, presented in figure 2.11. A residual current causes net sediment transport since sediment transport is a nonlinear function of instantaneous flow velocity. The flow field of figure 2.11 explains the arising of a delta perpendicular to the inlet. The flow strength increases which induces erosion. Consequently the channel deepens and a main ebb channel in the middle arises. The flood flow is stronger at the sides. Typically flood marginal channels are seen there according to figure 2.3. Cayocca [2001] modelled the macrotidal Arcachon Basin in France. In most of the inlet at Arcachon Basin the ebb currents are stronger than flood currents. She found that in the absence of waves, the ebb tidal delta continues to extend seawards. No process prevents the tidal ebb current not to expand as long as there is sediment available and the inlet retains its flushing action [Cayocca 2001]. The inlet retained its flushing action because the simulation did not include any process that might induce the breaching of existing sandbars [Cayocca 2001].
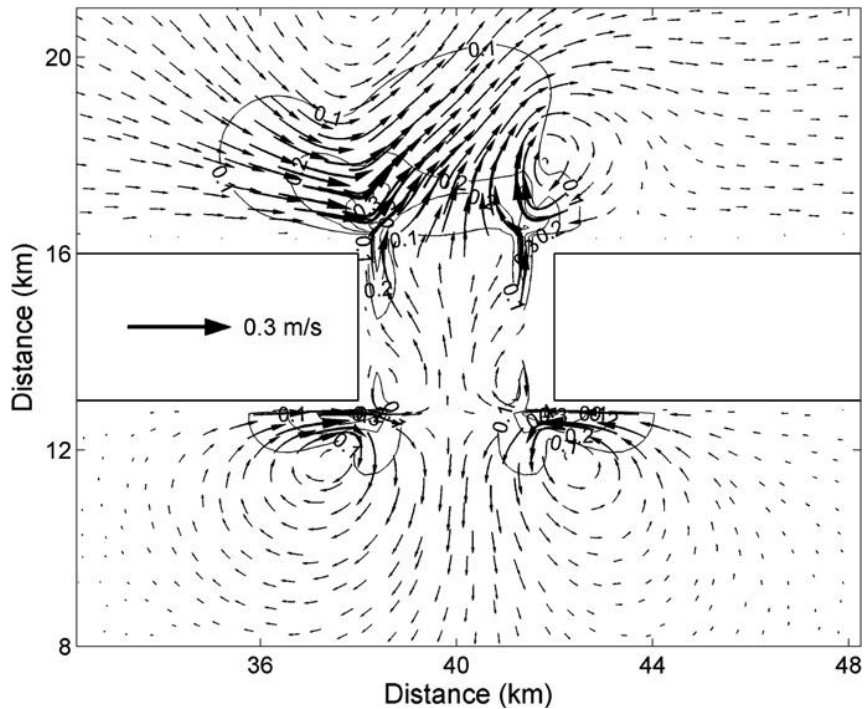
Figure 2.11 Mean residual tidal flow vectors from modelling study of Dissanayake et al. [2009] which illustrates presence of tidal residual circulation for Western Wadden Sea.

Some ebb-tidal deltas are (almost) symmetric with respect to the mid-axis through the inlet such as for the US Atlantic Coast. Van der Vegt [2006] modelled typical parameter settings from the USA coast to investigate how the symmetric ebb-tidal delta is maintained. The sediment that forms the ebb-tidal delta most importantly originates from stirring of sediment by waves and tides and the transport by the residual currents. The ebb-dominated channel does not form in the direction of the residual currents (figure 2.12). The presence of waves causes a larger delta. Van der Vegt [2006] achieved equilibrium between the ebb-tidal delta and the channels. The equilibrium is maintained by the balance between the bed slope and the average strength of currents and waves over a tidal cycle. The model results of Van der Vegt [2006] also showed differences with observations. Most importantly, the length of the ebb-dominated channel in the model is considerably smaller than observed in nature. Neither does the model recover the folding of the ebb-tidal delta around the ebb-dominated channel. The modelled sand volumes are about a factor five smaller than observed in nature. It indicates a limitation in available sediment transport formulation to model morphological change. Still, it was concluded that if sand transport by tides prevails over that by waves and alongshore tidal currents are small, a nearly symmetric ebb-tidal delta results.
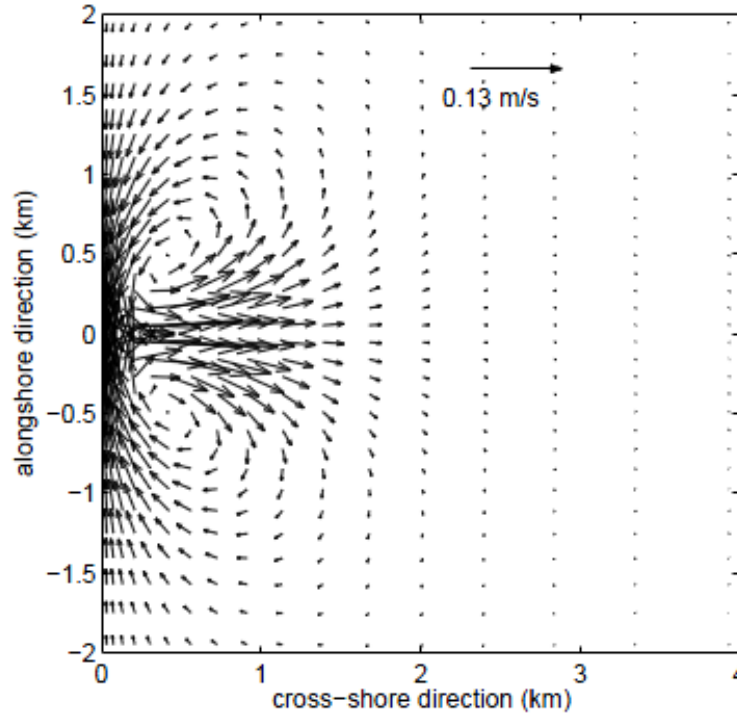
Figure 2.12 Mean residual tidal flow vectors from modelling study of Van der Vegt [2006] which illustrates presence of two tidal residual circulation cells (with maximum currents in the order of 0.13 m/s). The width of the tidal inlet is 1 km.

The occurrence of asymmetric deltas is prominent for the Dutch Wadden Sea coast (figure 2.1). Two important agents can be distinguished that give way to asymmetry of deltas. Waves that arrive at the delta with an angle cause the ebb-dominated channel to be oriented in the direction of the wave-driven currents. The second agent is the direction of the tidal current which is shore-parallel for at the Dutch Wadden Sea coast. The ebb current at the Dutch Wadden Coast travels from east to west. It causes the ebb-dominated channel to be oriented to that direction, which is to the left for the Dutch Wadden Coast [van der Vegt 2006]. When the flood flow enters the tidal basin, the tidal signal can deform because of decreasing water depths and long flow paths. At the time the ebb-flow leaves the basin, the open sea tidal signal can be of a different type (travelling wave) as the one leaving the basin (standing wave). When there is no difference between the open sea tidal wave and the tidal wave from the basin an ebb-dominated current exists that flows to the left-hand side. The flood flow enters from that direction too so the current is bi-directional there. The jet like character of the ebb flow is locally dominant over the more radial inflow at flood. As a consequence the delta is left oriented . On the right-hand side of the inlet the currents are weaker, more rotary and flood-dominated [van der Vegt 2006]. Usually flood dominated channels emerge there. When the phase difference between the open sea tidal signal and the basin tidal signal is 90 degrees the tidal flow behaves differently (travelling wave versus standing wave). In this case the ebb current through the inlet significantly lags the strength of a shore-parallel ebb-current to the left. The result is a less asymmetrical delta [Van der Vegt 2006]. Dissanayake et al. [2009] describe the same phenomenon in their models. Van der Vegt [2006] also found that wider inlets tend to have an ebb-dominated current which is oriented to the right. The orientation of the main inlet channel and the ebb-tidal delta is not influenced by the orientation of the basin with respect to the inlet [Dissanayake et al. 2009]. The Coriolis force is of minor influence on the orientation of the ebb-tidal delta. On the Northern Hemisphere the centre of mass will slightly be shifted to the right and on the Southern Hemisphere slightly to the left [Van der Vegt 2006]. In short, the orientation of the ebb-tidal delta is to a large extent determined by the interaction of the alongshore tidal current in the open sea and the tidal currents through the inlet. An asymmetrical ebb-tidal delta is maintained by strong

bypassing currents at the ebb-tidal delta front and the weaker and rotational character of the currents at the east of the inlet [Dissanayake et al. 2009].

For most coastal regions the M2 tidal constituent - the semi-diurnal lunar tide with a period of 12 hours and 25 minutes - is the dominant tidal constituent. The M4 tidal constituent is an overtide to the signal. When the tidal wave enters shallow water the tidal wave signal changes because in shallow water the tidal wave crest moves faster than the wave trough (propagation speed of the wave $u_w = (gh)^{1/2}$). The flood period becomes shorter with a peaked crest and the ebb becomes longer with a flat trough. It is referred to as tidal asymmetry. Consequently flood velocities will increase and ebb velocities will decrease but last longer. The higher flood velocities favor a basin inward sediment transport. The model of Dissanayake et al. [2009] showed that offshore asymmetry from the M2 and M4 tidal constituents leads to a decreasing volume of the ebb-tidal delta (ESV) on the longer term (figure 2.13). So the M4 tidal constituent causes higher flood velocities which results in a smaller ebb-tidal delta. In the model of Dissanayake et al. [2009] there is no wave generated alongshore transport which contributes sediment to the ebb-tidal delta. Therefore the flood current can continue to transport sediment from the ebb-tidal delta into the basin. In case of the M2 tidal constituent only the ebb-tidal delta sand volume first increases and then stabilizes. Figure 2.13 shows that the ebb-tidal delta of (b) from M2 and M4 has one main channel. In comparison, (a) from M2 has two channels and a more extensive ebb-tidal delta. The ebb-tidal deltas of both models show asymmetry in the ebb-tidal delta. These models did not consider wave driven currents. Meanwhile the basin was located asymmetrically with respect to the inlet in the model domain. As a result, higher concentrations of ebb currents developed at the west of the inlet which resulted in a more pronounced channel to the west and an asymmetry in the ebb-tidal delta. It is concluded that initial basin configuration influences the ebb-tidal delta orientation when wave driven currents are absent. Offshore tidal wave asymmetry from M2 and M4 influences the volume of the deltas.
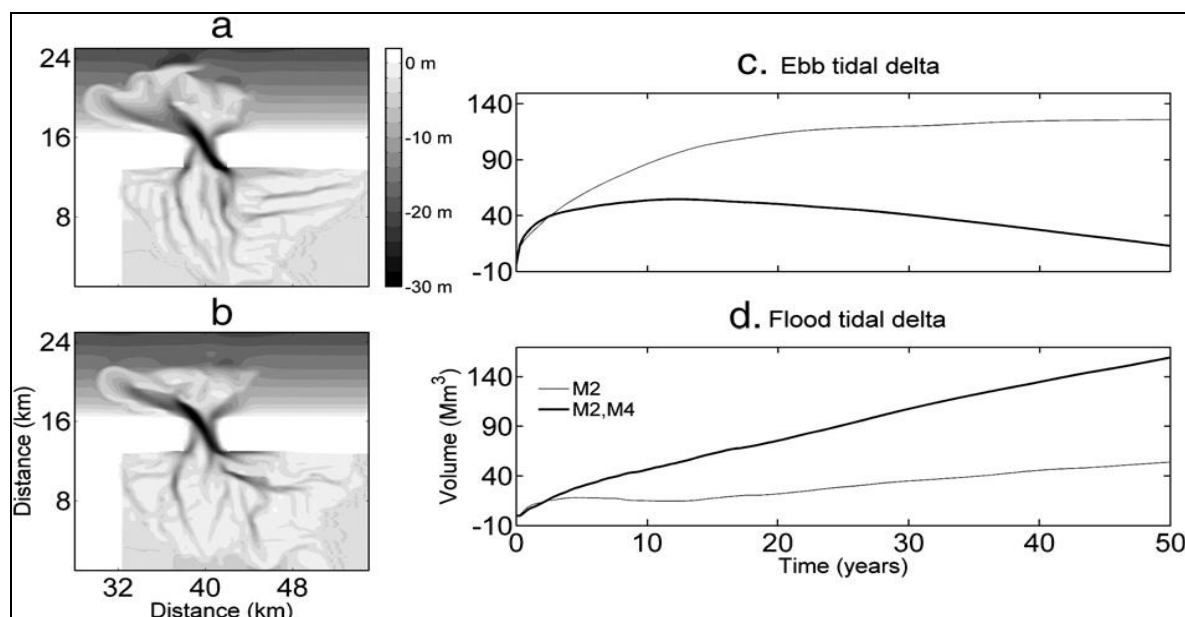
Figure 2.13: 50-year bed evolutions from model of Dissanayake et al. [2009] with (a) no tidal asymmetry (M2), (b) with tidal asymmetry (M2, M4), and volume change, (c) ebb-tidal delta, and (d) flood-tidal delta.

2.3.3 Flood-tidal delta

Just landward of the inlet, sometimes a flood-tidal delta is observed. The presence or absence of flood-tidal deltas and their size and development are related to the tidal range, wave energy, sediments supply and the back-barrier setting of the region [Davis Jr. and FitzGerald 2004]. Flood-tidal deltas are best revealed in areas with moderate to large tidal ranges (1.5 m to 3.0 m). They are

well exposed at low tide. The flood tidal delta can have single or multiple lobes. To some extent, the size of the flood-tidal delta is related to the open water area in the back-barrier and to the size of the tidal inlet [Powell et al 2006]. In general, a decreasing inlet channel width leads to a smaller flood-tidal delta [Davis Jr. and FitzGerald 2004]. At most stable inlets the sand of the flood-tidal delta is simply re-circulated. Strongest flood currents generally occur near high tide when the entire flood-tidal delta is submerged. Net sediment transport is up the flood ramp, through the flood channels and on the ebb shield. During the falling tide, strongest ebb-currents are generally reached near mid to low water. At this time the ebb shield is out of the water and the tidal current is diverted around the ebb shield while it erodes sand from the landward face of the ebb shield. The sediment is transported into the inlet channel. Then, the subsequent flood-current transports the sediment back up the flood ramp and ebb shield [Davis Jr. and FitzGerald 2004]. Like that the flood-tidal delta is maintained.

2.3.4 Channel networks

To model morphological change transport formulations are required. Dissanayake et al. [2009] used two different formulations to model the initiation and development of a tidal inlet system. The VR (Van Rijn) formula tended to produce twice the sediment transport rates compared to the EH (Engelund-Hansen) formula and gave a stronger evolution than that of the EH formula. The difference resulted from a different degree of non-linearity of sediment transport versus depth-averaged flow velocity of the two formulas. The VR formula better described the initiation of motion. The results from using the VR formula best followed the conceptual hypotheses of initiation and development of a tidal inlet over a time period of 50 years. But channel pattern was more refined and pronounced in the EH model result [Dissanayake et al. 2009]. The latter indicates that in order to achieve pronounced channel network configurations in the model, low sediment transport rates were preferred. At the same time, the bar theory from Struiksma et al. (1985) suggests that an increasing degree of non-linearity between sediment transport and depth-averaged flow velocity increases the tendency to form bars and islands [Van Dijk et al. 2010]. When there are many bars and islands, channel network is less defined in the sense of existence of long channel sections. Modelling efforts thus suggest that sediment transport rates determine channel network configuration, most importantly in early stages of development.

2.3.5 Long basins

Van der Wegen and Roelvink [2008] modelled 1D-profile adjustment of long basins from horizontal sediment bed. After 8000 years the profile from -10MSL is a landward sloping bed in figure 2.14. In case of a shallower basin higher sedimentation rates are observed. The shallower a basin becomes, the more ebb flows and ebb wave propagation are hampered so that ebb duration increases. As a result flood duration is smaller and velocities are higher. At the same time more sediment is transported landward during flood [van der Wegen and Roelvink 2008].
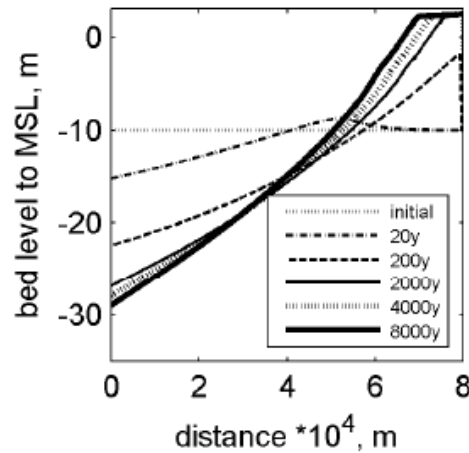
Figure 2.14 1D model results of profile evolution from horizontal flat bed at 10m-MSL

The 2D-modelling of van der Wegen and Roelvink [2008] provides knowledge on equilibrium morphology in a long shallow basin. Figure 2.15 shows the emerging of a wide sinuous channel from smaller channels. Channel width decreases basin inward indicating a (funnel) shape of the estuary. A different morphology arises for a short and a long basin. Figure 2.16 shows that in a short basin multiple small sinuous channels arise. While for a long basin a wide sinuous channel arises that bifurcates in the back part of the basin.

Long-term, 2D, simulations by Hibma (2003) show stable patterns in estuaries. The patterns have a characteristic length scale with an order of magnitude of the tidal excursion [van der Wegen and Roelvink 2008]. Lanzoni and Seminara [2002] stress the impact of the (funnel) shape of the estuary. They found that the dominant factor in tidal environments is the presence of multiple sediment fractions including sand and mud. Tidal asymmetries in currents and water levels result in continuously changing suspended sediment concentration profiles during the tidal cycle. Erosion and settlings lags are particularly relevant at shoals around slack tide.
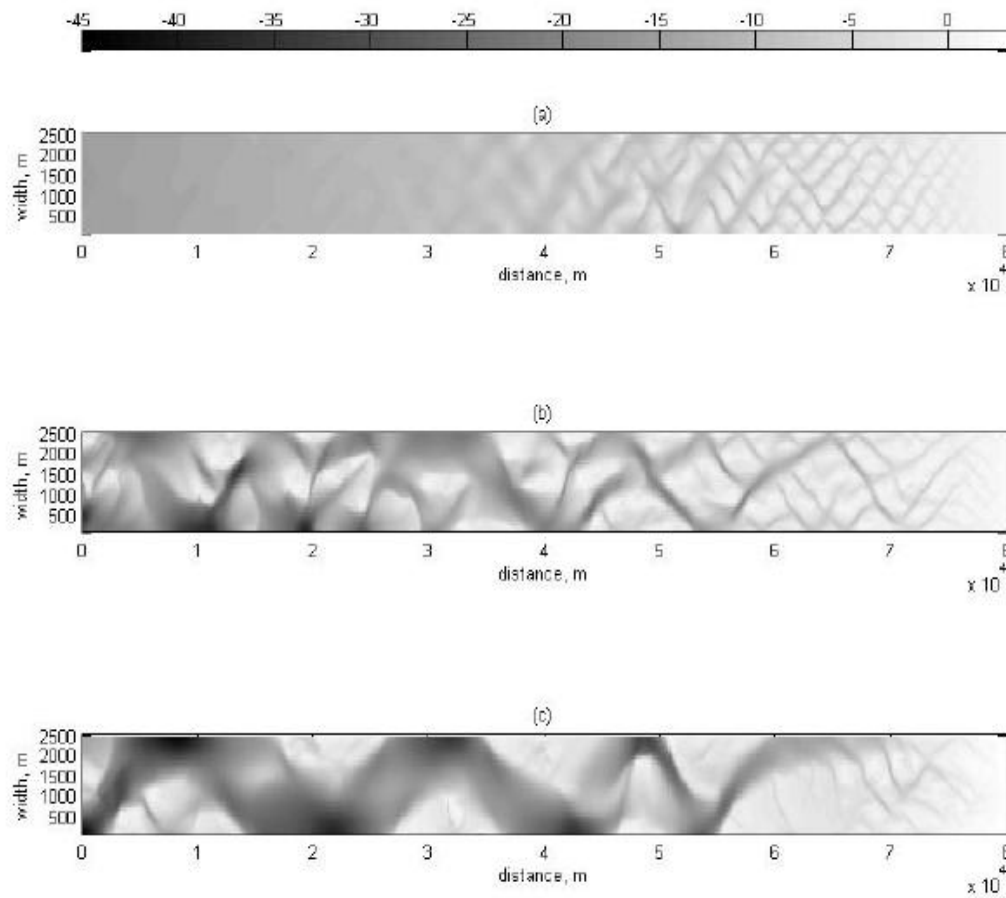
Figure 2.15 Pattern formation for a shallow basin in meters. The basin is 2.5 km wide and 80 km long. (a) is after 15 years, (b) after 100 years, (c) after 800 years. From van der Wegen and Roelvink 2008.
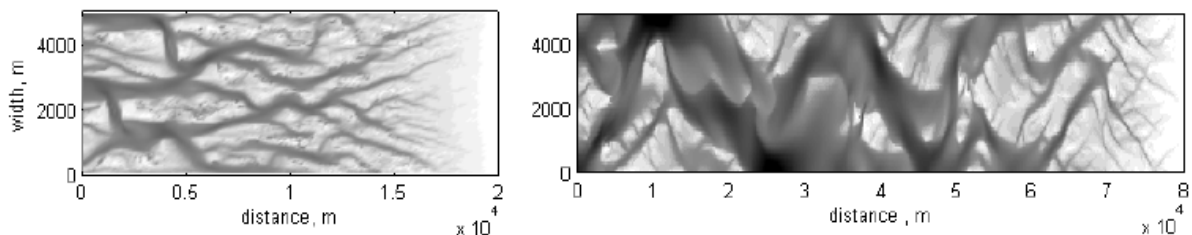
Figure 2.16 Pattern formation for, left, a short basin of 20 km long and, right, a long basin of 80 km long presented after 1600 years. From van der Wegen and Roelvink 2008.

2.4   Experiments

This section first gives an introduction to and summary of prior coastal morphological experiments. Secondly experimental findings will be given. Thereafter an analogue experiment to this research is summarized to finish with providing knowledge and experimental experience from delta experiments.

2.4.1 Experimental efforts and constraints

Relatively little amounts of laboratory experiments are done in the field of coastal morphological research [Hoyal and Sheets, 2009]. This is in contrast to the existence of a wide literature based on field observations, linear stability analyses and numerical modelling. Though experiments can provide a data-rich description of the evolution of tidal channel networks, ebb-tidal deltas and estuaries in fully controlled boundary and initial conditions. Reynolds already stated the importance of experimentalising about 120 years ago.

> *Experimentalising on the small scales allows to test in whatever condition we want to test and readily observe the effect produced. On a large scale we can only test the conclusion by actual observation [Reynolds 1887-1891].*

The results will be the same on a small scale as on a large one if the character of the motion of the water is the same at all points [Reynolds 1887-1891]. But only few research teams have ever created features of tidal inlet systems in the laboratory [de Swart and Zimmerman 2009]. So far, no research group ever succeeded creating a dynamic tidal inlet system that is close to equilibrium.

Stefanon et al. [2009] aimed at reproducing a typical lagoon environment subject to tidal forcings. Tambroni et al. [2005] investigated equilibrium conditions of a longitudinal bed profile for both a rectangular basin and a basin with an exponentially decaying width. Garotta et al. [2007] studied the long term morphodynamic evolution of an experimental tidal meandering channel connected to a tidal basin. Valeria et al. [2007] and Van Dijk [2009] created an ebb-tidal delta and a flood tidal delta respectively. Reynolds [1887-1891] simulated tidal flow paths and sediment distribution in Mersey estuary in the United Kingdom. Mayor-Mora [1977] investigated ocean-inlet-bay system subsequently subjected to ocean tide and wave action. The ocean-inlet-bay system varied in geometry. Spatial variation of important parameters such as tidal range damping and mean current velocity time lag were analyzed.

Generally these experiments faced problems because of the emergence of unrealistic deep scours and large ripples. Their systems were mostly ebb-dominated and experimental times were long (weeks to months). In addition, none of the experiments did consider the evolution of the channel network and the ebb-tidal delta simultaneously even though they mutually affect each other [i.e. Dissanayake et al. 2009; Masselink and Hughes 2003; Van der Vegt 2006; de Swart and Zimmerman 2009;]. Another major drawback of small-scale experiments is that the mobility of sediment must be similar to real situation to suit scaling conditions. In experiments the flow depth in channels is relatively low, therefore very fine sediment (clay) should be used. Clay cannot be used because it proved far too strong [Kleinhans et al. 2008]. Besides, the debate on up scaling experiments is withholding research on the experimental scale.

2.4.2 Experimental findings

Tambroni et al. [2005] found morphodynamic equilibrium both in the inlet region and in the channel. The channel exhibited a weakly concave bed profile seaward while landward the profile was weakly convex. Small-scale bed forms were found to develop in the channel and in the basin. Larger scale forms such as tidal bars developed in the channel [Tambroni et al. 2005]. Their findings agree with 1D-modelling of Seminara and Tubino [2001]. Garotta et al. [2007] developed a quasi equilibrium pattern of the average bed profile (figure 2.16B). A deep scour developed at the inlet and a shoal formed (a wet and dry area) in the inner reach of the channel. It appeared that the bed topography was strongly affected by the boundary conditions at the inlet and at the inner end. Mayor-Mora [1977] found that for a given tidal prism, an experimental inlet will have a smaller cross-sectional area for a test with waves and tides, than an inlet with tides only. This suggests that waves carry sand to the inlet and reduce the inlet area. Reynolds [1887-1891] mimicked an estuary in a rectangular basin of about 4m long and 1.2 wide. He shared a lot of experimental experiences on hydrodynamics and described key scaling issues. Van Dijk [2009] showed autocyclic behaviour to exist on the

experimental flood-tidal delta once it had grown to mean water level. The development of river dominated deltas has been studied by Hoyal and Sheets [2009] in small-scale experiments (figure 2.16B). He observed a cyclic pattern of delta evolution. Weak channelization was observed because of the use of simple non-cohesive sand mixtures which limited the ability to generate complex channels on deltas at the experimental scale [Hoyal and Sheets, 2009]. Hoyal and Sheets [2009] suggests the use of a polymer to achieve strong self-channelization.

Mayor-Mora [1977]
Inlet with tidal forcing

Hoyal and Sheets [2009]
Experimental delta with flow patterns
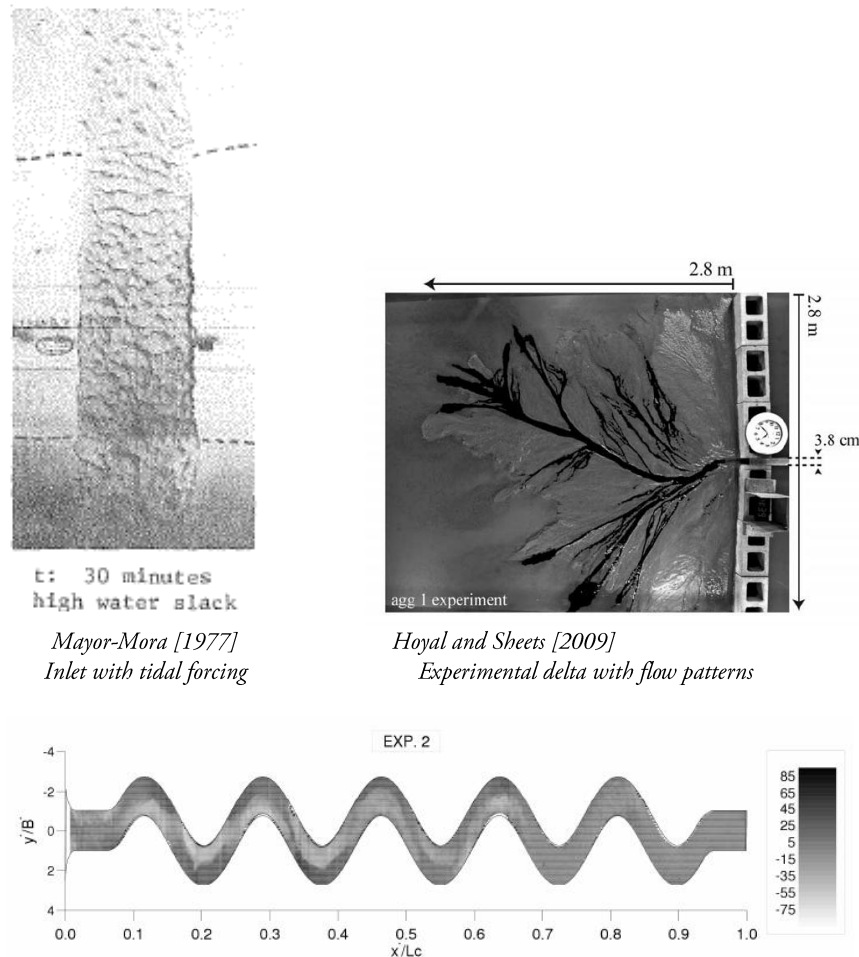
Garotta et al. [2007] Map of bed topography (mm) showing the bar-pool pattern in the final stage of experiment 2

Figure 2.16B Representation of experimental findings

2.4.3 An analogue experiment

Stefanon et al. [2009] state they were the first ones to do an experimental analysis on the processes governing the initial formation and subsequent development of a tidal channel network on a coastal lagoon behind a barrier island. The objectives of Stefanon et al. [2009] were as follows: What are the processes governing the initial channel network formation? Does the channel network evolve towards an equilibrium state? Do the laboratory network configurations exhibit morphological features similar to those observed in nature? The research questions correspond to the objectives of the proper laboratory experiment. Therefore it is meaningful to discuss the research of Stefanon et al. [2009]. This section shortly summarizes the efforts done by Stefanon et al. [2009] and their major findings.

The experimental set-up used by Stefanon et al. [2009] is shown in figure 2.17. The lagoon basin was about 5.3 m long and 4.0 m wide. The sea was separated from the lagoon by a barrier of wooden panels and the lagoon inlet was located in the middle of this barrier. The shape and width of

the lagoon inlet were varied in the different experiments. The tide was generated by a vertically oscillating weir and reproduced a sinusoidal tide of fixed amplitude and period oscillating around a prescribed average level.
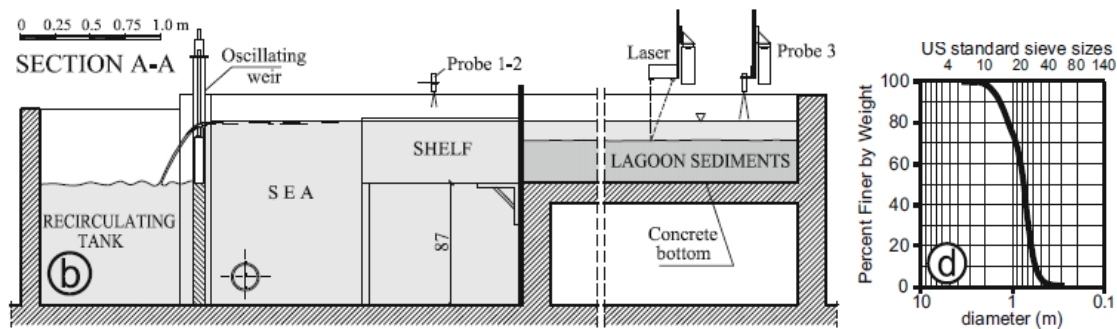
Figure 2.17 Side-view of experimental apparatus used by Stefanon et al. [2009] and sediment characteristics.

The sediment in the lagoon bed was cohesionless. It consisted of plastic grains with a density of 1041 kg/m^3. The grains ware characterized by a nearly uniform grain size distribution with a median grain size (d_{50}) of 0.8 mm. Stefanon et al. [2009] chose this sediment to ensure sediment transport throughout most of the tidal cycle, with the values of friction velocity typically generated in the experiments.

Four experiments were reported aimed at understanding the physical processes and the effects of boundary and initial conditions on the morphological evolution of a tidal inlet system. A summary of the experiments that were carried out is given in the table below. They varied tidal amplitude a, period T, width of the tidal inlet B and average depth of the initial tidal flat configuration D_0. The time required to complete a single experiment ranged from 30 to 60 days.

Table 2.1 Experimental properties of Stefanon et al. [2009]

Run	Tidal amplitude a (cm)	Tidal period T (s)	Inlet shape	Inlet width B (cm)	Average initial depth of tidal flat D_0 (cm)
1	2.0	480	Rectangular	100.0	0.0
2	2.0	600	Trapezoidal	20.0	1.5
3	1.0	480	Trapezoidal	20.0	0.0
4	1.0	480	Trapezoidal	20.0	0.0

For a given tidal period (8-12 minutes) a channel network was observed to form only for small enough values of the tidal amplitude (1.0-2.0 cm). Higher flow depths enhanced the formation of bed forms (ripples and dunes) and prevented the formation of well defined channels. It indicates that flow velocities were very low (in the range of centimetres per second) and so were sediment transport rates. Important were the wetting and drying processes of the lagoon bed at the beginning of the experiment. Isolated channels started to form in front of the inlet. The channels progressively elongated through headward growth, in particular during the ebb phase. Multiple major channels were present. Smaller tributaries of these channels proved to be unstable because they sometimes abandoned the main channel to join another one or they migrated laterally.

The third experiment of Stefanon et al. [2009] gave the best results (figure 2.18 left). A first channel formed after about 130 tidal cycles and a second channel formed after about 600 tidal cycles. These channels branched out, deepened and further developed through headward growth until they reached the landward side of the tidal basin. Headward growth was particularly active during the partial drying of the sediment surface when flux concentration within the channels enhanced and, therefore, higher bed shear stresses occurred. Stefanon et al. [2009] list that these behaviour agrees with field observations from Myrick and Leopold, 1963; Bayliss-Smith et al., 1978; Pethick, 1980; Healey et al., 1981. It indicates that in tidal creeks maximum ebb velocities occur once the water has left the adjacent intertidal surface and is flowing through the channels. The rate of

network growth was particularly high during the early stages of each experiment after a certain degree of network formation was achieved. Channel elongation was approximately 1.5–2 cm every 150 tidal cycles in a phase of rapid growth. At the end of such a phase, the tidal network experienced only small adjustments. After 36 days (7845 tidal cycles) the network configuration was characterized by the presence of two lateral nearly symmetrical channels. The channels exhibit two meanders and various tributaries. In the centre there was another channel characterized by one meander and some branching links. The fourth run was done in order to reproduce the tidal network configuration (figure 2.18 right). This was not achieved. Experiment four also exhibits a nearly symmetrical channel configuration but now the central channel is the main channel. Concluding, Stefanon et al. [2009] suggest that the chief land-forming processes for network formation in unvegetated real settings are:
- Channel headward growth, driven by the spatial distribution of local shear stress.
- Tributary addition (possibly originating at sites where the stress increases along bends).
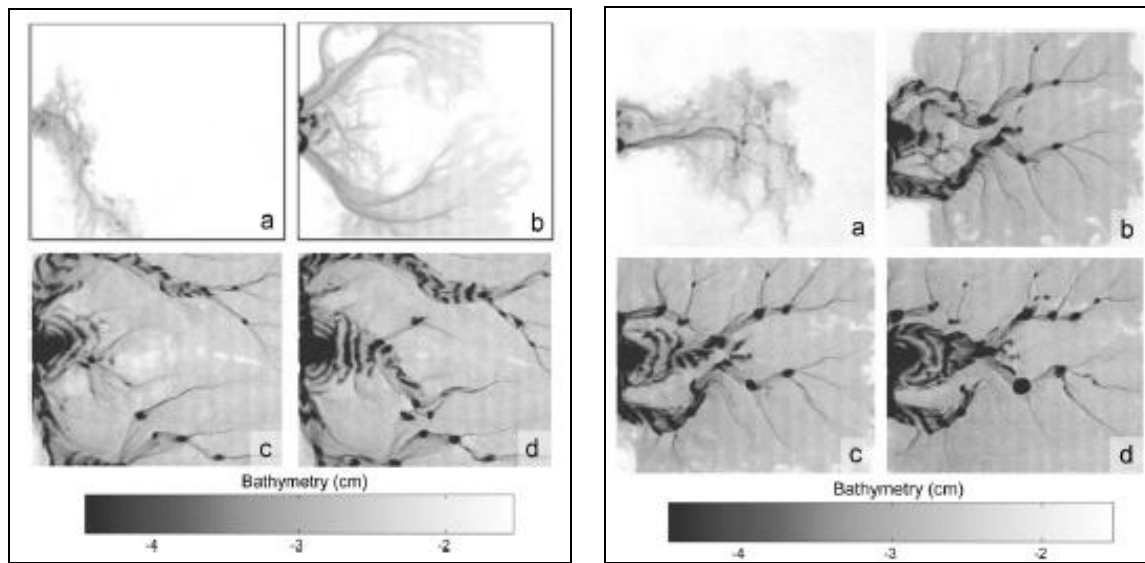
Figure 2.18 Distribution of bottom elevations within the lagoon in run 3 (left) after: (a) 127 cycles; (b) 756 cycles; (c) 3660 cycles; and (d) 6471 cycles. The right figure is the distribution of run 4 which was done in order to reproduce run 3 with (a) 750 cycles; (b) 2828 cycles; (d) 4757 cycles; and (d) 7845 cycles.
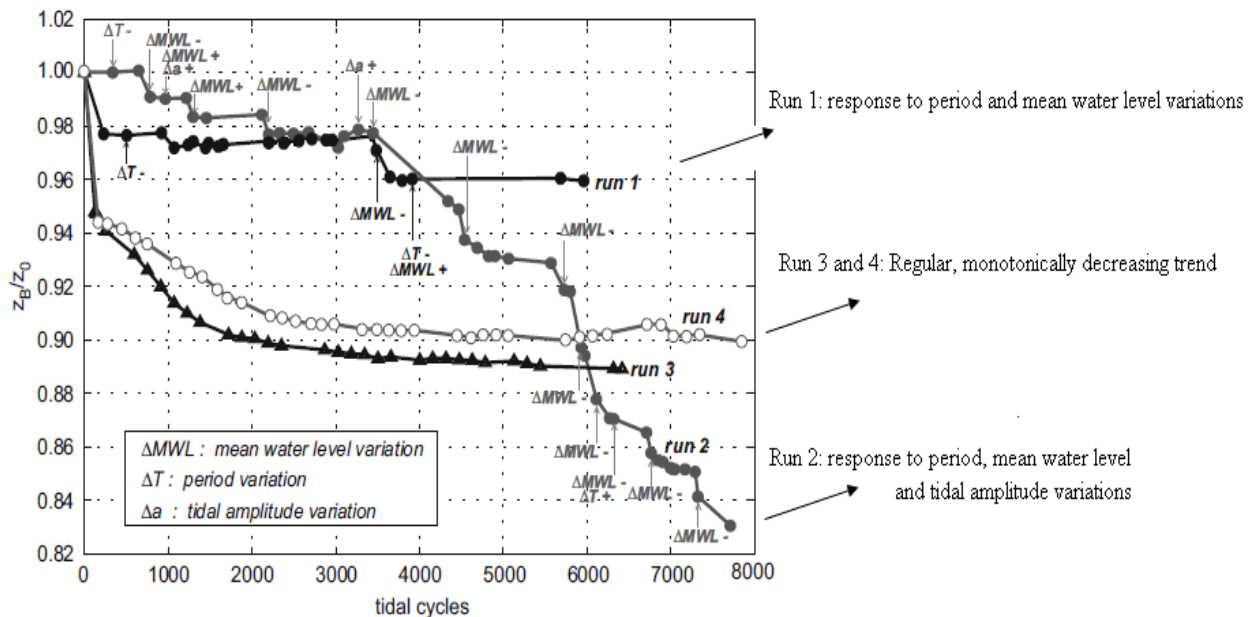
Figure 2.19 Temporal evolution of the mean lagoon elevation (z_b/z_0 means that bottom elevation is scaled with initial elevation). From four experiments by Stefanon et al. [2009]. The arrows at run 1 and 2 denote the instants at which the characteristics of the forcing tide were changed.

Figure 2.19 represents the evolution of the mean lagoon elevation and the response to changes in the forcing tide such as mean water level and tidal amplitude. It emerges that variations in tidal amplitude and tidal period only weakly affect mean lagoon elevation. While a decrease in mean water level produces abrupt increases in bed erosion processes with a deepening of the mean lagoon bottom. In contrast, an increase in mean water level does not result in a significant variation in the mean bottom elevation.

Stefanon et al. [2009] were able to create a channel network in the laboratory that displayed geomorphic features which compare favourably with those of actual networks. In any case, a wide scour formed near the inlet as a result of sediment transport only with the ebb flow and not with the flood flow. The channel network originates from the landward border of such a scoured region. In addition, all channels displayed deeper scoured regions at bifurcations or channel bends (figure *2.18 right (c)*). This is commonly observed by actual tidal channel networks [Stefanon et al. 2009], still the scour dimensions are not in accordance with actual channel network dimensions.

The lagoon always experienced a progressive net erosion. As a consequence the mean bottom elevation reduced. This was due to the lack of sediment inputs from external sources such as rivers and a net export towards the sea (with the ebb flow). It is representative for present conditions in the Venice Lagoon [Stefanon at AGU 2011]. Small scale bed forms extended from the inlet throughout the lagoon owing to the progressive lowering of the lagoon bottom produced by the net export of sediment. These bed forms tended to destroy the channel network. In order to solve this problem the mean water level had to be lowered (about 0.5 cm). This worked rather well to smooth out the small scale bed forms. But lowering of the mean water level also leads to enhanced flux concentration during the ebb phase over large portions of the lagoon. In case of higher tidal amplitudes intense sediment transport occurred and large bed forms formed over the entire basin. Then channel network growth was inhibited by the bed forms.

Stefanon et al. [2009] found an almost linear relationship existing between channel width and mean channel depth. The scatter of points in their experiments was mainly related to the presence of scours at confluences and bends. The width to depth ratio was found to vary mainly between 10 and 30, with a lower limit of 5 and an upper limit of 60. Lower beta-values characterize the smaller channels. These channels usually got dry during the tidal cycle. The larger beta-values characterized the larger channels.

2.4.4 Delta experiments

The research of van Dijk [2009] and Hoyal and Sheets [2009] consider river-dominated deltas in contrast to the subject of tidal deltas. Yet the results are discussed here because they consider deltas formed by a current in the direction of a relatively steep bed slope. The ebb-current is also a current in the direction of the bed slope. Also for an estuary system the ebb-current will be promoted because the river discharge is additional to the tidal discharge. Van Dijk [2009] describes alternating stages of sheet and channelized flow in the evolution of so called fan deltas. During sheet flow, aggradation of sediment on the delta increases the surface slope. As the slope reaches a critical value, incision is initiated, which is followed by headward erosion connecting the incision to the feeding channel. Channelized flow diminishes the surface slope and therefore leads to a lower gradient. After the incision is filled, renewed sheet flow occurs [Van Dijk 2009].

Hoyal and Sheets [2009] describe depositional cycles of river-dominated deltas by purely autogenic conditions. The experimental results allowed isolating and identifying a series of positive and negative feedback cycles persisting on the long-term scale. The so called intrinsic instability drives the system away from an equilibrium state (e.g. channelization). However self-regulation (e.g. deposition and lowering of the slope) returns the system to quasi-equilibrium conditions [Hoyal and Sheets 2009]. Examples of such self-regulation cycles are the bar cycle, avulsion cycle and the delta cycle. Cyclic bar behaviour was also described for ebb-tidal deltas at Ameland inlet [De Swart and Zimmerman et al. 2009; Ehlers 1988 in Dissanayake et al. 2008]. The bar cycle described by Hoyal and

Sheets [2009] involves a transition from inertial to gravitational flow and deposition at a channel mouth. On river deltas, avulsion cycles are integrated bar cycles that are promoted by morphodynamic backwater effects that can propagate upstream over surprisingly long distances [Hoyal and Sheets 2009]. The long-term behaviour of a delta cycle is governed by upstream controlled avulsion and abandonment of large regions of the delta. Relating this to tidal inlet systems, delta cycles would be the result of changes in the basin channel network. It indicates that ebb-tidal deltas and tidal basin configuration are directly linked on the longer term.

Van der Vegt [2006] describes that the ebb-tidal delta most importantly originates from stirring of sediment by waves and tides and the transport by the residual currents. While Hoyal and Sheets [2009] experimental setup made it possible for the delta to prograde free and radially into "deep water". Also ebb channels are deep compared to river channels that lay relatively high due to extensive sediment deposition. Such differences between tidal experiments and river experiment should be taken in mind when comparing experimental results. The present experiment considers delta growth and therein analogy is expected with the experimental deltas of Hoyal and Sheets [2009] and Van Dijk [2009]. Most importantly, non-cohesive deltas experienced a smoother coastline as a result of the diffuse effect of faster channel migration. Hoyal and Sheets [2009] showed that at low Froude number, more realistic channel and shoreline patterns were created which enabled strong channelization (small channel width, slow channel migration, low-wetted area). The key to increased complexity in fluvial systems is enhanced cohesion [Hoyal and Sheets 2009]. Enhanced cohesion was achieved through the addition of an artificial polymer.

2.5 Scaling / Correlation of hydraulic variables

Whether, and to what extent the present results can be translated to reality it is of interest to analyze the dimensions, flow characteristics and sediment mobility of the experimental scale model and compare it to natural systems. First the principle of upscaling is given followed by suggestions on relaxing scale rules and what sediment to use. Methods of scaling from literature are outlined to allow comparison of results to previous experimental work and comparison to nature. The scaling methods are theory of wave motions and hydraulic similarity.

2.5.1 Relaxing scale rules and sediment mixture

The main reason for the lack of laboratory experiments is the difficulty in analyzing to what extent the present results can be transferred to reality. This subject is referred to as up scaling of laboratory results to real situations. Usually the flow depths in experiments are shallow while the mobility of the sediment must be similar to real situations. This would imply the use of very fine sediment. But such sediment is cohesive which hinders the experiments because it increases the critical threshold for erosion while shear stresses are generally low in experiments. Deficits in experiments are the occurrence of low sediment mobility, ebb-dominance, hydraulic smooth boundaries reflected in unrealistic deep scour holes and a static equilibrium because of shear stresses below motion [Kleinhans et al. 2010].

Traditionally, rivers were downscaled to the laboratory through similarity of the non-dimensional Froude number, Shields number and Reynolds number.

$$Fr = u / (gh)^{0.5} \qquad\qquad (2.6)$$
$$\theta = \tau_b / ((\rho_s - \rho_w) g d_{50}) \qquad\qquad (2.7)$$
$$Re = (\rho_w h u) / \mu \qquad\qquad (2.8)$$

Where u = depth-averaged flow velocity (m/s), h = water depth (m), g = gravitational acceleration (m/s^2), θ = Shields parameter (-), τ_b = bed shear stress (N/m^2) equation 2.1, ρ_s = sediment density (kg/m3), ρ_w = water density (kg/m3), d_{50} = median sediment size and μ = dynamic viscosity (kg/m/s). In order to have similar sediment mobility in a scale model as in reality the Reynolds (*Re*) and Froude (*Fr*) numbers should be equal in prototype and scale model [Van Dijk, 2009]. The Reynolds number

contains water depth (h) while the Froude number contains the root of water depth (√h). It is impossible to fulfil both conditions and obtain the same velocity scale [Kleinhans et al. 2010]. So the scale rules should be more relaxed in experiments. For the Froude condition it is more important that the flow remains subcritical and is near uniform [Kleinhans et al. 2010].

Smooth conditions causes ripples or scour holes to form which do not scale with water depth and thereby create unrealistic morphology in experiments. For instance, the experiments on the evolution of tidal channel networks by Stefanon et al. [2009] show unrealistic deep scour holes and unrealistic large ripples at the inlet. Kleinhans et al. [2010] recommend the use of a sediment mixture with a coarse tail to avoid smooth conditions. The large particles cause turbulence whereby fine sediment is suspended from the bed. To avoid flush-embedding it is important that the sediment mixture does not have a separate mode. Armoring tendencies increase if the mixture is more bimodal rather than unimodal. So the mixture should be unimodal. Then, usually median grain size (d50) is used to scale hydraulic resistance. Use is made of the Particle Reynolds Re* (-) number, given by

$$Re^* = \rho_w \, u^* \, D \, / \, \mu \qquad\qquad\qquad (2.9)$$

with u* is the shear velocity (m/s) and D (m) the particle size that is relevant for the roughness. The particle Reynolds number must be larger than the transition from hydraulic smooth to rough (Re* > 11.63). Usually median grain size d_{50} is used but it can be argued that the 90th percentile grain size d_{90} is more representative of near-bed roughness because the coarse grains add turbulence to the flow. Experiments by Kleinhans et al. [2010] showed that even when Re* for d_{50} of their sediment mixture was far below the transition to hydraulic rough conditions, neither ripples nor scour holes were observed. It suggests that Re* can be calculated using d_{90}.
For mobile bed experiments, the mobility of sediment must be similar. Usually flow depths are small in small-scale experiments so very fine sediment should be used. But silt and clay becomes cohesive which can inhibit channel migration and bar migration. Therefore one has to use coarser sediment that is less mobile. The decrease in mobility is mostly solved with a higher bed slope. It is then easier to transport the relatively coarse sediment in the down-slope direction (chapter 2.1.3). But transport of the coarse sediment in the up-slope (flood) direction is then inhibited. The models become purely ebb-dominated models. The novel method of tilting the experimental apparatus increases sediment mobility in the ebb- and flood phase. The bed surface slopes in downstream direction both during flood and ebb phase. Most importantly, transport in the flood-phase is facilitated.

Applying relaxed scale rules becomes problematic in cases of low flow depth such as on small-scale floodplains. The flow depth on the flood plains might become too low to achieve realistic floodplain formation. Herein hydraulic resistance is important which scales with flow depth divided by particle size. However, silt and clay become cohesive [Kleinhans et al. 2010] and flow might become laminar (smooth). Kleinhans et al. [2008] and Hoyal and Sheets [2009] suggest the use of silica flour or plastic grains. Such light-weight sediment has a low critical shear stress (equation 2.2) and is thus more easily entrained than sand. So silica flour or plastic grains scale much better with flow depth but are not as cohesive as clay. When fine sediment is deposited adjacent to channels it can control bank strength. Bank strength promotes morphological evolution of channel networks [Hoyal and Sheets 2009]. Channel width and depth are determined by the balance between floodplain formation and bank erosion. Without cohesion, banks erode until a braided threshold channel has developed. In order to secure meandering, bars should not erode too fast so that erosion is focused at a specific bank location for long enough time. The width-depth ratio is a parameter often used to determine bar pattern and therefore channel pattern. Kleinhans et al. [2010] selected wide unimodal sediment with about 20% of silica flour from testing and scaling conditions. With this mixture and low-density vegetation the formation of meandering channels was achieved in a flume. Without the silica flour, a moderately braided river was formed. Hoyal and Sheets [2009] state the key to achieving strong self-channelization is the addition of a cohesive product, namely a polymer. The polymer enhances the substrate strength and thereby increases the

critical erosion stress. For small-scale experiment the rate of cohesion onset can account for increased rates of morphodynamic evolution. In real deltas these cohesive effects are accounted for by vegetation [Hoyal and Sheets 2009].

It is concluded that the composition of a sediment mixture is essential when relaxing scale rules. Besides the availability of fine sediment that scales with flow depth on the flood planes, a coarse sediment tail is important to avoid smooth conditions in a laboratory scale model. Low sediment mobility can be overcome with the use of light-weight sediment. Sediment cohesion determines strength of banks, spatial variation in roughness and as such bar dynamics and channel pattern which is essential to simulate morphodynamics [Kleinhans et al. 2010].

2.5.2 Theory of tidal wave motions

Reynolds assimilates the theory of tidal wave motions to scale flow characteristics and dimensions. He scales the velocity, tidal wave height, tidal period and horizontal scale of his experimental set-up to Mersey estuary in the United Kingdom. The subsequent example is based on the proper experimental set-up (e) and two prototype natural systems (p), hereinafter, identified with the suffix e and p. The theory of wave motions according to Reynolds [1887-1891] first describes that the scale of velocities (u_e/u_p) varies as the square roots of the scales of wave heights ($\sqrt{h_e}/\sqrt{h_p}$) [Reynolds 1887-1891]. For the prototype Beaufort Inlet with a velocity approximation of 0.8 m/s (figure 2.20) and an experimental velocity in the range of 0.15 m/s, it gives a ratio of 1/5 in table 2.2. The corresponding experimental wave height is 4 cm provided that the tidal wave height at Beaufort inlet is 1 m (rule A). The flow in the experimental apparatus is generated by tilting in comparison to a wave signal. Therefore the model wave height might need further analyses.

Secondly, the ratios of the periods would be as the ratio of the horizontal scales divided by the ratios of the velocities [Reynolds 1887-1891]. To meet the rule (B) for a certain prototype system, the horizontal scale and tidal period of the experiment need to be tuned accordingly. Hence, consider a semi-diurnal tide (T_p = 44.700 s) as the tidal period and an experimental period of 30 seconds. It gives a ratio of 44.700 / 30 = 1.500 (-) which agrees with the horizontal scale of 2.0 / 16.000 m divided by the ratio of velocity of 0.15 / 0.8 m/s. Reynolds [1887-1891] assimilates that the ratio 1/1500 provides a time factor (1500) that directly translates experimental time to real time. Reynolds method shows that the smaller the horizontal scale of the experiment, the smaller the experimental tidal period needs to be. The prototype system demands an experimental period in the range of 15 to 55 seconds. This is based on the physical feasibility of the experimental apparatus (maximum horizontal scale of about 3.5 m and minimum period of 15 s). Then, the experimental horizontal scales would be in the range of 1.0 to 3.7 m.

Figure 2.20 Microtidal Beaufort Inlat at east coast of United States. The centre of the inlet is at 34.7°N, 76.6°W. Yellow lines are approximately 16 kilometres in length, which is defined to be the horizontal

scale. The maximum tidal current is 1 m/s and the tidal wave height is approximately 1 m. The tidal period is a semi-diurnal tide. The spatial extent of the ebb-tidal delta is several kilometres [van der Vegt, 2006].

Table 2.2 theory of wave motions

		experiment	prototype	ratio	Description	Reynolds	Inter relation
Tidal velocity	m/s	0.15	0.8	1/5	rule A	33	A B
tidal wave height	m	0.04	1				
square root wave height	$m^{1/2}$	0.200	1	1/5	rule A	33	A
tidal period	s	30	44700	1/1490	rule B		C
horizontal scale	m	2	16000	1/8000			B
ratio of horizontal scale / ratio of velocity		(-)		1/1500	rule B	950	C
period of the model	s	29.8			rule C	42	

Remark: Green values are based on prototype systems, yellow values are tuned accordingly. The yellow values embody achievable properties of the experimental apparatus.

In short, the theory of wave motion implies that when the velocity and wave height conditions agree (rule A), the tidal period and horizontal scale to velocity scale ratio of experiment and prototype should more or less agree (rule C). To accomplish the latter, one has to adjust the experimental tidal period or the horizontal scale of the experiment and/or prototype. It follows that by applying the theory of wave motions, one knows to what horizontal scale prototype system the experiment should be compared, or vice versa (arising from rule B).

2.5.3 Hydraulic similarity

In order to ensure a complete hydrodynamic similarity relevant parameters must attain the same values in the experiment and the prototype [Stefanon et al. 2009]. The question arises what parameters are relevant, and whether at all it is possible that they agree one to one. In section 2.5.1 it was argued that it is impossible to fulfil equality in the Froude and Reynolds conditions and obtain the same velocity scale [Kleinhans et al. 2008]. So the scale rules should be more relaxed in experiments. Nevertheless, one wants to compare the experimental results to prototype systems so scaling rules should be applied.

In experiments flow velocity and flow depth are usually smaller than in nature. A simple way to compare the flow velocities and water depth is to convert the values to a non-dimensional scale. Then it allows direct comparison. In order to make a parameter non-dimensional one can either divide the parameter by a characteristic value or by a selection of other parameters. Typical examples of the latter are the Froude number and the Shields number (equation 2.6 and equation 2.7). Another formulation that results in a non-dimensional comparison factor is given by:

$$\frac{U_e * T_e}{L_{experiment}} = \frac{U_p * T_p}{L_{prototype}} \qquad (2.10)$$

wherein U is maximum velocity (m/s), T is tidal period (s) and L is length scale of tidal intrusion (m). Consider typical values for these parameters found for Ameland Inlet in the Dutch Wadden Sea and Beaufort Inlet at USA Atlantic Coast (table 2.3). The solution of the right-hand side of the equation is about 2 for both prototype systems.

Table 2.3

	velocity	tidal period	length	solution
	m/s	s	m	(-)
Ameland Inlet	1	44700	25000	1.8
Beaufort Inlet	0.8	44700	16000	2.2

Experimental velocities are in the range 0.05 - 0.15 m/s and experimental tidal period in the range 40 - 80 seconds. Solving the equation for experimental conditions and solution 2 gives that corresponding experimental length scales are 1 to 6 meter in table 2.4. The experimental apparatus allows a maximum length scale of 3.7 m. Experimental velocities of 0.15 m/s would thus be too high. It is concluded that dominant velocities near the inlet of 0.05 – 0.10 m/s and tidal periods of 40- 80 seconds scale with Ameland Inlet and Beaufort Inlet.

Table 2.4

velocity	tidal period	length	solution
m/s	s	m	(-)
0.05	40	1	2.0
0.1	40	2	2.0
0.15	40	3	2.0
0.05	60	1.5	2.0
0.1	60	3	2.0
0.15	60	4.5	2.0
0.05	80	2	2.0
0.1	80	4	2.0
0.15	80	6	2.0

For comparison of the parameters in the formulations of prototype and model Stefanon et al. [2009] define non-dimensional parameters. They define a characteristic planar length L*, an average flow depth of the tidal basin D* and a typical value of the depth-averaged flow speed U*. Then they calculate Froude number, relative importance of inertia and friction with respect to gravity and the normalized tidal amplitude. A complete hydrodynamic similarity is expected when the values are the same for the prototype and the experiment. A comparison factor can be defined by introducing the scale factor λ. The scale factors are given by

Planimetric reduction scale $\qquad \lambda_L = L^*_e / L^*_p \qquad$ (2.11)

Vertical reduction scale $\qquad \lambda_D = D^*_e / D^*_p \qquad$ (2.12)

Distortion rate $\qquad \lambda_D / \lambda_L \qquad$ (2.13a)

One of the purposes of the distortion rate λ_D / λ_L is to convert width to depth ratios by:

$$\beta_p = \beta_e \, \lambda_D / \lambda_L \qquad (2.13b)$$

Stefanon et al. [2009] found that for higher tidal amplitudes the distortion rate increases. When a complete hydraulic similarity is satisfied, the planimetric and vertical reduction scales relate to scale ratio of velocity r_u, scale ratio of time r_t, scale ratio of sediment r_{ds} and scale ratio of flow conductance r_c by:

$$r_u = \lambda_D^{1/2} = \lambda_L / r_t \qquad (2.14a \text{ and } 2.14b)$$

$$r_c = \sqrt{(\lambda_L / \lambda_D)} = r_u r_{ds} \qquad (2.14c \text{ and } 2.14d).$$

Flow conductance is a measure of the ease of the flow to transport the sediment. The Shields diagram (figure 2.4) shows that it is easier to mobilize a small sediment particle than a larger one. Although the effect of cohesion of very fine sediment shows an exception on this rule. Also, the higher the flow velocity, the easier to it is to transport the sediment. To implement the hydrodynamic scale ratios one needs to define the values of the non-dimensionalized parameters.

Unfortunately there is no consensus in defining the parameters between the different experimental researches. The bed friction is usually a very important parameter when determining flow and sediment transport. But bed friction changes when the sediment bed changes and when the flow changes. Also there is no consensus yet in what formulation best describes average bed friction. Stefanon et al. [2009] embody that the so called roughness condition is usually not fulfilled because of too large roughness characterizing the model. Experimental channels are shallow and narrow so the bottom and channel walls exert relatively high friction.

2.6   *Thesis outline*

This thesis will first describe the experimental method and experimental conditions. The next chapter four defines the experimental parameters. Chapter five is the result section and covers a description of the evolution, equilibrium state, morphology, effect of sea level rise and experimental conditions. Where after in chapter six, the discussion section, scale rules are applied and discussed. Also experiments are compared to reality, models and other experimental and a selection of results is translated to the physical system. Chapter 7 gives conclusion of this thesis. The appendix is a separate document.

Chapter 3: Method

The main objective of this research is to create a tidal inlet system in dynamic equilibrium state in an experimental scale model. This chapter describes the experimental apparatus that was used for this purpose. Furthermore the settings of the different experiments are described. Last data collection and processing is explained for.

3.1   Experimental design

The experiments were carried out on a small indoor apparatus, depicted in figure 3.1 and figure 3.2. The tide was generated by vertically tilting the set-up, instead of pumping water in and out (figure 3.3). For simplicity, the experimental apparatus will be referred to as "tilting basin". The tilting basin is a plastic tub of 3.8 meter in length, 1.2m wide and 0.25m deep. The tub was placed on a metal frame, designed and assembled by Chris Roosendaal of Utrecht University. Its legs are in contact with the floor at the middle and at one end of the tub. There a mechanical jack was attached that tilts the basin by vertical movement of its leg. The pivot point was in the middle, over the horizontal width. Suitable software for the mechanical jack was developed by ing. Henk Markies of Utrecht University. The software allowed setting the amplitude of the tilting from the horizontal level, the tilting speed and a delay at high and low water. The delay allowed the tidal flow to come to rest before the tide turns. To prevent the loss of water by evaporation an overflow pipe was installed at the end of the sea basin. The overflow drained water to a minimum water level while water was continuously pumped into the sea basin. The excess of water was drained into a storage tank. Thus a minimum water level was guaranteed. The height of the overflow pipe could easily be shoved up or down to manage the water level in the sea basin. The pump discharge could be modified by means of a valve. Both the overflow height and pump discharge determine the water level in the tilting tub at a certain time step.
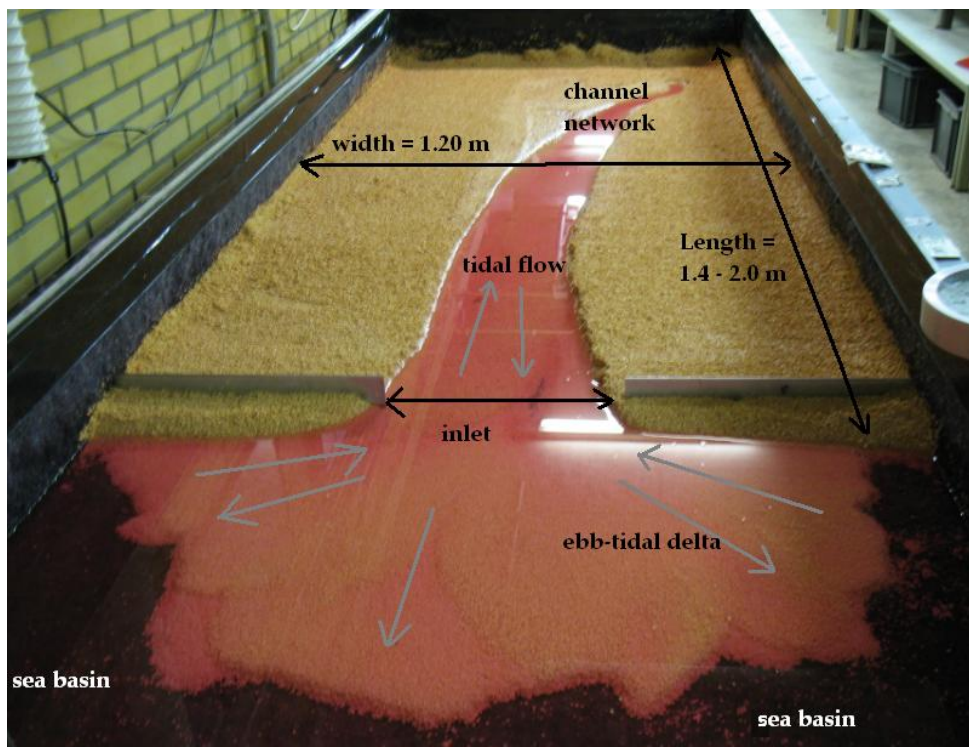
Figure 3.1 Terminology and dimensions of the tilting basin.

The experiments consisted of an artificial sediment basin directly connected to a shallow sea. The initial bottom topography was either flat horizontal or constantly upward in the landward direction. Henk Markies of Utrecht University constructed a tool to flatten the bottom at an adjustable sediment level. In general the sediment basin was 2.3 metres long, 1.2 m wide and 3 to 4.5 cm high. The sediment basin contained about 0.1 m^3 of sediment. The level of the sediment bed was usually higher than mean sea level. The sea was generally 1.5 meter long, 1.2 meter wide and 2 to 4 centimetres deep. It contained 35 to 70 litres (L) of water. The water level in the inlet at horizontal level (no tilt) represented mean sea level (MSL). The tilting of the basin generated a flow from a change in water surface gradients. At the narrow inlet the flow converged and at the same time the back-barrier flooded. The flooding of the back-barrier area and the retreatment of the water (figure 3.4) both induced a cycle of sediment erosion, sediment transport and deposition. The character of the flow during the two phases was different so residual sediment transport occurred. It resulted in a morphological evolution of the initial perturbation. The effect of experimental conditions amplitude of tilting, speed of tilting, inlet width, horizontal water level (MSL), sediment level, sediment slope and sediment type on evolution and morphology were investigated.

The spatial distribution of bed elevations and tidal water levels within the tilting basin were surveyed through two digital photo cameras. The photo cameras were suspended to permanent spots at the ceiling. The photo release was in phase with the mechanical jack and connected to computer software (Photoboot and PSRemote). The software allowed selecting four moments within the tidal cycle at which photos were taken. The moments were low water, MSL during flood flow, high water and MSL during ebb flow, depicted in figure 3.4. To cut back on data storage a certain number of tidal periods was skipped. The apparatus also consisted of a stereo system for rapid automated DEM production. The DEM-scan measured the sediment level over a plot of approximately 70 x 50 cm. The software VX Studio resulted a 3-dimensional image of the morphology from the scan. The appendix section provides the Matlab scripts that were run in order to generate the figures presented in this thesis. The appendix section also provides experimental recommendations. Improvements create more opportunities to display the morphology and its evolution and allows better quantification.

Figure 3.2 Photo of the tilting basin in the laboratory at the basement of the Zonneveldvleugel at Utrecht University. The arrows represent the vertical movement of both ends with the pivot point over the short axis in the middle.
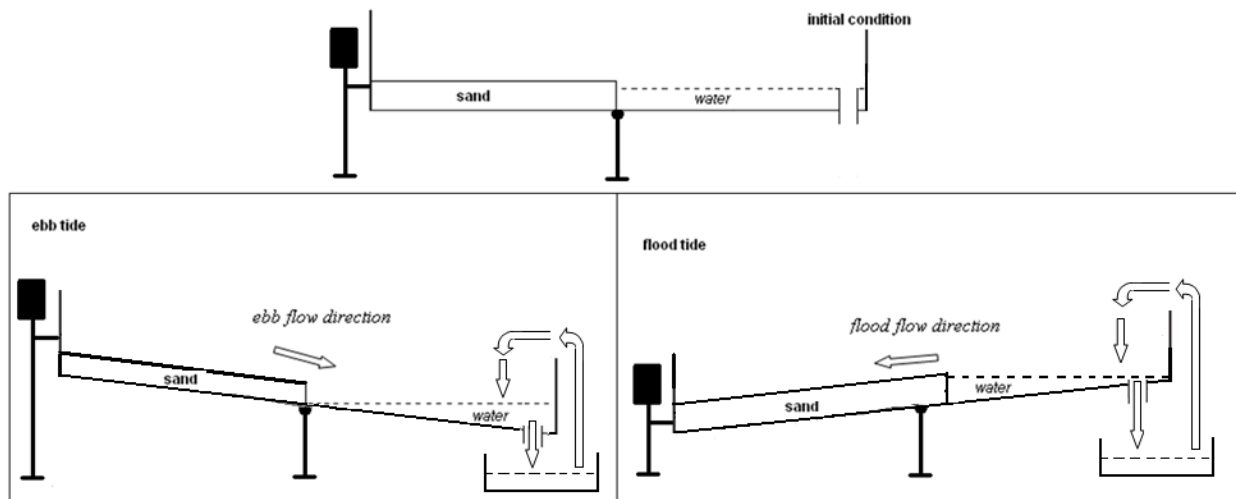
Figure 3.3 Schematic cross-sectional view of the tilting basin with a representation of the effect of tilting on the water flow. Water is continuously pumped around to avoid loss of water through evaporation.
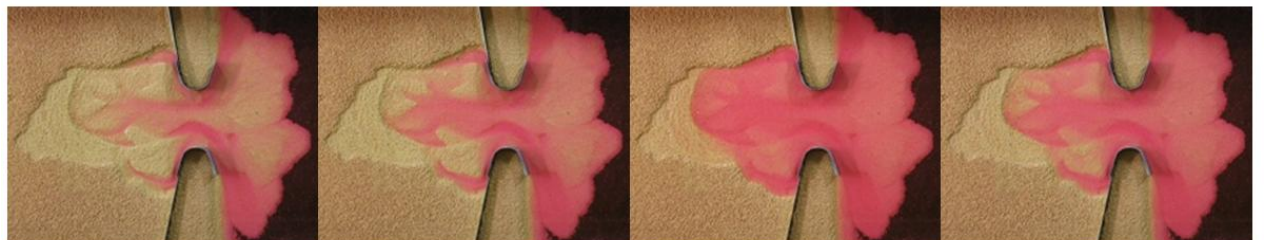
Figure 3.4 The software allows selecting four moments within the tidal cycle at which photos are taken. The moments are low tide, MSL during flood flow, high tide, MSL during ebb flow. The photo series show the flooding and draining of the back-barrier over a tidal cycle.

3.2   Experimental conditions

A total of 35 experiments were performed for this research. Fourteen experiments were performed in a smaller experimental apparatus. The smaller apparatus was 1.5 by 1.5 meter and tilted over the diagonal. A description of the experimental apparatus and a summary of the preparatory experiments (experiment 1 to 9) can be found in the appendix. Twenty experiments were performed in a larger experimental apparatus of 3.5 by 1.2 meter, the tilting basin. The experiments may be classified into three categories (table 3.1). It was either an experiment in the small apparatus or in the tilting basin. The sediment used was poorly sorted sand or light-weight plastic grains. To initiate the development of a tidal inlet system from the sediment platform the existence of a perturbation in the coastline was required. The initial configuration is a start perturbation (tidal inlet) or a long initial channel (estuary) which is visualized in figure 3.5. The idea originates from the initial topography of an estuary in numerical modelling studies which is usually a long rectangular channel of fixed or sloping depth [Dissanyake et al. 2008a and Geleynse et al. 2011]. The experiment numbers are listed accordingly in table 2.1. Freshwater was used. Temperature effects were not investigated.

Table 3.1 Experiments grouped according to the apparatus, sediment and initial configuration.

Experiment number	Apparatus	Sediment	Initial configuration
1 - 15	small (1.2 x 1.2)	poorly sorted sand	start perturbation
15 - 17	tilting tub (3.5 x 1.2)	poorly sorted sand	start perturbation
18 and 19	tilting tub (3.5 x 1.2)	poorly sorted sand	long channel (estuarium)
20 and 21	tilting tub (3.5 x 1.2)	poorly sorted sand	start perturbation
23 – 29	tilting tub (3.5 x 1.2)	light-weight polymers	start perturbation
30 – 36	tilting tub (3.5 x 1.2)	light-weight polymers	long channel (estuarium)

The light-weight plastic grains were cohesionless grains provided by Utrecht University. The grains were 1.0 mm to 3.0 mm in size with a median size of 2.1 mm (figure 3.6). The grains were light-weighted, reflected in their density of 1042 kg/m^3. The porosity was 0.31 (-). The method of determination was such that it is likely that the density may slightly be underestimated and the porosity slightly overestimated. Because of their low weight the grains were easily entrained and transported despite of low flow depths. Therefore they better met scaling conditions than when using sand. The poorly sorted sand was also provided by Utrecht University and is commonly used in river research at Utrecht University. The sediment contained sand in the range of very fine sand to very coarse sand with a median grain size of 0.5 mm and a 90th percentile of 1.4 mm. The very find sand particles describe sediment transport, while the coarse grains add roughness to the flow. Rough flow is important to avoid unrealistic deep scour holes and ripples [Kleinhans et al. 2010]. The grain size of poorly sorted sand is given in figure 2.6. In order to achieve channel network development and sediment rearrangement cohesiveness can be added to the sediment by introducing silica flour or polymers. Appendix B describes the effect of addition of silica flour on the tidal system morphology. Addition of silica flour was tested in preparatory experiments (appendix). The addition of silica flour resulted in higher water content and did not necessarily favour channelization and morphological evolution as river research on the experimental scale by Hoyal and Sheets [2009] and Kleinhans et al. [2008].

Figure 3.5 Top-view of initial configuration 'small inception' and 'long initial channel' in the tilting tub. The terminology of fixed inlet width, back-barrier basin and sea basin are visualized.
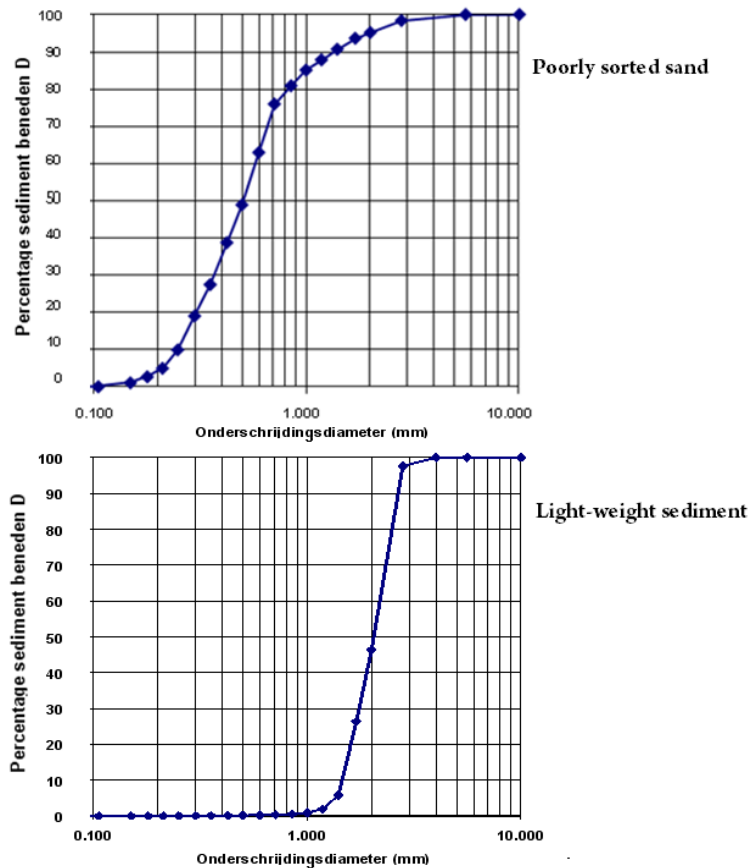
Figure 3.6 sediment distribution of poorly sorted sand and light-weight sediment.
poorly sorted sediment (2650 kg/m^3): d10 = 0.14 mm, d50= 0.5 mm and d90 = 1.4mm
light-weight polymer (1042 kg/m^3): d10 = 1.03 mm, d50 = 2.1 mm and d90 = 2.8 mm

Dependent variables in the experiments besides initial configuration and sediment type were amplitude of tilting from horizontal level, speed of tilting, initial bed level, mean sea level and inlet width. Inlet width was determined at the end of each experiment when equilibrium state was assumed. Initial bed level and mean sea level were measured in the inlet and represented the height with respect to the sea bottom. The effect of the variables on the morphology was interrelated. It means that a similar response on evolution occurred for a decrease of the relative sediment level to mean sea level and an increase in the amplitude of tilting. A sea level rise was simulated in experiment 29 by increasing the drainage level in the sea basin. As a result both the flood and ebb level increased. This is consistent with observations in nature where there exists a non-linear relation between tidal amplitude and water depth [van der Wegen et al. 2008]. The mean water level at the inlet increased from 2.8 cm to 3.6 cm in five steps. An increase of 0.8 cm signifies a rise of 29%. A single step describes more or less 6% of rise in water level. The sea level rise was tuned by visualization of the flooding area in the back-barrier. During evolution, a part of the back-barrier filled up with sediment reflected in channels that do not reach to the basin margin anymore. The sea level rise was such that the abandoned area in the back-barrier flooded but did not overspill.

Table 3.2 presents the experimental conditions of experiment 10 to 36. The colours represent the categories and typical settings.

Table 3.2 Overview of experimental settings of experiment 10 to 36. Poly is an abbreviation of polystyrene, the light-weight plastic grains. The sediment bed is sloping when the sediment level increases basin inward. In this way the upward sediment bed outweighs the effect of tilting such that the bed is plane at high tide. Colours are provided when the condition is one out of two options. The orange coloured numbers at inlet width represent an inlet of metal barriers. The ↑ sign means that the inlet was still prone to widening and thus in disequilibrium. The (~) sign at equilibrium state means that the system is neither static (because of bank migration) nor dynamic (in the sense of channel migration).

Nr.	Sedi-ment	Initial con-figuration	Ampli-tude of tilting	Speed of tilting	Delay	Tidal period	Total cycles	Back-barrier	Sand level	Equilibrium state	Inlet width
	type		mm	mm/min	s	s	nr		cm		cm
10	sand	tidal inlet	20	100	10	72	72	plane	2.9	static	10
10b	sand	tidal inlet	15	65	10	58	248	plane	2.8	static	13
11	sand	tidal inlet	20	50	10	96	81	plane	2.8	static	9
12	sand	tidal inlet	25	70	10	64	131	plane	3	static	13
13	sand	tidal inlet	35	90	10	108	78	plane	2.8	static	13
14	sand	tidal inlet	20	80	10	71	93	plane	2.8	static	13
15	sand	tidal inlet	15	45	15	88	102	plane	*4*	static	13
16	sand	tidal inlet	30	30	10	214	50	plane	4	static	19
17	sand	tidal inlet	30	30	10	213	44	plane	4	~	16
18	sand	estuary	15	50	10	166	152	plane	4	dynamic	14
19	sand	estuary	15	100	15	68	128	sloping	3	~	12
20	sand	tidal inlet	20	100	10	71	127	sloping	3	static	13.5
21	sand	tidal inlet	25	60	10	106	57	sloping	3	static	20
22	sand	tidal inlet	25	60	20	136.5	66	sloping	2	static	17
23	poly	tidal inlet	10	50	20	79	775	sloping	3	static	62
24	poly	tidal inlet	7	50	20	67	5158	sloping	3	~	49
25	poly	tidal inlet	7	50	20	67	6448	plane	3	dynamic	85
26	poly	tidal inlet	10	50	20	79	12030	plane	4.1	dynamic	25↑
28	poly	tidal inlet	10	50	20	79	6619	plane	4.1	dynamic	23
29	poly	tidal inlet	10	50	20	79	9857	plane	4.1	dynamic	23
30	poly	estuary	6	50	20	65	185	sloping	4.5	dynamic	23
31	poly	estuary	6	50	20	65	203	sloping	4.5	dynamic	23
32	poly	estuary	2 − 6	6-12	20	44 − 48	*3400*	sloping	4.5	dynamic	23
33	poly	estuary	3	30	20	60	1440	plane	4.1	static	23
34	poly	estuary	3 − 3.8	40	*25*	65 - 70	5926	plane	4.1	dynamic	35
36	poly	estuary	3.8	30	20	63	4114	plane	4.1	dynamic	44

3.3 Experimental measurements

This section describes experimental parameters, their definition and how they were collected from the data.

Sediment properties

The density, porosity and sediment distribution of light-weight plastic grains were determined according to the methods described for in the appendix. Sediment characteristics of poorly sorted sand were available at Utrecht University.

Tidal period

Experimental tidal period was the time needed for the experimental apparatus to succeed a tilt cycle of upward movement, delay, downward movement, delay. The experimental tidal period was a function of tilt amplitude, tilt speed and delay. The higher the tilt and delay, the longer the tidal period was. A higher tilt speed shortened the tidal period. Tidal period was determined with a timer.

Water depth

The water used in the experiments was coloured pink by a colour additive. The intensity of the colour was a measure for water depth, the deeper the more intense the colour in the green band of the red green blue colour band. The calculated water depth maps from images were most consistent for the images taken when the experimental apparatus was horizontal during ebb (MSL ebb). Figure 3.7 represents water depth calculated from the pink intensity of water in a stable channel on the ebb-tidal delta. The channel depth varied as a result of migration of the inlet channel(s). The signal consisted of many peaks and falls. From 122.5 hours to 124 hours the water depth gradually decreased apart from one data point at 123 hours. The value at this peak was about 0.2 cm higher than it would have been if the signal had followed the declining trend. Such small peaks of maximum 0.2 cm water depth were distinguished multiple times (red circles) during a gradually increasing, decreasing or stabilizing water depth. These small peaks might have been a result of experimental variability. But it is more likely that the small peaks described the inaccuracy of the depth scale since they deviate from the overall trend. So the inaccuracy of the depth scale was determined to be smaller than 0.2 cm which we consider to be a good estimate of water depth.
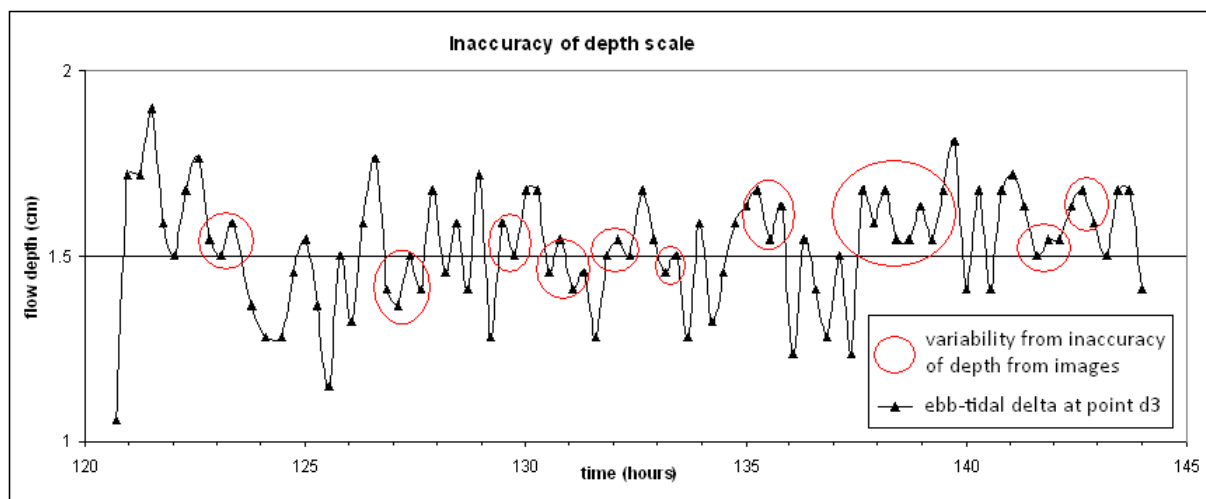

Figure 3.7 Variability in water depth in a channel on the ebb-tidal delta. Small peaks of maximum 0.2 cm water depth were distinguished multiple times (red circles) during a gradually increasing, decreasing or stabilizing water depth.

Width to depth ratio
The width to depth ratio of channels was calculated from depth maps. Cross-sections were drawn perpendicular to channel walls. The length of the cross-sections was measured and converted to the experimental width of the channel. The depth that was attributed to the cross-section was the depth that was most prevalent in the section indicated average depth.

Tidal wave height
Flow resulted from vertically tilting the set-up at the end of the experimental apparatus. So the flow did not result from a wave signal. The actual water level depended on the location, tilt amplitude and water level and was a function of time. The water level differences between low water and high water ranged from 0.1 to 1.0 cm for experimental settings suitable for experiment with light-weight plastic grains. In experiment 28 the maximum water level difference at the inlet was 0.5 cm. In the sea it was 0.2 cm and in the back-barrier it was more or less 0.8 cm. The water level difference at the inlet was investigated for different experimental settings. But the water level did not show a quantifiable signal despite different experimental settings. Defining an experimental tidal wave height was thus not straightforward. A suggestion to define experimental tidal wave height is to use maximum water level difference in the middle of the back-barrier and multiply it by a certain factor to meet scaling conditions.

Horizontal scale
The experimental horizontal scale was determined by connecting the outer corners of the morphology, similar to figure 2.20. The length of the two lines were determined and averaged over both to obtain a length (m) referred to as the horizontal scale.

Typical flow velocity
Experimental flow velocity in poorly sorted sand experiment was done through tracing colour additive over a given distance. Determination of experimental flow velocity in experiments with light-weight plastic grains was based on the transport of a single grain. A sediment grain was visible throughout the tidal cycle. A taper and a stopwatch allowed calculating the average speed of the grain. The speed of the grain is not necessarily the flow velocity because transport is delayed by interaction with other grains and the sediment bed. So determination of experimental flow velocity from grain transport resulted in an underestimation. Since the density of the light-weight sediment is only slightly smaller (1042 kg/m^3) than water (998 kg/m3) it was adopted that the underestimation of average flow velocity by 'particle tracing' is small for light-weight sediment and that the method serves its purpose.

Simple formulation to calculate experimental flow velocity from experimental settings
The most important variables that determined the flow velocity in the model were water depth, tilt and tilt speed. To approach experimental flow velocity the relative importance of the variables might be implemented with:

MSL at inlet (m) * tilt from MSL (m) * tilt speed (mm/s) / 3 * 1.000.000 = estimate flow velocity (m/s)   (3.1)

The estimated flow velocity that results from typical experimental values and a constricted inlet width of 23 cm are given in table 3.3. A tilt amplitude of 1 cm and a speed of 50 mm/min results in a flow velocity estimate of 0.07 to 0.10 m/s depending on water depth. These values resemble measured experimental flow velocities. Experiments were performed with tilt 0.5 to 2 cm, tilt speed 5 to 100 mm/min and water level 2.0 to 3.5 cm. Table 3.3 provides that whatever combination of these ranges results in a flow velocity of 0.03 to 0.19 m/s. These were indeed typical values observed during experiments. The exceptional case with 4 cm tilt, maximum tilt speed and high water level

results in a flow velocity of 0.78 m/s according to the proposed formulation. A value of 0.78 is impossible. It is recommended to incorporate a friction effect when doing experiments with high settings. Yet, experience with the experimental apparatus suggests the formulation is a good first estimate. More experiments and an accurate method to determine flow velocity are needed in order to verify the formulation.

Table 3.3 Solving equation 3.1 for experimental conditions to obtain an estimate of flow velocity

mean water level	tilt from MSL	tilt speed	tilt speed	typical velocity estimate
cm	cm	mm/min	m/s	m/s
2.5	0.5	50	8.3E-04	0.03
3	0.5	50	8.3E-04	0.04
3.5	0.5	50	8.3E-04	0.05
2.5	1	50	8.3E-04	0.07
3	1	50	8.3E-04	0.08
3.5	1	50	8.3E-04	0.10
2.5	1.5	50	8.3E-04	0.10
3	1.5	50	8.3E-04	0.13
3.5	1.5	50	8.3E-04	0.15
2.5	2	50	8.3E-04	0.14
3	2	50	8.3E-04	0.17
3.5	2	50	8.3E-04	0.19
3	1	20	3.3E-04	0.03
3	1	40	6.7E-04	0.07
3	1	60	1.0E-03	0.10
3	1	80	1.3E-03	0.13
3	1	100	1.7E-03	0.17
3.5	*2*	*100*	*1.7E-03*	*0.39*
3.5	*4*	*100*	*1.7E-03*	*0.78*

Tidal prism / high water volume
The tidal prism results from subtracting low water volume from high water volume in the back-barrier. The water volumes were calculated from water depth maps of images at low water and at high water by summation of water depth at every pixels and multiplying by the area of a single pixel. But the images at high water and low water were taken while the experimental apparatus was at a different angle. As a result, illumination was different and low water volume was highly overestimated. There was no signal found that could substitute for the low water volume. In the thesis high water volume serves as an indication of tidal prism.

Cross-sectional channel area
Channel area was calculated from water depth maps at MSL ebb. A cross-section was drawn in the middle of the inlet (686 in figure 4.10). Water depth at every pixel was summed. The summation was multiplied by the length of a single pixel to obtain cross-sectional area.

Chapter 4: Results

The results chapter reports a selection of experiments that were performed. The objective of this research was to experimentally create a tidal inlet system from plane bed with typical morphology and investigate whether a dynamic 'equilibrium state' exists. We were the first ones to achieve so in our experiment number 28. This experiment shows the emergence of typical morphology that is in a dynamic state. Chapter 5.1 visualizes, describes and analyzes the evolution from plane bed to a dynamic equilibrium state in experiment 28. The next section, chapter 5.2 is on the dynamic behaviour of channels, bars and shoals at the 'equilibrium state' of experiment 28. The ebb-tidal delta, inlet and back-barrier area are considered separately. Third, chapter 5.3 describes the effect of a rise in sea level on typical morphology investigated in experiment 29. Thereafter chapter 5.4 considers the observed cyclic behaviour in switching of number of inlet channels. Last, chapter 5.5 describes the effect of the variables that were investigated in all other experiments (number 1-36).

4.1 Experiment 28: evolution of a dynamic tidal inlet system

The subsections of this section describe the emergence from plane bed to a dynamic tidal inlet system in different approaches. First the change in morphology from plane bed to an end state is considered. Then the expansion of the tidal area and ebb-tidal delta as a result of a growing tidal inlet system is described for. Thereafter the subject of equilibrium state is covered in chapter 5.1.2. Next it is shown how width- to depth ratios develop in the expanding system. Chapter 5.1 finishes with describing patterns of erosion and deposition of the expanding tidal inlet system of experiment 28.

4.1.1 Morphological evolution from plane bed to an end state

In experiment 10 - 27 variables were investigated aimed at finding the experimental conditions for the evolution of a dynamic tidal inlet system from plane bed. It was found that most importantly the use of light-weight grains, an initial perturbation, a tidal flat level (4.1 cm) considerably higher than MSL (2.8 cm) and a non-erodible barrier were necessary. Figure 4.1 presents the evolution of experiment 28 by twelve photo images in time taken at low water. The back-barrier basin is seen to the left and the ebb-tidal delta is seen to the right. In between the back-barrier and the ebb-tidal delta there was a constricted metal inlet of 23 cm width. A tidal period consisted of flooding and subsequent draining of the back-barrier by tilting the experimental apparatus and lasted 79 s. The total experiment time was 144 hours (6 days) and represented 6550 tidal cycles.

The initial perturbation was a channel after 20 tidal periods. The channel lengthened and at the same time a delta formed in the sea. The outflow over the ebb-tidal delta was radial. Then after 350 tidal periods the outflow occurred to the sides of the ebb-tidal delta. At the same time the inlet and back-barrier consisted of two channels. At 800 tidal cycles the inlet showed three channels of which one was separated by a wide bar. The ebb-tidal delta grew by expansion in lobes. At 1100 tidal periods the ebb-tidal delta had become more symmetrical. The back-barrier showed two small channels near the inlet and a main channel in the middle of the back-barrier extending furthest land inward. From 1400 to 4500 tidal periods the channels in the back-barrier showed multiple curves indicating meandering behaviour. The channel in the middle of the back-barrier shifted northward, southward and back. The small channels near the upper and lower inlet increased their curvature and length. Thereby the back-barrier width increased. The ebb-tidal delta continued to expand into the sea basin. The expansion occurred more or less radial. After 4500 tidal periods the ebb-tidal delta had reached its seaward length. Thereafter the ebb-tidal delta most importantly built up vertically and expanded its width slightly. The middle channel in the back-barrier continued to migrate. Also the tips of the lower and upper small channel aside the inlets changed their morphology. Most of the time the inlet existed of two channels but a switch to one main channel was observed occasionally. In short, the evolution from initial plane bed to 'equilibrium morphology' (will be discussed hereafter)

described about 6000 tidal cycles. It was accompanied by migration of channels in the back-barrier and inlet and switching of the numbers of channels.
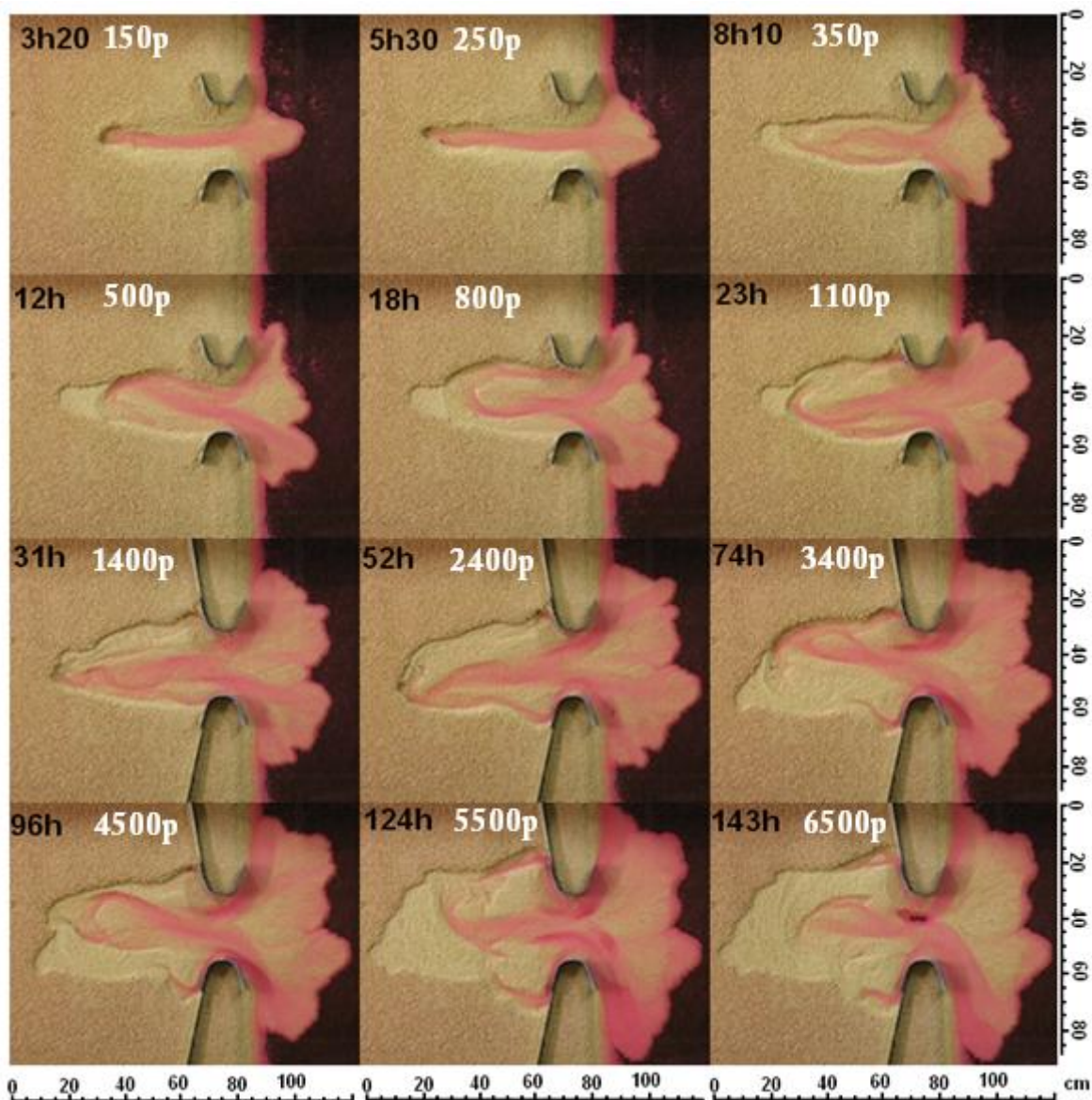
Figure 4.1 Photos of evolution of experiment 28 taken at low water. Time (black) and tidal period (white) were displayed in the figures. Initially, tidal flat bed was 4.1 cm high and MSL was 2.8 cm. The inlet was constricted and use was made of light-weight grains.

4.1.2 Tidal system area expansion

Figure 4.2 represents the contour of the area that contributed to sediment erosion or deposition at fifteen time steps of evolution. The contour areas were distracted from the images at high water. In the back-barrier and inlet the flooded area contributed to the area. While the ebb-tidal delta was displayed when sediment deposition had occurred on the sea bottom. The time steps are given in table 4.1 and numbered one to fifteen. Step one to five each described four hours of evolution, step five to ten each described eight hours, step ten to thirteen each covered twelve hours and the last two steps covered about twenty hours.

The initial configuration was a small perturbation of 10 cm width. After 50 tidal cycles the perturbation had become longer and a small circular ebb-tidal delta was deposited. During the first hours the channel lengthened more and the ebb-tidal delta grew circularly. The subsequent tidal

periods (time step 3) the channel in the back-barrier retreated slightly in contrast to former lengthening. The intertidal area widened and the ebb-tidal delta expanded to the sides, both north and south. The inlet widened considerably. During time step (4) and (5) an asymmetrical expansion occurred of the intertidal area in the north and of the ebb-tidal delta in the south. During the sixth time step the asymmetrical expansion reversed in position. The lateral expansion of the intertidal area was southward while the northern ebb-tidal delta expanded. At the same time the inlet widened extensively and adopted the entire constricted width of 23 cm. During the seventh time step the signal continued as during the sixth time step. But now the back-barrier lengthened again and also adopted intertidal area aside the northern inlet. At the same time the ebb-tidal delta attached to the northern barrier. Ebb-tidal delta expansion also occurred at three other locations. Next the main ebb-tidal delta expansion shifted to the south while the back-barrier lengthened slightly at its northern end. Also the back-barrier adopted the area near the southern inlet. The next time step (9) was one of little of expansion but the signal of the previous time step continued. Then time step (10) showed growth over the diagonal again. Time steps (11) to (13) showed expansion of the intertidal area at the northern end of the back-barrier. At the same time both northern and southern ebb-tidal delta lobes grew. Also more intertidal area aside the barriers was adopted. Time step (14) covered 1250 tidal periods. Both the back-barrier and the ebb-tidal delta expanded still. The expansion occurred over the width, both north and south. The last time step (15) did not show considerable expansion of the back-barrier and the ebb-tidal delta. Summarizing, the description of the evolution from initial plane bed to equilibrium state provided reoccurring signals and persisting signals. The most prominent observations were:

- Overshoot lengthening of the main-channel in the back-barrier area
- Lateral expansion in the back-barrier often coincided with expansion of the ebb-tidal delta over the diagonal (either north-south or south-north).
- The ebb-tidal delta grew by lobe expansion which resulted in a net circular outgrowth.
- The ebb-tidal delta distinguished a northern lobe and a southern lobe.
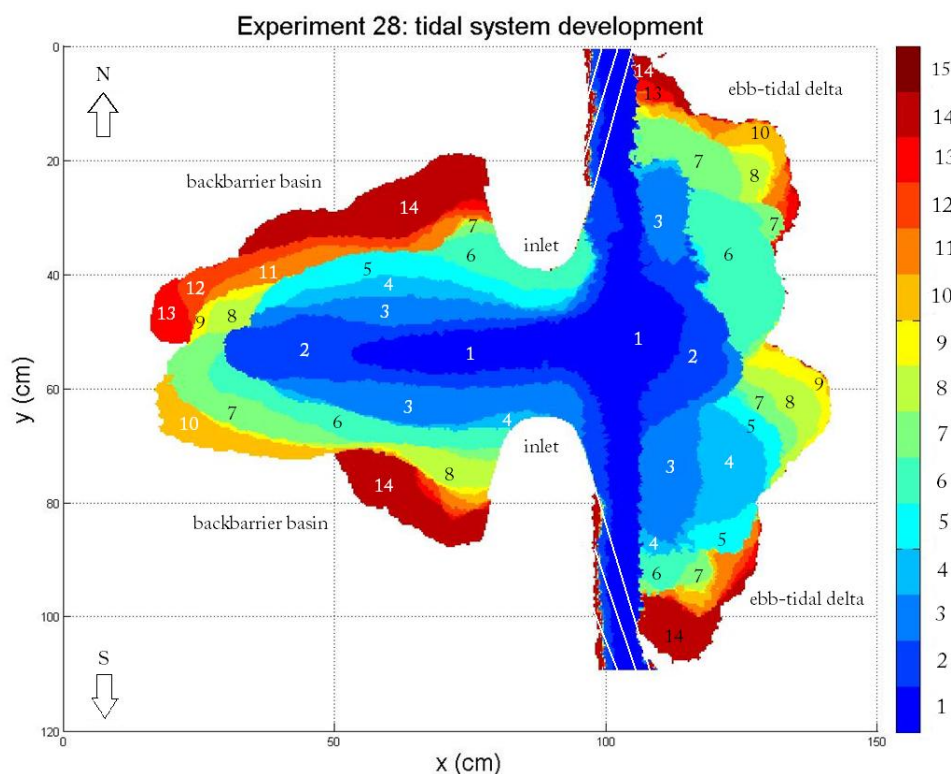- Net expansion of the ebb-tidal delta and intertidal area decreased in time

Figure 4.2 Contour of the area that contributed to sediment erosion or deposition from images at high water. Figure presents the contour of fifteen nonlinear time steps as in table 4.1. Area of white stripes should be neglected.

series number	elapsed time (hours)	elapsed tidal cycles
1	1	50
2	5	220
3	9	410
4	13	590
5	17	770
6	25	1140
7	33	1500
8	41	1860
9	49	2240
10	57	2600
11	69	3150
12	81	3700
13	93	4250
14	121	5500
15	144	6500

4.1.3 Equilibrium state

There was no expansion of the intertidal area and ebb-tidal delta observed over 1000 tidal periods during timestep (15) in figure 4.2. It was assumed that the experimental tidal inlet system had arrived at its equilibrium state since channel area, ebb-tidal delta and tidal prism were about constant. Since the inlet was constricted further expansion of the inlet and coinciding expansion of the intertidal area was impeded. Figure 4.3 shows that the flood volume in the back-barrier was about constant after 60 hours. Figure 4.4 shows that channel area was about constant after 70 hours. Assuming flood volume to closely resemble tidal prism, constant flood volume and channel area indicated that the inlet system was in the vicinity of equilibrium state. In figure 4.2 intertidal area and ebb-tidal delta still expanded after 60 hours. Figure 4.1 indicated that after 60-70 hours morphology still changed. Constant flood volume and channel area after 70 hours thus coincided with tidal system area expansion and morphological change. A temporal increase in flood volume in figure 4.3 around 125 hours coincided with the high tidal area expansion during timestep (14) in figure 4.2. Afterwards the flood volume recovered to the volume of before the temporal increase. Small temporal increase in flood volume, morphological change and tidal area expansion occurred simultaneously with flood volume and channel area being constant. It indicated that the subject of defining equilibrium state is not straightforward. However constant flood volume and channel area and ceasing of tidal system area expansion indicated the system being in the vicinity of equilibrium state.
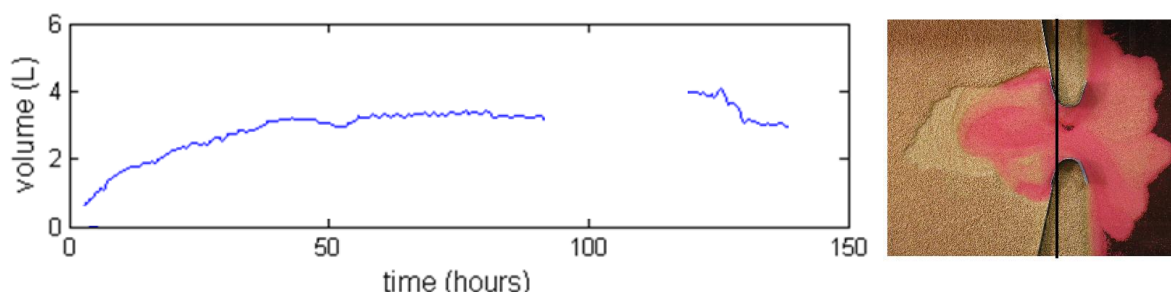

Figure 4.3 Volume of water in the back-barrier at high water during experiment 28. The volumes were calculated from water depth derived from colour intensity of water as in figure to the right. The back-barrier was defined left of the thick line. Moving average was taken over 15 points (15*12 = 180 tidal periods).
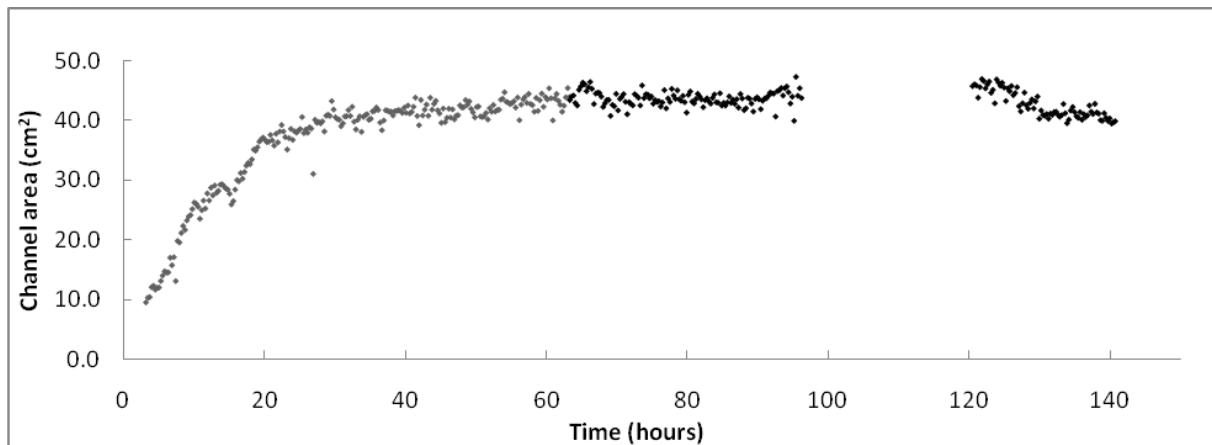
Figure 4.4 Inlet channel area during experiment 28. The areas were calculated from the water depth maps at MSL during ebb. Moving average was calculated over 15 points (15*12 = 180 tidal periods).

4.1.4 Width to depth ratio

Figure 4.5 is a flow depth map of the four stages represented by the middle row in figure 4.1. The flow depth was calculated from the photo taken at mean sea level during ebb. At this phase water depth was slightly lower than during high water and channels were clearly distinguished. The width to depth ratio is a much used non-dimensional parameter that describes channel geometry in rivers. The values were calculated for different cross-sections. The numbers and cross-sections were displayed in figure 4.5. The maximum flow depth was 2.8 cm at 124h at the location of a scour in the inlet. Width to depth ratios varied between 1.5 and 5.5 (-). In general the width to depth ratio was lowest in the back-barrier. The width to depth ratio in the main channel and the inlet both showed a trend during evolution. The width to depth ratio of the main channel in the back-barrier at 5h30 was 3 (-), it then increased from 3.5 to 4.5 to 5.5 (-) at 124h. The trend for the inlet channels is opposite. At 5h30 and 18h it was about 4 (-). It decreased to 3.5 at 52h to 2.5 (-) at 124h. The width to depth ratios of the small channels aside the barriers did not change considerably during evolution. The ratios were about 2 (-). In short, during evolution to equilibrium state the main channel in the back-barrier widened with respect to its depth while the inlet channels deepened with respect to their width. Channel ends in the back-barrier were relatively deep with respect to their width indicated by low width to depth ratios.
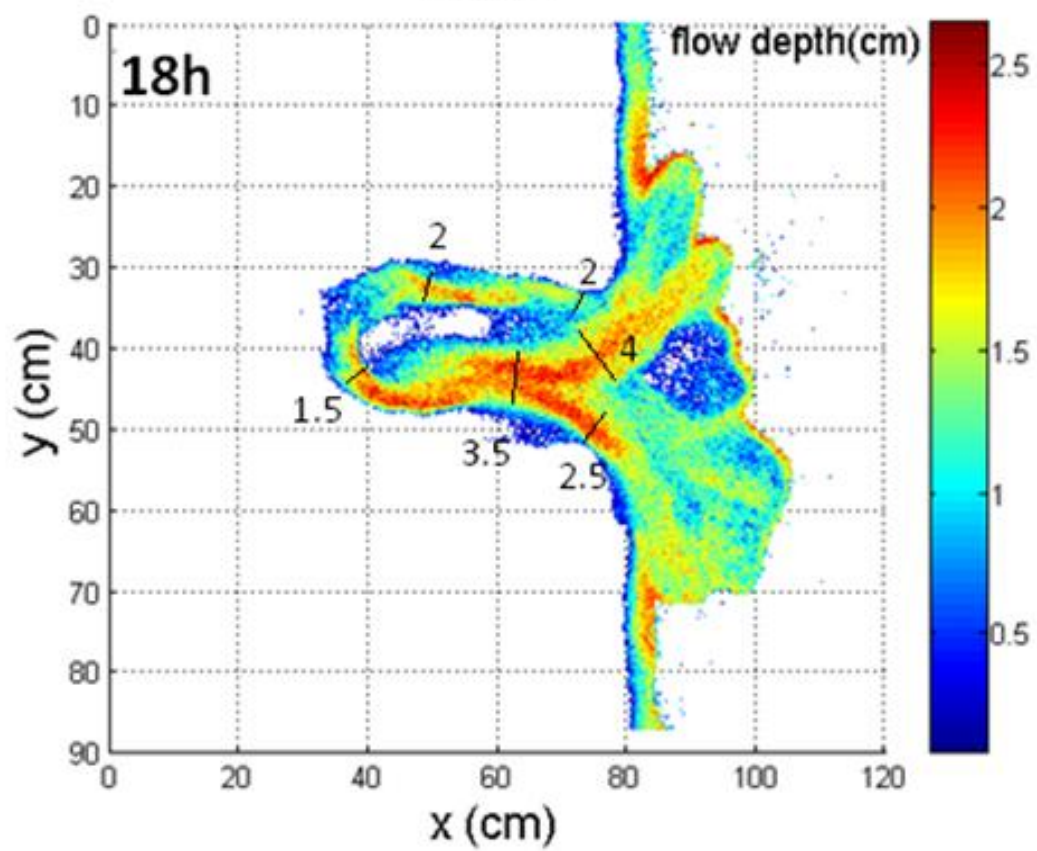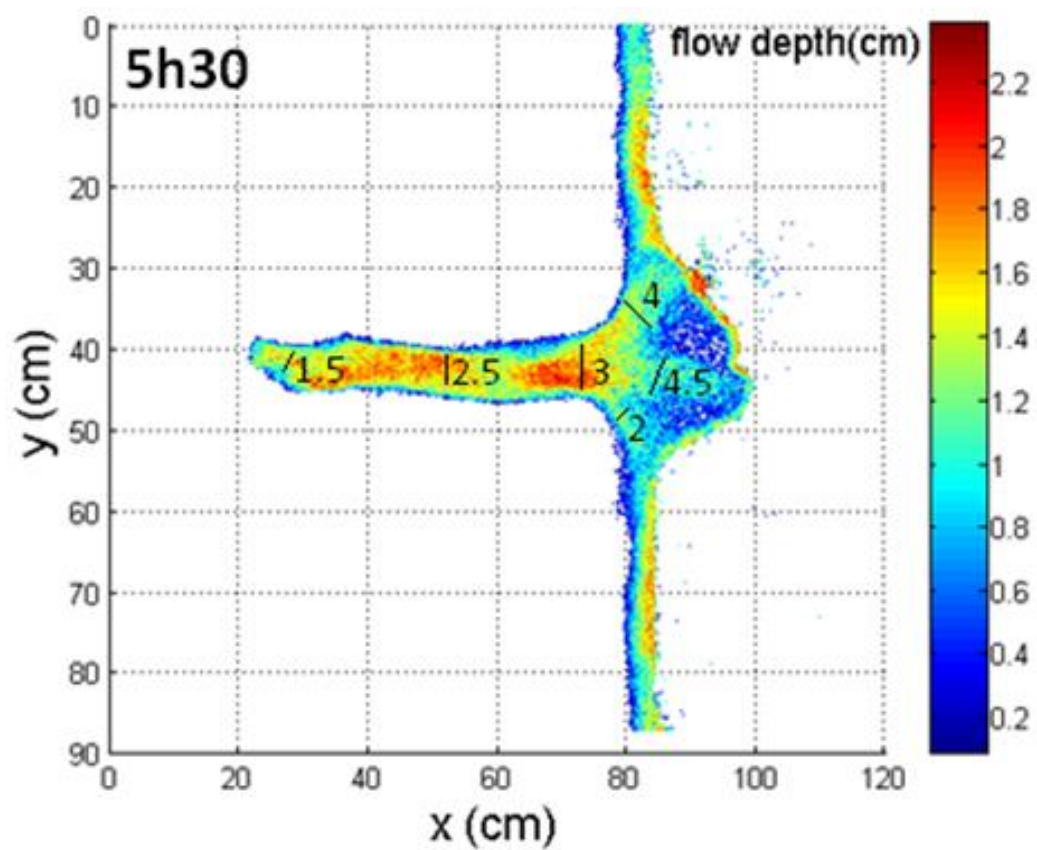
Figure 4.5 Flow depth maps were calculated from photos taken at MSL (mean sea level) from high water to low water. The numbers represent the width to depth ratios (-) at the cross-sections (rounded at 0.5).
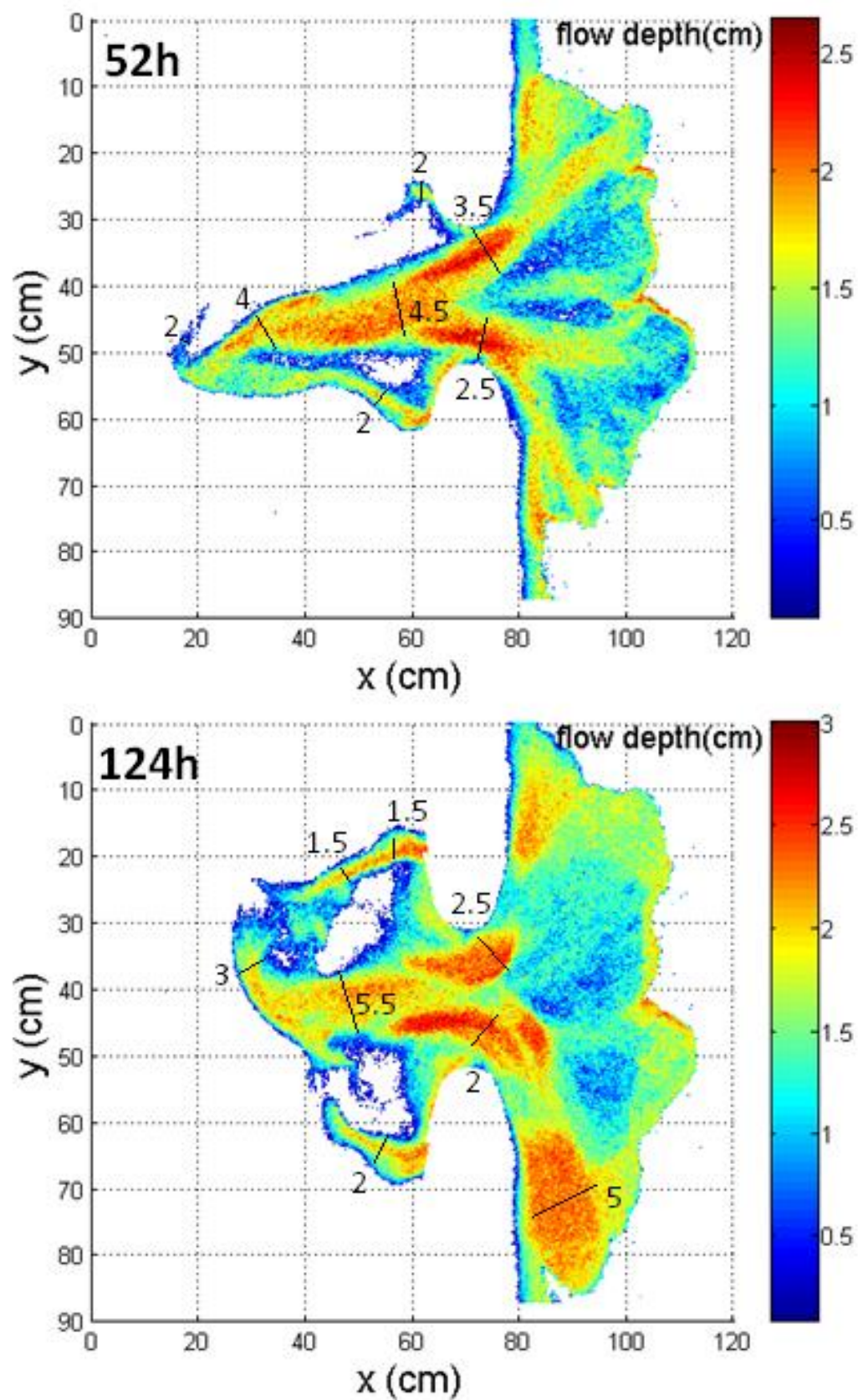
4.1.5 Net average erosion rate pattern in the inlet and back-barrier

This subchapter quantifies the erosion in the inlet and back-barrier from analyses of three-dimensional images (figure 4.8, evolution 1-7). Erosion rates over time were calculated from subtracting digital elevation models of two consecutive time steps and displayed in figure 4.6. The coverage of the stereo system for rapid automated DEM production was 70 x 50 cm which was insufficient to cover the entire active system. The focus was on the inlet and a part of the back-barrier.

Figure 4.6 shows two data signals. The diamonds represent net erosion rate (L/hour) over seven timesteps of the experiment (evolution 1-7). Triangles are the erosion rates averaged over eleven timesteps. Erosion rates were high in the beginning of the experiment and approached zero at the end of the experiment. The values of erosion rates deviated considerably between the two classes. It indicates that net erosion rate depended on the choice of time steps. This can imply that erosion occurs in peaks and falls. This statement is supported at 100 hours of elapsed time. Data points were dense there and the signal consisted of peaks and falls. Another possibility is that the deviation between the plots was a result of inaccuracy of the method. This is underlined by the coverage of the DEM image not covering the entire model. If the peaks and falls were a result of inaccuracy of the method, the erosion rate should better be represented with a trendline through the data points. The coefficients of determination (R^2) represent the percentage of varation that can be explaneed. The values 0.79 for seven data points and 0.46 for twelve data points indicate a certain relation between net erosion rate and elapsed time.
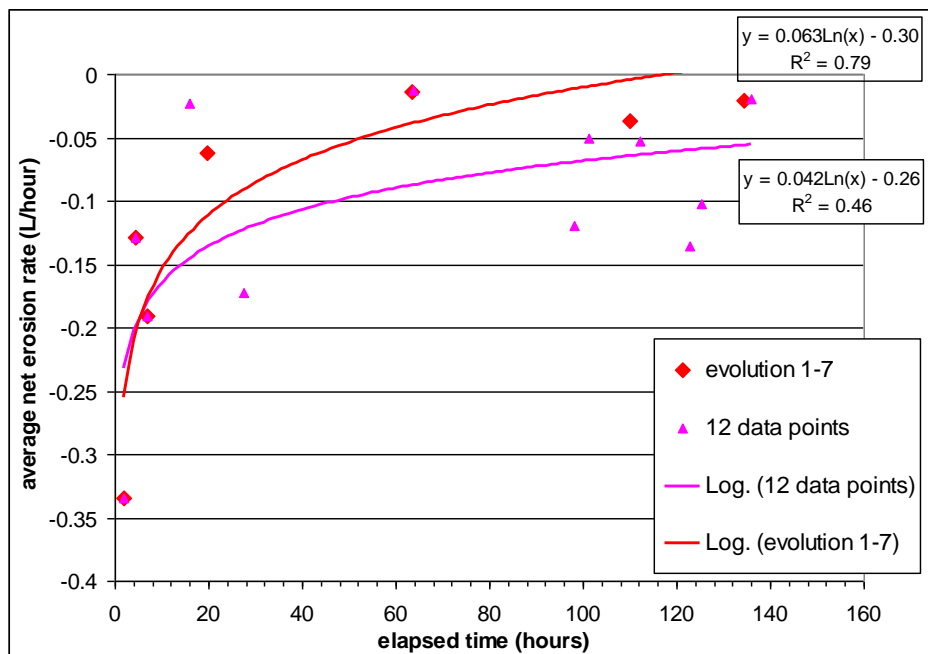
Figure 4.6 Net erosion rate from DEM images calculated over seven time steps (figure 4.7) and over twelve time steps. The time steps were chosen arbitrarily.

The DEM-images also allowed calculating net deposition rates in time. Most deposition occurred on the ebb-tidal delta. The ebb-tidal delta was only partly covered in the DEM-image so the deposition rate was highly underestimated. Interestingly, the average deposition and erosion rates did reflect an opposing signal in figure 4.7. When the erosion decreased, the deposition increased and vice versa. During this period of increased erosion and deposition the channel changed from being one long main channel to two shorter channels (evolution 3 in figure 4.8). Over time, the net average deposition rate showed a decreasing trend similar to the net average erosion rate.
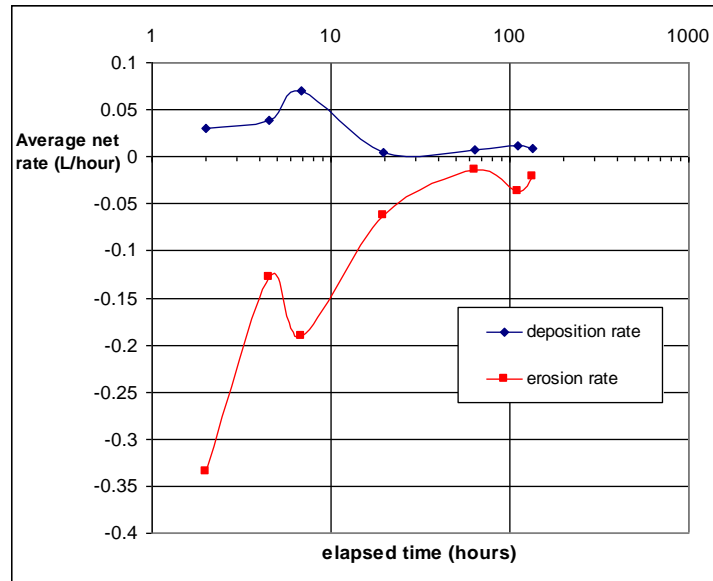
Figure 4.7 Average net deposition and erosion rate from the DEM images. The deposition rate was underestimated because the ebb-tidal delta was not within the coverage of the image. Nevertheless the peaks and falls coincided.

Total erosion and deposition were calculated in table in figure 4.8. Net erosion was 5.5 L for seven data points. Net deposition was 1.4 L. The difference between net erosion and deposition was 4L. Maximum flood volume was 4L in figure 4.3. The maximum flood volume would be slightly lower than total erosion since a part of the back-barrier was abondoned at that time. But the DEM-images neither covered that part of the back-barrier. So net sediment loss over coverage of the DEM-image was 4L which closely resembled maximum flood volume and validates the method.

	elapsed time (hours)	Erosion (dm^3)	Deposition, corrected (dm3)
Evolution 1	3.5	-1.00	0.09
Evolution 2	5.5	-0.26	0.08
Evolution 3	8.2	-0.51	0.19
Evolution 4	31	-1.43	0.11
Evolution 5	96	-0.87	0.45
Evolution 6	124	-1.04	0.33
Evolution 7	145	- 0.43	0.18

Figure 4.8 Three-dimensional images of net evolution over time in experiment 28. The time periods of evolution 1 to 7 are given in the table and resemble stages as in figure 4.1.

4.2 Dynamic behaviour of channels, bars and shoals at equilibrium state

Channel, bar and shoal migration are typical for tidal inlet systems so quantification of experimental dynamic behaviour at equilibrium state is relevant for comparison. This section visualizes and describes the dynamic behaviour of the ebb-tidal delta (5.2.1), the inlet (5.2.2) and the back-barrier area (5.2.3).

Data points were selected in the back-barrier (b), in the inlet (i) and on the ebb-tidal delta (d) and numbered according to figure 4.9. Cross-sections were drawn according to figure 4.10. Deepest were the channels. Channels in the back-barrier and ebb-tida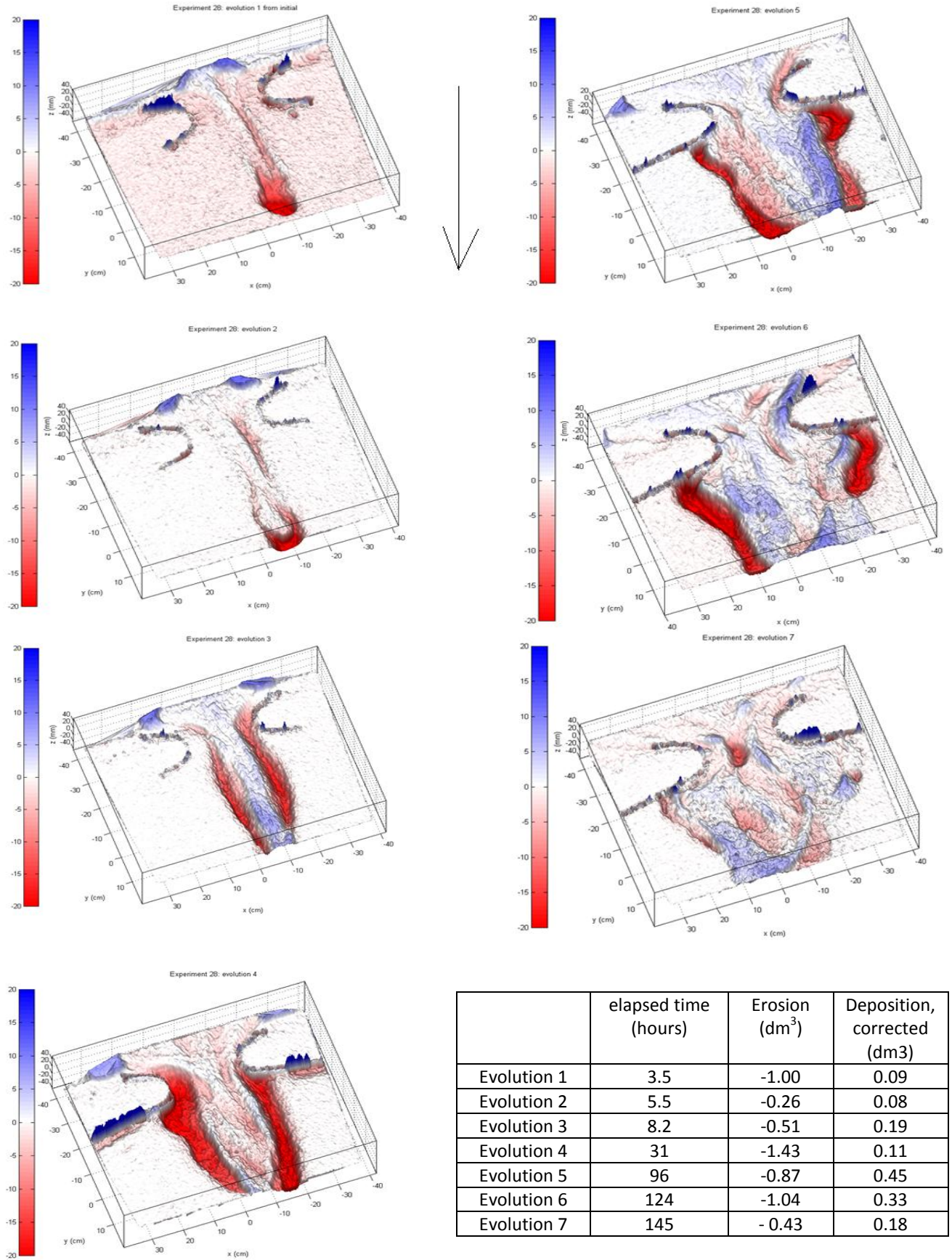l delta were about 1.5 cm deep. A shoal in the back-barrier was observed at flow depth below 0.5 cm. Channels in the inlet were deeper than 2.2 cm and banks had a flow depth of less than 1.8 cm. A change in water depth of > 0.2 cm indicated migration of channels or erosion/deposition.
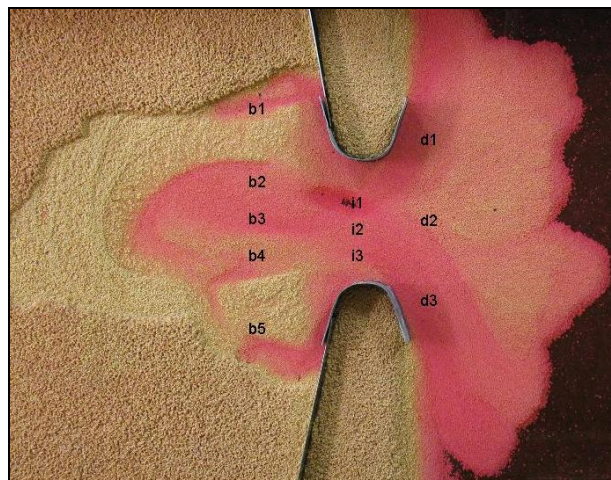
Figure 4.9 Codes represent data points in time series of images in which b = back-barrier 1 to 5, i = inlet 1 to 3 and d = ebb-tidal delta 1 to 3.
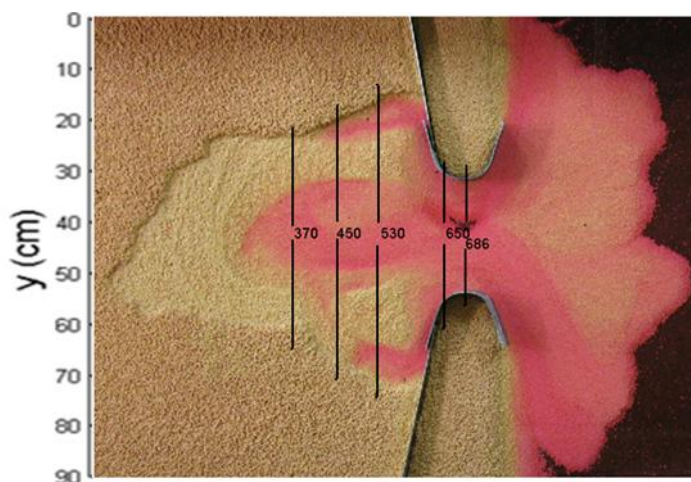
Figure 4.10 Cross-sections in experiment 28 over which time stacks of water depth were calculated. Location of cross-sections were represented by coordinate 370, 450, 530, and 686.

4.2.1 Ebb-tidal delta

The variation in water depth on the ebb-tidal delta at data points d1, d2 and d3 was presented in figure 4.11. The signal for point d3 was a more or less stable channel depth of 1.5 cm. Point d2, the middle section, showed a decrease in water depth from 127 to 133 hours. It was associated with the

67

formation of a bar between two inlet channels. The formation of the bar lasted 5 hours, while the removal succeeded in 2 hours. Thereafter the sediment level remained more or less constant and sediment level was higher than it was before. Point d1 showed a moderate decrease in time of water depth indicating vertical accretion of sediment on the ebb-tidal delta.
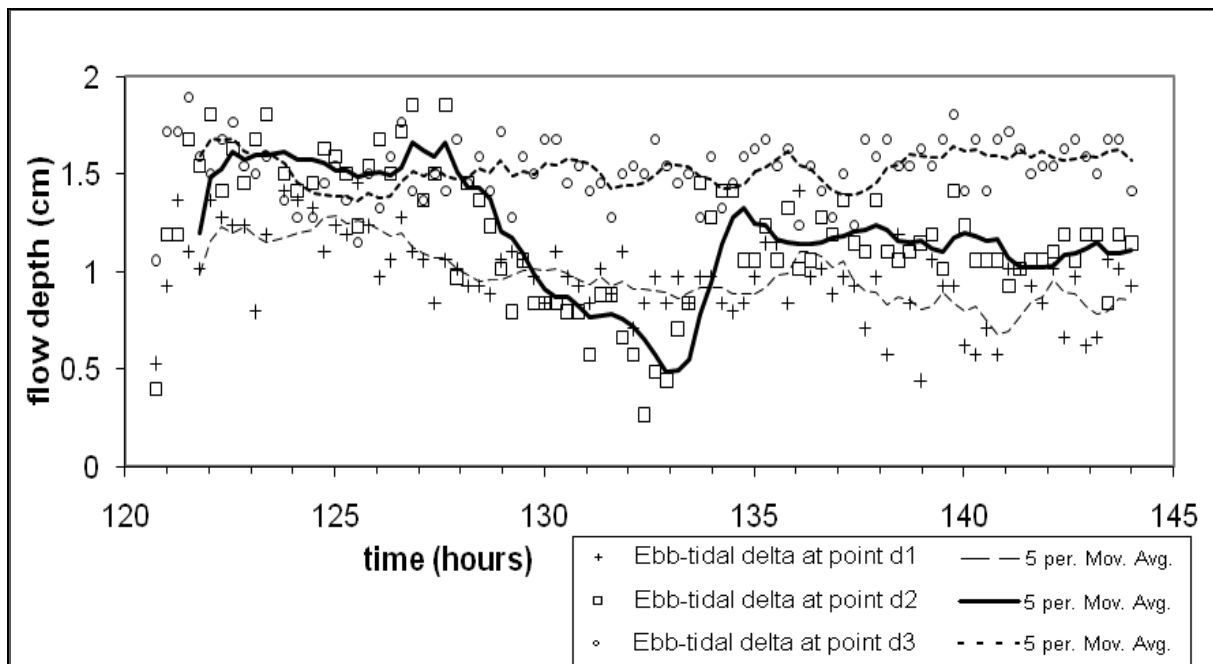
Figure 4.11 Variation in flow depth on the ebb-tidal delta of experiment 28 at data points d1, d2 and d3 according to figure 4.10. The lines present the 5-period moving average of data points. Note that moving average in excel has a known bug of shifting the moving average to the right. Therefore the moving average is not adequate. Still the signal serves its purpose.

4.2.2 Inlet

The inlet dynamics of formation of bars and channels was displayed in figure 4.12. The three data points presented a high variability in water depth. The high variability indicated the dynamic state of the inlet. The depth varied in the range 1.4-2.6 cm. In general point i3 described the shallowest part of the inlet. Flow depth varied between 1.5 cm and 2.2 cm, representing switching between a bank and a shallow channel. The signals of point i1 and i2 were often anti-phase indicating that the inlet consisted of one deep channel. The deepest point of the channel migrated between point i1 and i2. Two simultaneous peaks indicated one wide deep channel or two narrow deep channels. The movie of successive images shows that simultaneous peaks usually represented two channels separated by a bar. Figure 4.13 presents flow depth at cross-section 686 (figure 4.10, through the inlet) from 120 hours to 144 hours. The inlet first consisted of 2 deep channels whereas after 125 hours one of the channels became shallower and got filled up. Thereafter the inlet showed a laterally migrating channel and emerging of a new channel on the opposite side of the migrating inlet channel. In about 10 hours (132 – 142 hours, 450 tidal periods) the main channel shifted from and to north – south – north – south – north. The inlet also shifted between having one inlet channel and having two. The switching of two inlet channels to one was visualized in cross-section in figure 4.14. Between each cross-section there were 35 tidal cycles. First two channels were distinguished of which one was slightly deeper than the other. Then both channels obtained the same flow depth. Subsequent the bar between the two channels was eroded in 3 * 35 = 105 tidal cycles to form one wide channel. In the following 70 tidal cycles the channel became narrower. Next a sudden shift of the location of the main channel occurred which then persisted (figure 4.13).
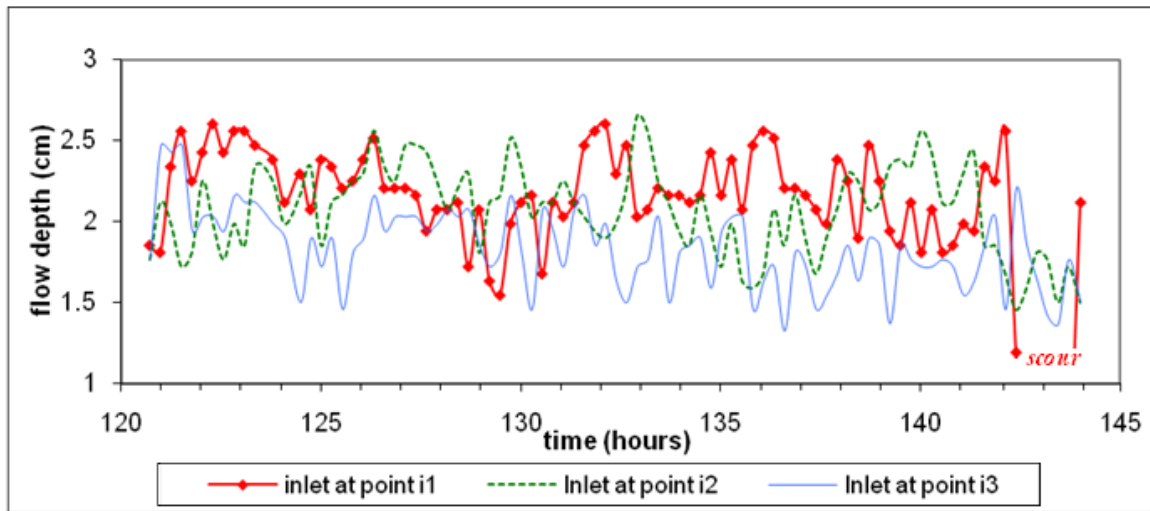
Figure 4.12 Inlet channel migration in experiment 28 of data points at i1, i2 and i3 according to figure 4.9 over time series 120 hours to 144 hours.
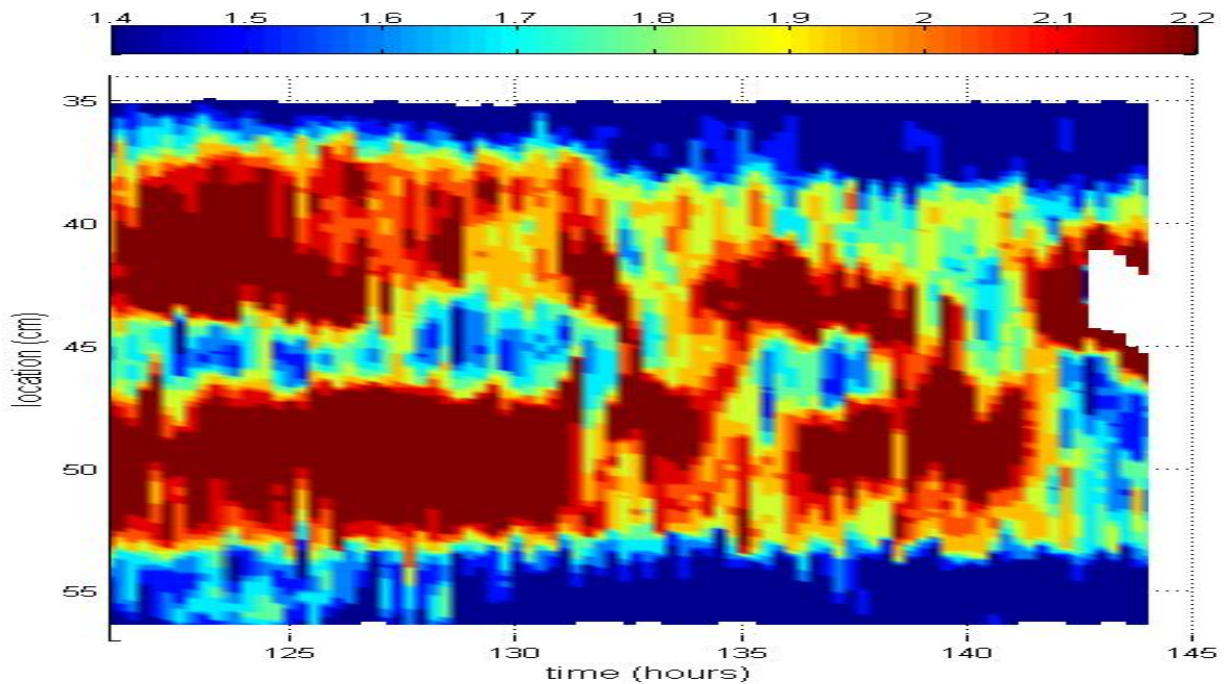
Figure 4.13 Flow depth at cross-section 686 (figure 4.10, through the inlet) indicating inlet channel migration and formation of new channels. The white hole indicates a scour hole.
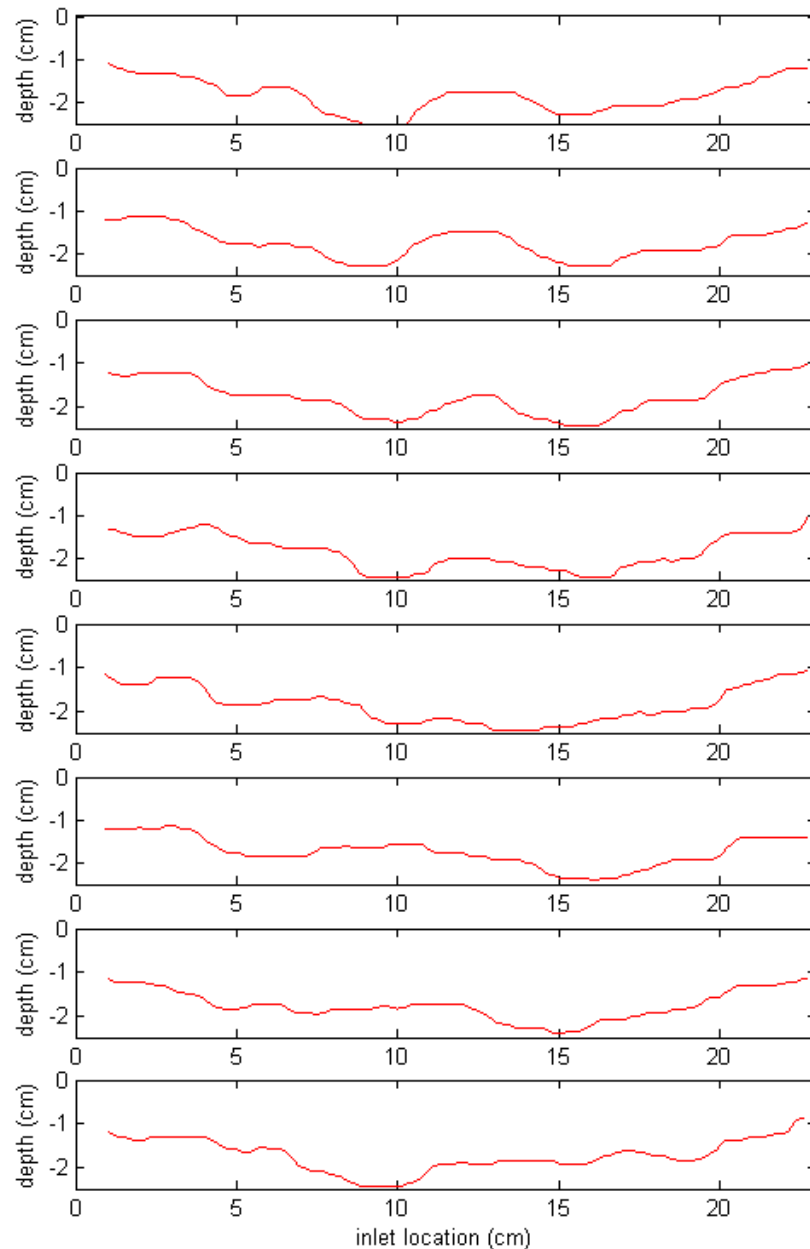
Figure 4.14 Inlet cross-sections at 136.3 h to 142h. Between each cross-section 35 tidal cycles (45 minutes) took place.

4.2.3 Back-barrier

In the back-barrier area channel migration was prominent for the middle, main channel. Figure 4.15 presents the cyclic behaviour of the middle channel. Point b2 and b4 were located above and below the centre. The flow depth varied between 2.1 cm and 0 cm. A water depth of 0 cm indicated a shoal since there was no water present at that time. The signal of b2 and b4 were in anti-phase. It indicated that when a channel was present at point b2, there was a shoal at point b4 and vice versa. There were four major peaks (flow depth > 1.5 cm) in 21 hours resulting in an average channel existence time in the back-barrier of 5 hours (21/4). All major peaks showed a fall between two peaks indicating that the channel migrated slightly further away from the point and then came back. So the middle channels swapped back and forth in a period of about 5 hours. Figure 4.16 distinguished back and forth sweeping to occur between y= 35 cm and y =55 cm. In the figure red – orange-yellow is a deep channel. At 122 hours a channel is migrating southward from y=40cm towards y=55cm. Both southward and northward migration of channels in the back-barrier area was observed. The

70

migration rate was generally 3-4 cm/hr. Some of the channels got abandonment after migration to the margin while others switched direction and migrated back. New channels emerged from bifurcations or by gradual deepening. When the channel had migrated towards y=55cm a new channel formed at y=45cm. A cycle in channel migration of southward migration seemed to exist and occurred seven times within 1000 tidal periods. This gave a channel migration cycle of 1000/7 = 140 tidal periods (4h/7 = 3h). The flip of direction of lateral migration or abandonment occurred relatively quickly. In short, the channels in the back-barrier show channel migration, bifurcations, channel abandonment and switches of migrational direction.

Figure 4.15 flow depth in the back-barrier at b2 and b4 indicating back-barrier channel migration in experiment 28 over time series 120 hours to 144 hours.

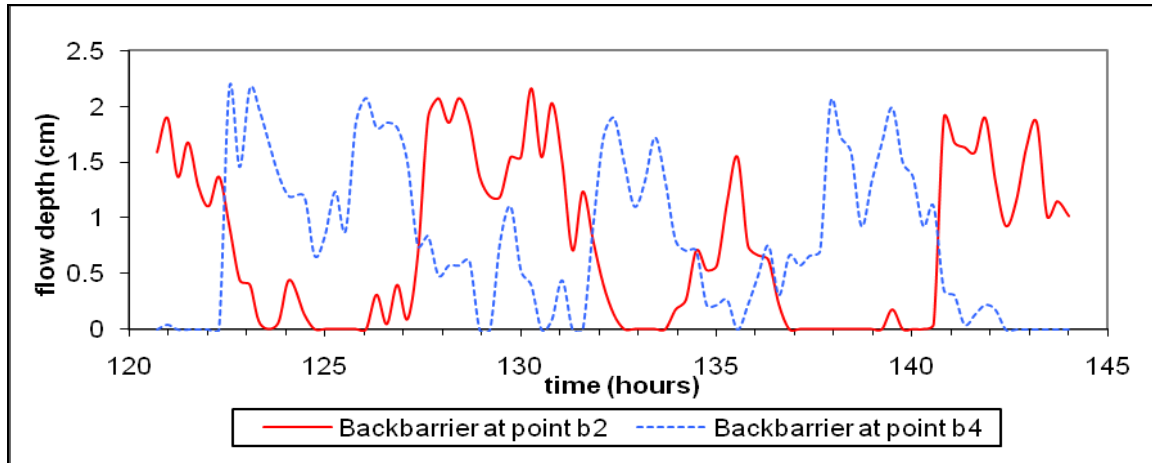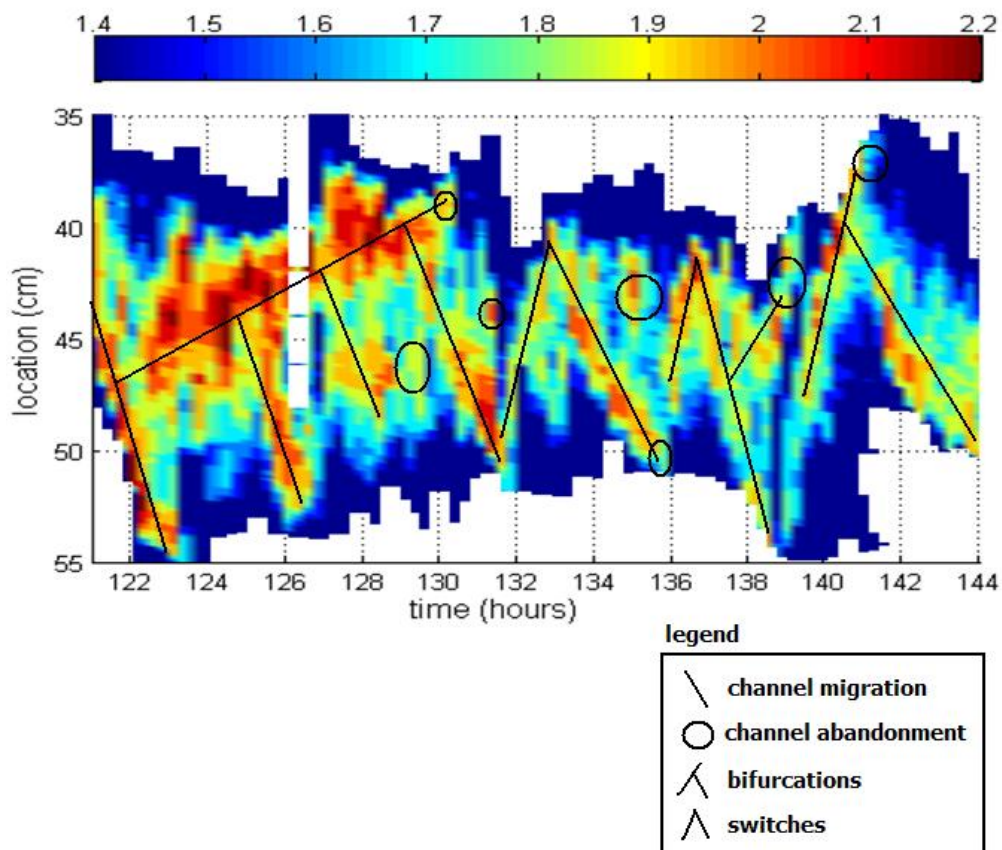Figure 4.16 flow depth in the back-barrier at cross-section 450 indicating back-barrier channel migration (~ 3 to 4 cm/hr), channel abandonment, switches and bifurcations in experiment 28. Time was at 120 hours to 144 hours (5500 to 6500 tidal cycles).

4.3   Experiment 29: Sea level rise

The response to sea level rise of dynamic equilibrium state (experiment 28) was investigated in experiment 29. The direct response and the effect of sea level rise on typical morphology will be described for in this section.

Sea level rise was simulated by a stepwise increase of water depth. After every sea level rise the system needed about 1000 tidal cycles (24 hours) to adjust to the change in water level where after a next sea level rise was imposed. This method allowed studying the short term and long term effect to an instant sea level rise. Figure 4.17 presents the volumes at high water. The high water volume increased from 3.5 L at start to almost 5L after sea up 2, 6L after sea up 4 and 9L after sea up 5. The net increase in high water volume is (9 – 3.5) / 3.5 * 100 = 160 %. In contrast, the increase in water level was 30 % (section 3.2).
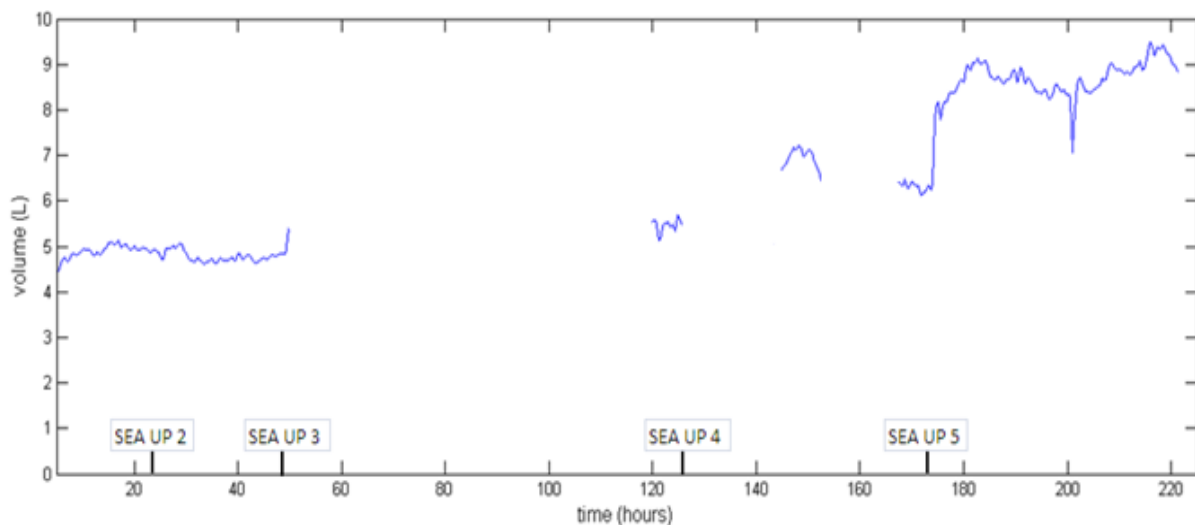
Figure 4.17 Volume of water in the back-barrier at high water during experiment 29. The water level was increased 5 times by about 5% according to 'sea up 1 – 5'. The back-barrier was defined left of the thick line in figure 4.3. Moving average was taken over 15 points (15*12 = 180 tidal periods).

Figure 4.18 presents the response to the first sea level rise and figure 4.19 the response to the fifth sea level rise. Short-term responses which were generally observed after each sea level rise were as follows:
- The middle channel in the back-barrier lengthened. At a certain distance of lengthening the channel curvature increased coinciding with the channel tip withdrawing from the back part of the intertidal area. The cyclic back and forth sweeping of the middle channel commenced again.
- The outer channels in the back-barrier eroded their outer bends and the flooded area widened. Thereby the channel tips retreated from the *landward side* of the basin.
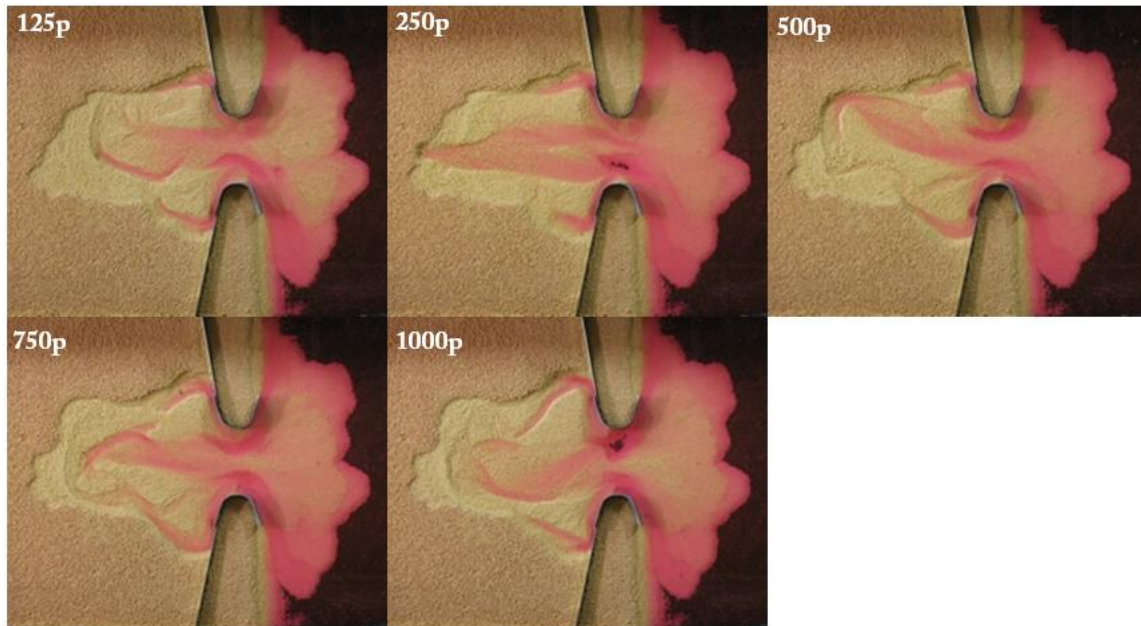
Figure 4.18 Response to an instant rise in water level of about 5% (sea up 1). The photos were taken at low water at 125, 250, 500, 750 and 1000 tidal periods after first rise in sea level.
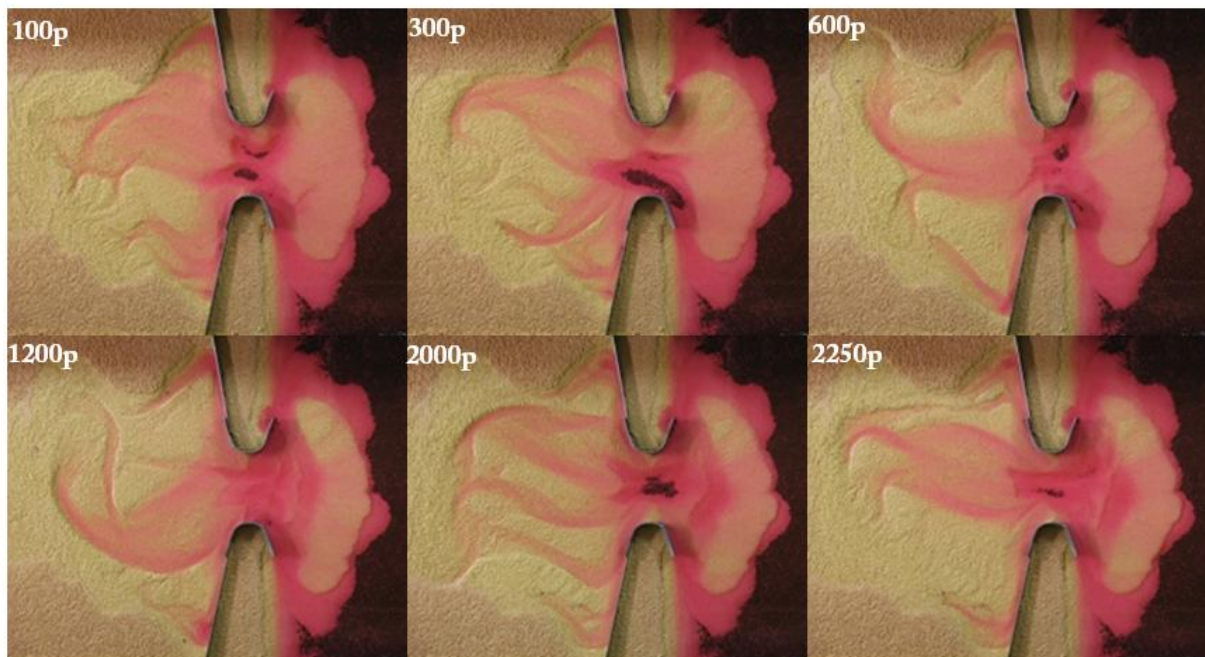
Figure 4.19 Response to an instant rise in water level of about 5%. The photos were taken at low water at 100, 300, 600, 1200 and 2250 tidal periods after fifth rise in sea level.

The erosion of the outer bends of the outer channels is presented in figure 4.20a. The erosion of outer bends of the outer channels showed a stepwise widening simultaneous with the instant sea level rises. Also the width over which the middle channels in the back-barrier migrated increased from location y at 35 – 55 cm to location y at 20 – 70 cm. The increase was (50 –20) / 20*100 = 150%. Channel migration rates after the second sea level rise were calculated from figure 4.20b and were about 22.5cm/4h = 5 - 6 cm/hr. In the last stadium of sea level rise the channel migration rates were slightly higher: 17.5/2.5 = 6.5 - 7.5 cm/hr. The rates became harder to deduce because the number of channels increased and often they merged but continued migration. Still a trend was observed of decreasing channel migration rates as a function of rise in water level. The cyclic channel migration also persisted. At the second sea level rise southward migration was

observed five times in the period 30h to 50h which gives a duration of 4h per migration cycle. Before the sea level rise the cyclic migration occurred every 3h. So a slight increase in migration cycle time occurred as a function of sea level rise. After sea level rises four and five the number of channels had increased. These channels merged often while they continued migration to one direction or the other. As a result the migration cycles were not as prominent anymore because they occurred both over small ranges and over large ranges. Therefore migration cycles in a later stage of sea level rise were not compared to migration cycles at an earlier stage. In short, channel migration and migration cycles in the back-barrier persisted during sea level rise. The trend in channel migration rate and cycle duration is an increase as a function of sea level rise.

The last sea level rise was continued for a longer time to study the equilibrium state of the experimental tidal inlet system after a significant sea level rise. Figure 4.21 is the final configuration after each sea level rise. The long-term effects are as follows:
- The back-barrier basin widened and lengthened which coincided with an increase in tidal prism (high water volume). In general a lengthening overshoot occurred before arriving at equilibrium dimensions.
- The number of channels in the back-barrier increased and varied in number between 3 to 6 main channels.
- The ebb-tidal delta built up in the vertical by forming a smaller delta on top of the former.
- The inlet channels deepened simultaneously with a rise in water level.
- The inlet channel extended further into the ebb-tidal delta.
- The inlet channel showed larger scours which appeared and disappeared. The inlet region was very dynamic as a response to migration of channels in the back-barrier.
- Width to depth ratios of the main channels showed a slight increase in figure 4.22. The increase indicated that channels became wider with respect to their depth. The channels on the ebb-tidal delta showed the opposite signal of deepening with respect to their width.
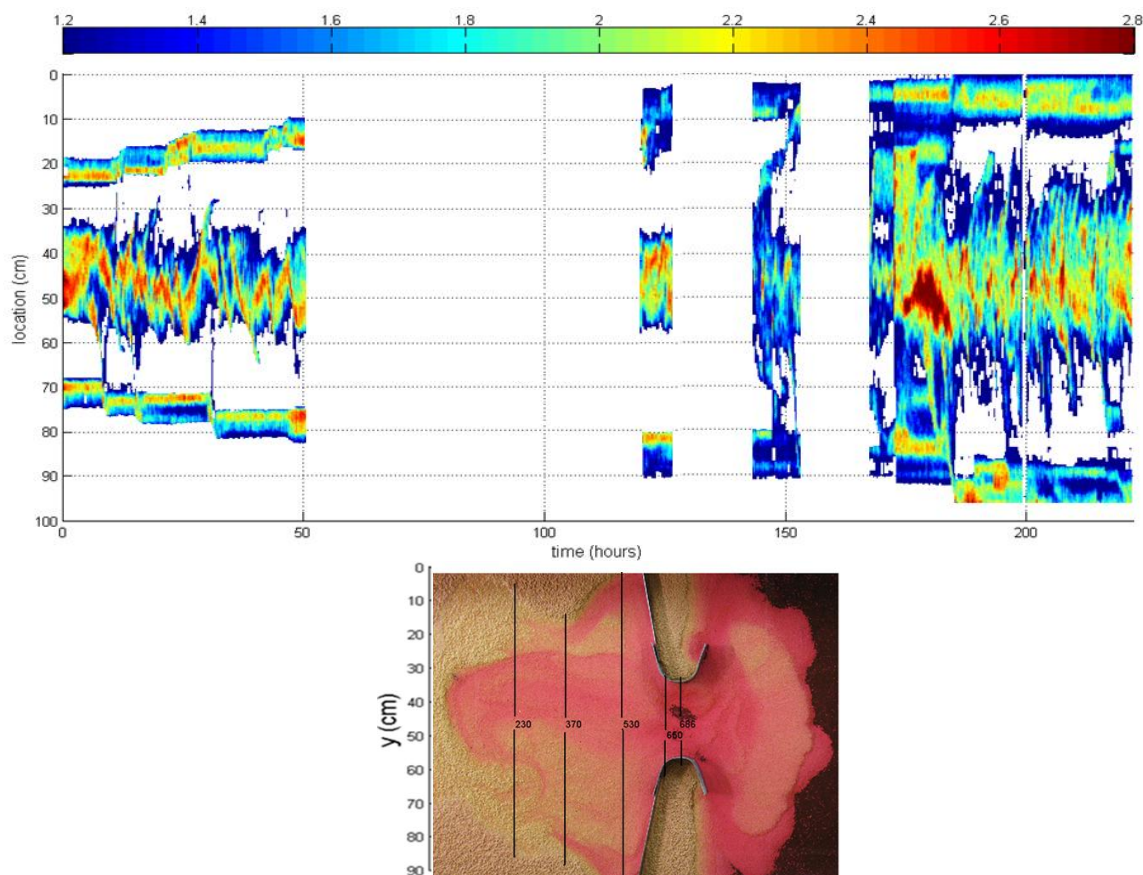
Figure 4.20a flow depth in the back-barrier at cross-section 530 over time (indicated in lower figure) showed back-barrier widening and lateral, cyclic migration of channels.
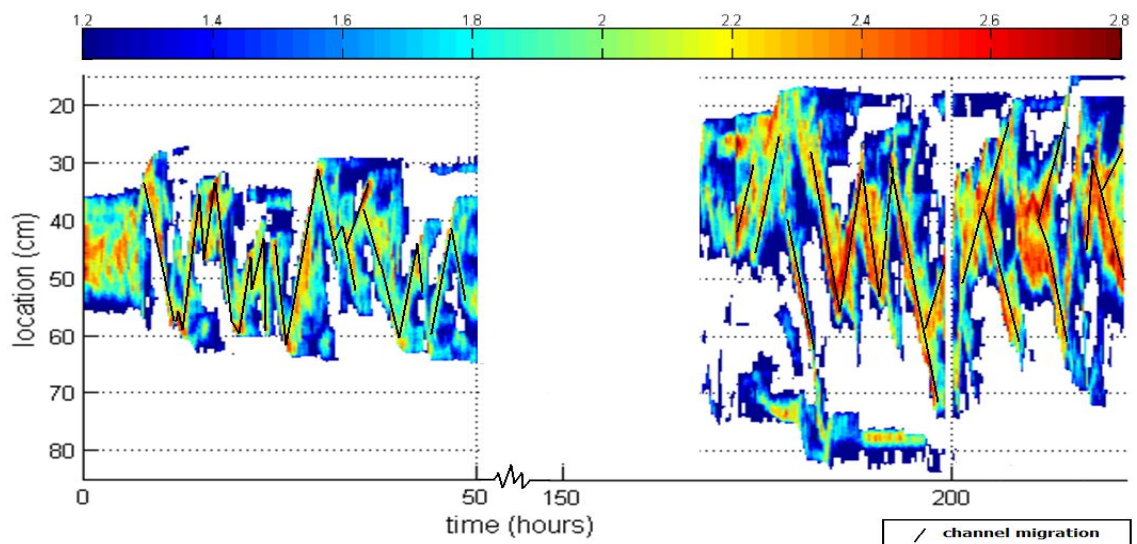
Figure 4.20b Visualization of channel migration in experiment 29 at location 370 which is in the middle of the back-barrier area. Channel migration persisted and the channel migration rates slightly decreased as a function of a sea level rise.
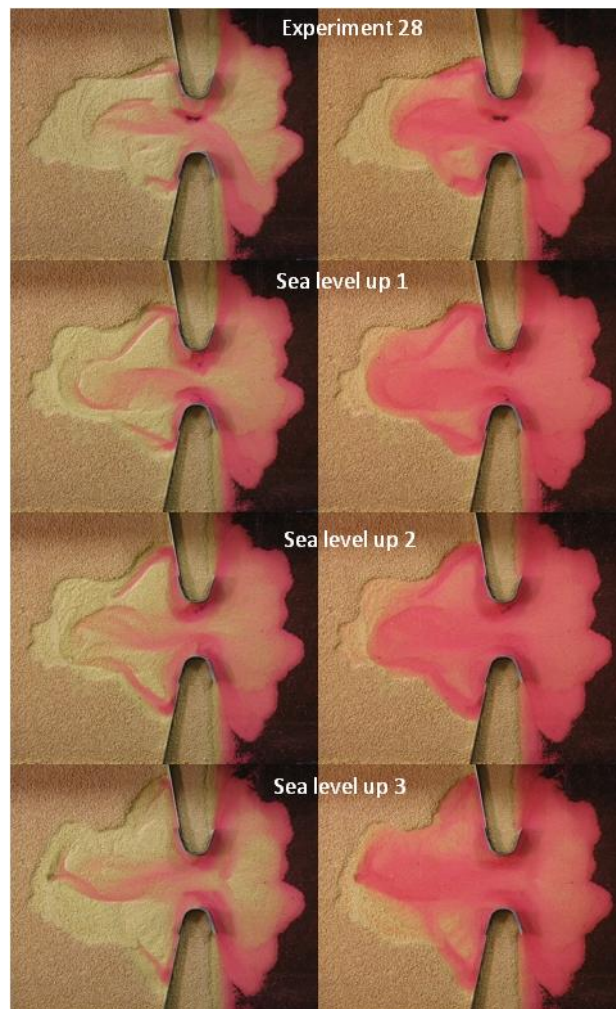
Figure 4.21 Final configuration of morphology at low water (left) and high water (right) after sudden increase in water level (sea level up 1 to 5). Experiment 29 photo numbers 349 and 351, 717 and 719, 856 and 858, 1102 and 1104, 1774 and 1776, 1842 and 1844.
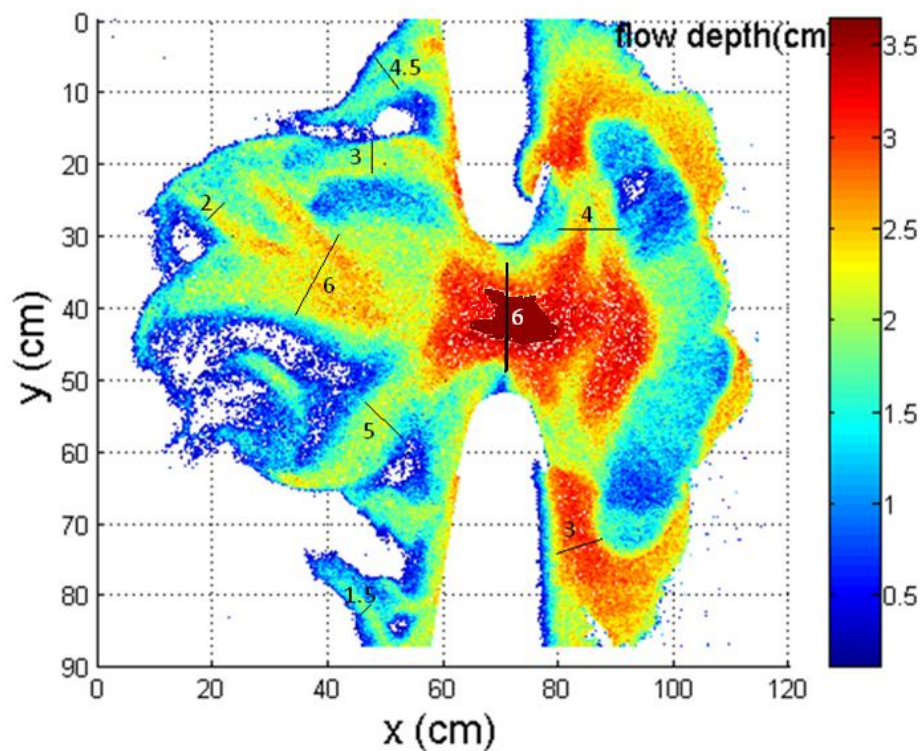
Figure 4.22 Width to depth ratio (-) at the cross-sections of experiment 29, final configuration (photo 1789). Flow depth map calculated from photo taken at MSL (mean sea level) at the phase from high water to low water.

4.4 Switching of number of inlet channels

The switching of the number of inlet channels is a cyclic phenomenon observed for in nature (literature background, chapter 2.2.8). This section visualizes, describes and quantifies the switching of number of inlet channels that was observed in the experiments.

Figure 4.13 showed switching of the number of inlet channels between one and two inlet channels. Figure 4.23 shows the flow depth in the inlet cross-section from plane bed to equilibrium state. First there was one channel. After about 1000 tidal cycles a second channel had developed. The existence of two channels persisted during morphological evolution. The switching between one and two inlet channels commenced after 127 hours. Between 127 hours and 143 hours seven switches were distinguished. The time to switch from two inlet channels to one and back to two was irregular. An average time of occurrence of a cycle was calculated from (143 – 127)/7 and was 2.3 hours (about 100 tidal cycles). Figure 4.24 shows the inlet during the first two steps of sea level rise of experiment 29. The existence of one deep main channel was observed six times (green/orange) in 50 hours. So average existence time was much longer after sea level rise than it was for experiment 28. Also existence time of a main channel was irregular but much shorter than existence time of two channels in the inlet. It is concluded that switching between numbers of channels occurred cyclically although the time of existence of one inlet channel or two inlet channels was very irregular.
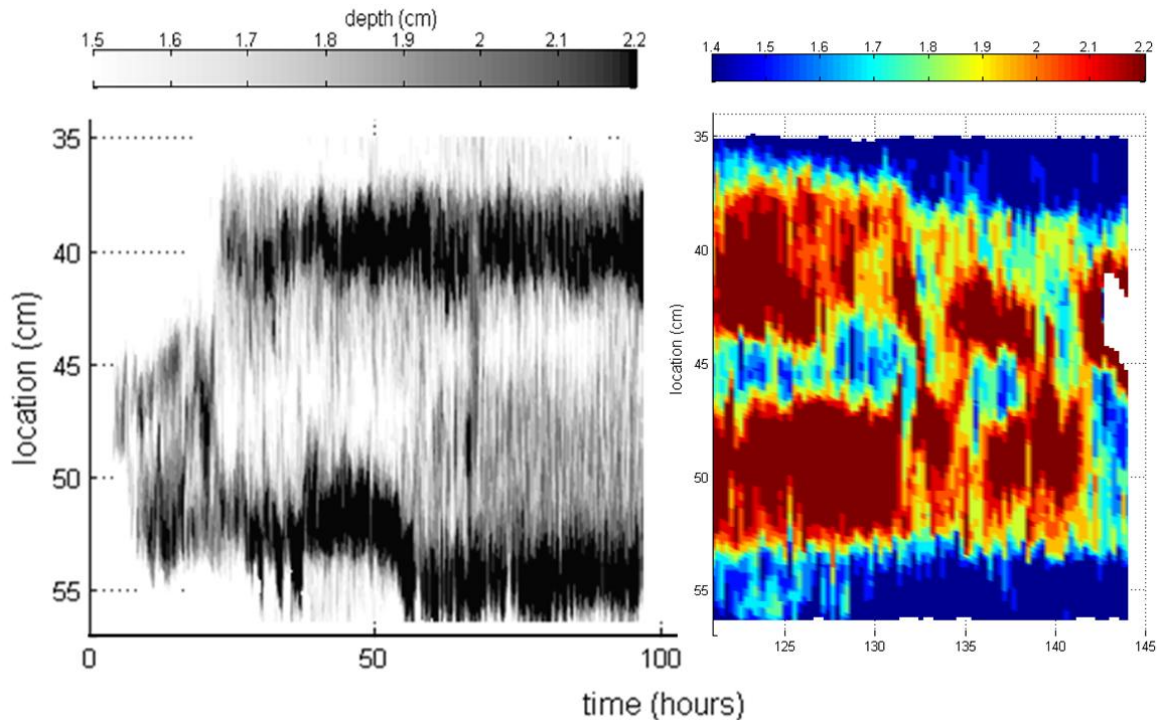
Figure 4.23 flow depth in the inlet at cross-section 686 of experiment 28.
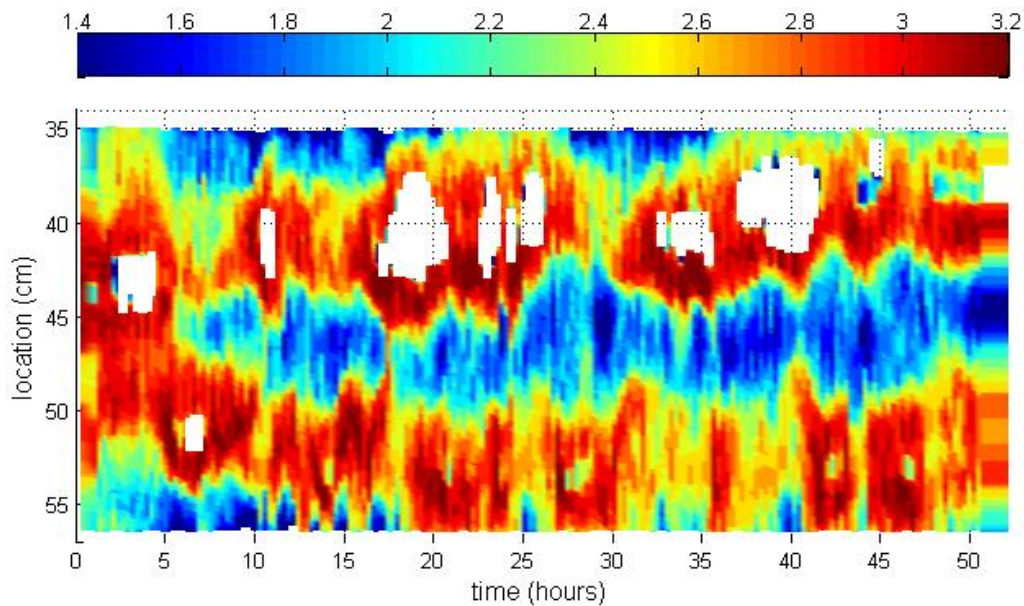
Figure 4.24 flow depth in the inlet at cross-section 686 in experiment 29 during first two steps of sea level rise.

4.5 Experiments and variables

The twenty-three experiments reported here aimed at understanding the physical processes, as well as boundary and initial conditions, which lead to experimental development of a dynamic tidal inlet system with channel network as presented in the previous sections. The experiments started from plane horizontal tidal flat located behind a barrier island and connected through the sea by a single inlet. Each experiment started forcing water to flow from tilting the experimental apparatus. A small perturbation in the inlet was a requirement for channel development. This section describes the effect of the variables on the end state of the morphology in the experiments that were performed. First experiments with poorly sorted sand will be considered and the effect of flow strength, water level and initial configuration given. Then experiments with light-weight grains are considered. The variables flow strength, water level, sediment level, start perturbation, bed slope and protected or unprotected inlet width were investigated.

4.5.1 Poorly sorted sand

In experiment 10 – 22 use was made of poorly sorted sand. A channel network formed only for large enough values of tilt amplitude so the lagoon bed wetted and for small enough water depths to dry the lagoon at ebb. Drying of the lagoon was important for headward erosion to occur. Channels developed mainly through headward erosion. In case of unequally levelled tidal flat an ebb-tidal delta developed that was non-symmetrical perpendicular to the inlet (preparatory experiments). Sediment transport was dominant during end of the flood phase and at beginning of the ebb phase. Also significant sediment transport occurred in the late ebb phase. Flood flow generally determined the inlet width. Ebb flow generally described channel network development. Sediment deposition occurred mainly on the ebb-tidal delta and some in the lagoon behind the channels. General observations were schematized in figure 4.25. The time required to complete a single experiment with poorly sorted sand ranged from 1 to 4 hours and presented 40 – 250 tidal cycles (table 3.2). Ultimately development ceased because of flow strength below threshold for sediment transport.
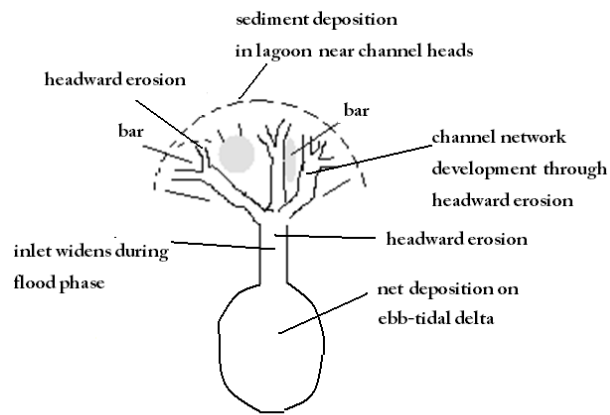
Figure 4.25 General observations op processes during morphological evolution in experiments with poorly sorted sand.

Variables: tilt amplitude and tilt speed

Experiment 10 and 13 showed the effect of the tilt amplitude. Tilt amplitude positively influenced flow strength and tidal prism. The channel network of experiment 13 wherein tilt amplitude was higher extended further into the lagoon and deposition occurred in the lagoon. The deposition in the lagoon was in a delta form and showed sediment rearrangement. In experiment 10 with lower tilt amplitude the ebb-tidal delta grew to a double bulge form. Sediment deposition in the lagoon was insignificant. The channel network resembled the one of experiment 15 in which transport only occurred at ebb. Tidal prism of experiment 10 was lower than for experiment 13, consequently the inlet width was narrower (10 cm versus 13 cm) and inlet area smaller.
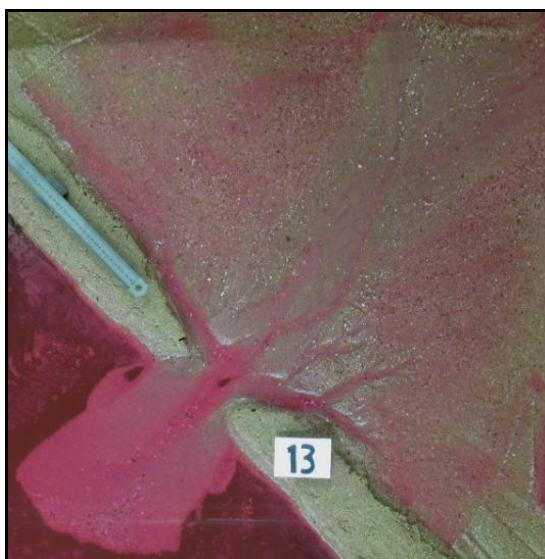
tilt 35 mm
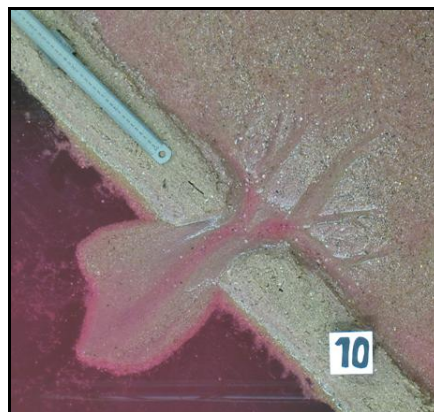
tilt 20 mm

solely ebb-transport

Tilt speed

The effect of the tilt speed was compared through experiment 10 and 11. Tilt speed positively affects flow strength. The channel network of experiment 10 and 11 resembled. But in experiment 11 the channel aside the barrier islands was relatively wide. A fast tilt of 100mm/min caused the water in the lagoon to first flow towards the barrier islands before leaving through the inlet. So fast tilting induces the water in the lagoon to be drained aside the barriers. Then the ebb-tidal delta became wide because flow paths generally extended straight on from the lagoon. For a tilt of 50 mm/min as in experiment 10 the water generally drained circularly around the channels (dashed line in figure 4.25). Speed of tilting thus affects the mode of drainage from the lagoon. Morphology in the back-barrier is similar while the ebb-tidal delta is more long-stretched for a higher tilt speed with further extension of the inlet channel over the ebb-tidal delta. It is concluded that the effect of speed of tilting on channel network development is small. Speed of tilting was thereafter set to best represent natural flow paths.
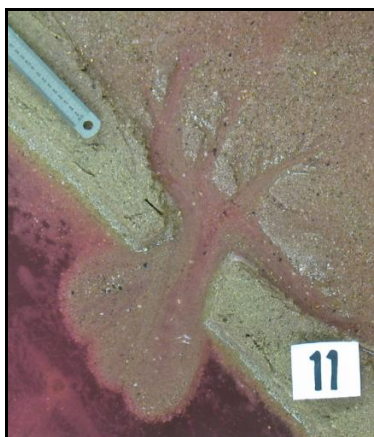
Average tilt 50 mm/min   *Fast tilt 100 mm/min*
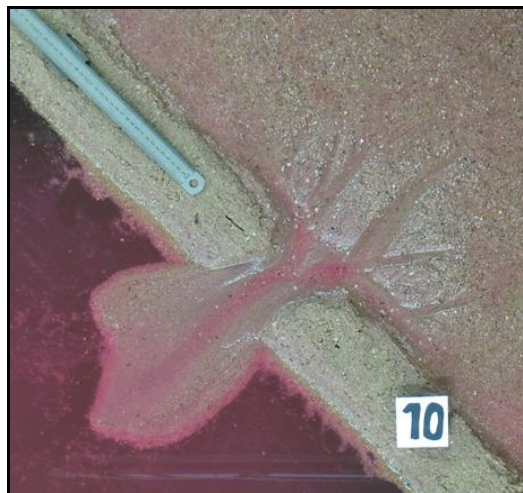
Variable: initial bed level

Experiment 22 had a low bed level difference between tidal flat (2cm) and sea (1 cm) compared to previous experiments (tidal flat of 3 cm and no sediment in sea). Experiment 22 did not show development of a channel network. While an extensive ebb and flood-tidal delta developed. It was concluded that a bed level step between sea and tidal flat is required for channels to develop.

Variable: initial perturbation

In experiment 16 and 17 the initial perturbation was varied. Experiment 16 started with a perturbation of about 5 cm like in previous experiments. Experiment 17 started with a perturbation

consisting of a 50 cm long channel. The final configurations of experiment 16 and 17 show a similar shape of the ebb-tidal delta. Different are the character of the channels and shoals in the back-barrier and the length of the system. Note that ultimately shear stresses became low for both experiments and the active area in terms of sediment transport retreated to covering only the inlet section. In that area, morphology is similar. Remnants of morphology in the former active areas showed considerable difference indicating that initial topography had a major control on morphology.
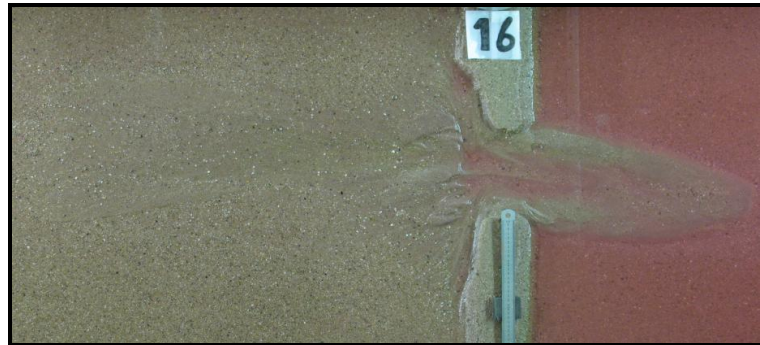
Perturbation of about 5 cm

Perturbation of about 50 cm length

4.5.2 Light-weight grains

In case of poorly sorted sand the evolution was ebb-dominated. Over time the transport capacity of the flow decreased. Eventually it was under the threshold to transport poorly sorted sand and morphodynamic change ceased. The use of light-weight grains was studied to accomplish continuation of sediment transport throughout the entire experiment. Because of the low density of the grains (1042 kg/m^3) the threshold for sediment transport is lower. Therefore it is assumed that flow capacity stays above the threshold for sediment transport, both during ebb-and flood phase. As a result sediment transport will be less ebb-dominated.

Variable: Tilt amplitude
The amplitude of tilt confined the strength of flow. The higher the amplitude of tilting, the higher the water surface gradients and the higher the flow velocities were. The tidal prism and the ebb-tidal delta obtained a larger volume. The light-weight sediment restricted maximum amplitude of tilting at 10 mm (experiment 23). At higher amplitudes large parts of the sediment bed were transported in bulk. At amplitudes lower than 5 mm the evolution was extremely slow and the flow strength eventually was under the threshold for sediment motion.

Variable: bed slope
The flow was generated such that flow was to lower parts within the experimental apparatus. The further away, perpendicularly, from the pivot point, the lower the sediment bed was at high water. To prevent the back-barrier from creating a 'deep lake' the sediment bed was designed to slope landward. In experiment 23 and 24 with a sloping bed the channels extended less far into the back-barrier and channel migration was slower. The ebb-flow was promoted since at ebb tide the bed

slope was higher. Relatively deep ebb-dominated channels emerged in the back-barrier (experiment 24). Experiment 25 showed that the system widened continuously until it ultimately covered the entire length of the experimental apparatus. Since sediment was reworked throughout the entire experimental apparatus it was assumed that sediment availability was too low.

Variable: bed level

A sufficient sediment level behind the barriers was a variable necessary to obtain a dynamic state of the morphology in experiment 26 and experiment 28. When the sediment level in the back-barrier region was lower the flow diverted over the plane surface and hereby channel development did not succeed (experiment 23-25). So flow concentration was needed to obtain shear stresses sufficiently high for migrational behaviour to persist (experiment 26 and 28). For low sediment levels migration of back-barrier channels only occurred at their tips. Likely flow concentration was higher at the tips. Channels near the inlet became wide and did not show migrating behaviour so shear stresses were low here. Scour holes in the inlet were slightly mobile. Flow converged passing through the inlet whereby flow velocity and bed shear stress increased. Higher shear stresses in the inlet occasioned migration of inlet channels and thus of scour holes.

Variable: initial perturbation in a long basin → see appendix for description of 7 experiments

Protected or unprotected inlet

The inlet width was an important variable for the final configuration of the experimental scale models. Flow converged when it had to pass through the inlet and hereby the flow velocity increased. Sediment transport was promoted. Experiment 23 -26 were performed with an unprotected inlet. The inlets showed ongoing widening prominent in experiment 23-25. The long run of experiment 25 showed that ultimately characteristic morphology of tidal inlet systems vanished because of inlet widening. Experiment 23 and 24 were stopped when the inlet widths had become 62 cm and 49 cm. Migration rates of channels in the back-barrier had become very low. Still characteristic morphology was present. It was concluded that to arrive at an equilibrium state, the barriers should be stronger. Strength was added by higher barrier level in experiment 26 and subsequent also a constricted metal inlet in experiment 28. When the constricted inlet was smaller than about 10 cm, insufficient volume of water entered the region and flow velocity remained low. No morphological evolution occurred.

Water level

The water level at a certain phase in the tidal period was a function of the sea volume and the amplitude of tilting. Low water levels at MSL in combination with a normal tilt for light-weight sediment (7 mm) gave rise to channels that extended far into the ebb-tidal delta (experiment 26). The ebb-tidal delta built out via narrow but relatively long lobes. The channels in the back-barrier were few in number and they were narrow and long. Channel migration occurred in stages accompanied with channel migration on the ebb-tidal delta. A higher mean water level gave rise to inlet channels that diverted the ebb-flow alongside the ebb-tidal delta (experiment 28). The ebb-tidal delta extended less far into the sea but was higher in level. The channels were wider than for experiment 26 with a lower mean water level. The channels extended less far into the back-barrier region and were more abundant in number. Migration rates were relatively high and continuous.

To summarize, tidal flat level (topography) and using light-weight grains (sediment mobility) both had a major control on equilibrium morphology and migration rates. Constricted inlet width was required to arrive at an equilibrium state. It is suggested by author that only certain combinations of tilt amplitude, inlet width and water level enable emergence of realistic equilibrium morphology. The conditions in experiment 28 were such that experimental creation of a dynamic equilibrium state of a tidal inlet system was achieved.
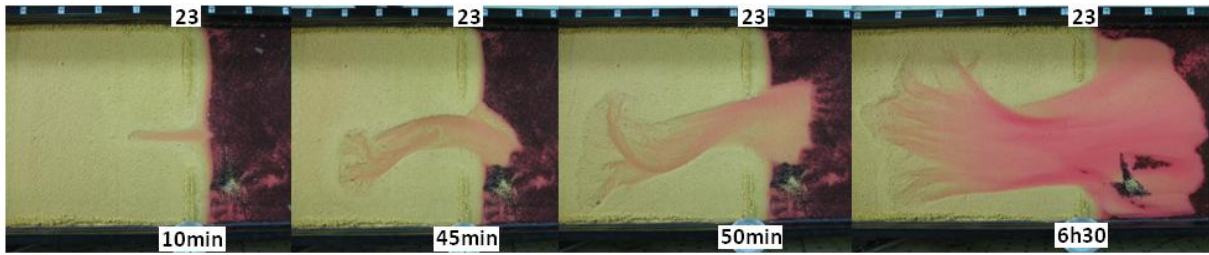
Experiment 23: Sloping bed – tilt 10 mm - 775 tidal periods
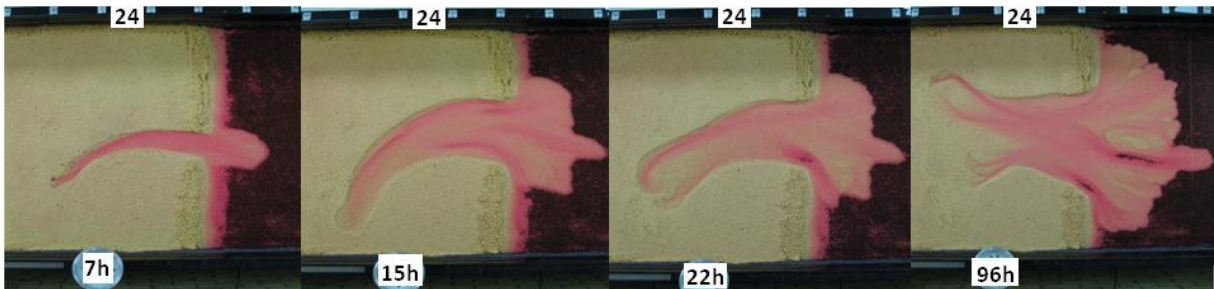
Experiment 24: Sloping bed – tilt 7 mm - 5150 tidal periods
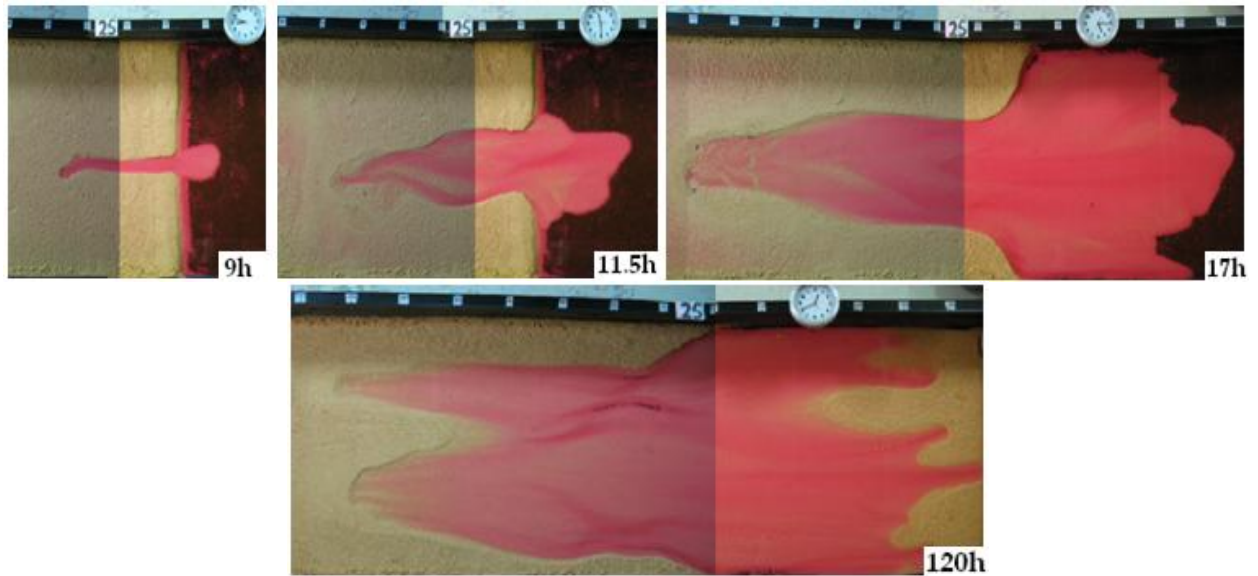
Experiment 25: Plane bed of 3 cm – tilt 7 mm – 6500 tidal periods
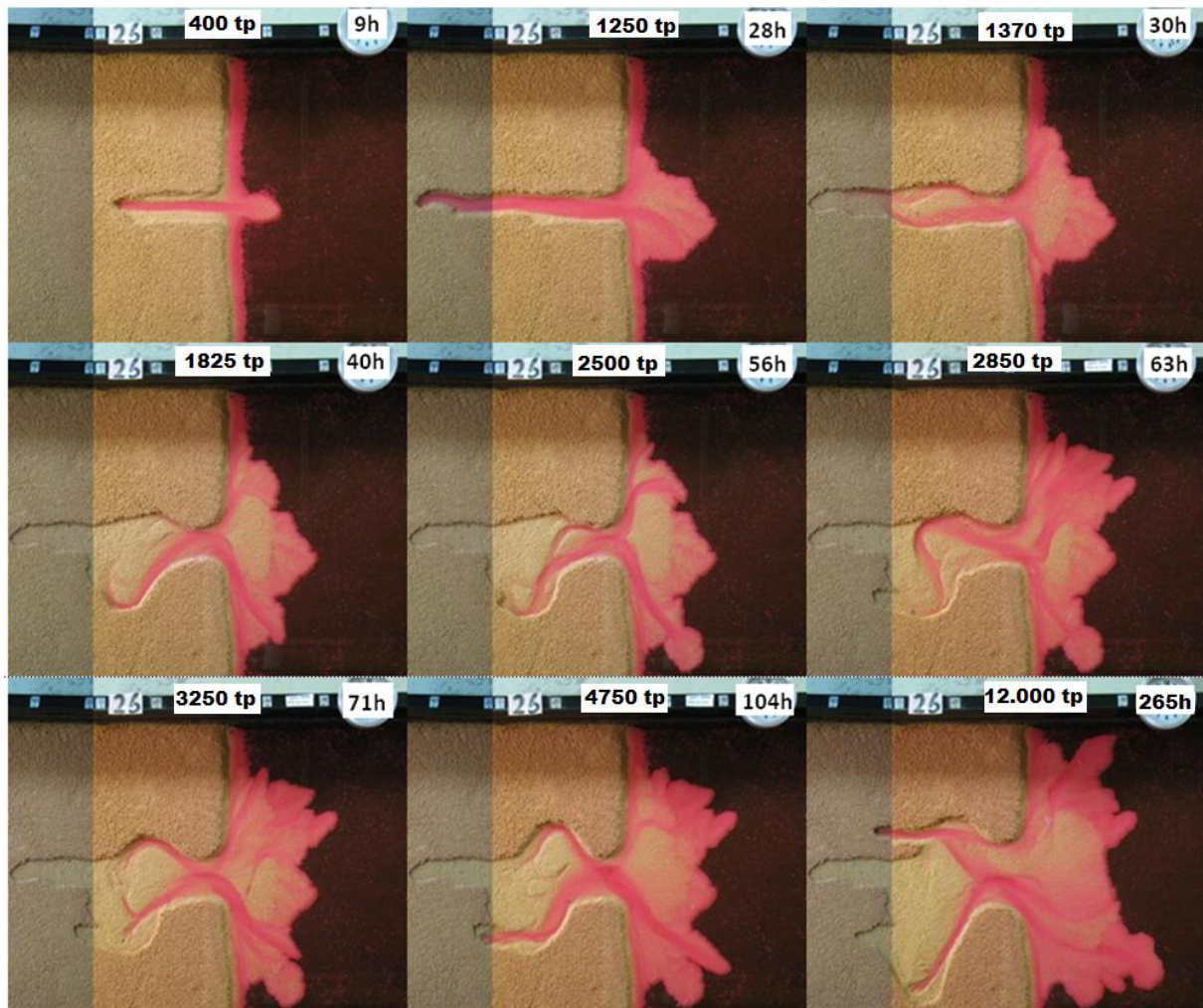
Experiment 26: Plane bed of 4.1 cm - tilt 10 mm – 12.000 tidal periods
Water level varied due to losses by evaporation. Maximum MSL was 2.8 cm.

Experiment 28: plane bed of 4.1 cm – tilt 10 mm – 6600 tidal periods - constricted metal inlet
Mean water level in the experiment was 2.8 cm.

Chapter 5: Discussion

The discussion chapter compares the experimental results to literature, observations, models and other experimental work. Chapter 5.1 is on scaling results to reality and applies different methods. Then chapter 5.2 compares the experimental results to full-scale systems. The basic phenomena, morphology, evolution and cyclic behaviour are discussed. The next section is on the comparison to computer models. Chapter 5.4 compares experimental results to prior experimental work. Last chapter 5.5 and chapter 5.6 translate the experimental findings to the physical system and provide recommendations for further research.

5.1 Scaling of results to reality

First the theory of tidal wave motions will be applied to scale experimental parameters to reality. Then scaling by similarity in flow parameters and sediment mobility is investigated and discussed. Last the different methods are compared by use of scale ratios.

5.1.1 Theory of tidal wave motions

The theory of wave motions [Reynolds 1887-1891] is implemented on experiment 28 to scale the experiment to prototype systems. An estimate of the velocity of experiment 28 was 0.06 m/s. An estimate of the tidal wave height was 1.0 cm. The tidal period was 79 s and the horizontal scale was 0.9 m. In nature maximum tidal currents through the inlet are about 1.0 m/s [Van der Vegt 2006]. Typical velocity in prototype tidal inlet is assumed to be slightly smaller, about 0.8 m/s. The corresponding tidal wave height is 1.8 m according to scaling method of Reynolds in table 5.1. So experiment 28 scaled with a prototype system with a tidal wave height of 1.8 m. The corresponding horizontal scale was 6.8 km. Google earth images from the US Atlantic Coast at North and South Carolina showed tidal inlet systems to exist in the range of 4 to 16 km for six randomly chosen inlets. A horizontal scale of 6.8 km is within that range. It is concluded that experiment conditions of experiment 28 scale with certain tidal inlet systems at the USA Atlantic Coast, for instance Fort George Inlet in Florida.

Table 5.1 Application of theory of wave motion on experiment 28.

		experiment	prototype	1/(ratio e/p)	Description
typical velocity	m/s	0.06	0.8	13.3	rule A & B
tidal wave height	m	0.01	1.8		
square root wave height	m$^{1/2}$	0.100	1.341641	13.4	rule A
tidal period	s	79	44700	566	rule B
horizontal scale	m	0.9	6800	7556	
ratio horizontal scale / ratio velocity		(-)	567	rule B
period of the experiment	s	78.9			rule C

The scaling of experiments to prototype systems by the theory of wave motions gives a good agreement for estimated values of parameters. Still the definition of the parameters is discussable. The experimental definition of tidal wave height and perhaps tidal period need adjustment when comparing to tidal wave height and tidal period in reality. The determination of typical velocity and horizontal scale for both model and prototype require a more accurate and unequivocal method. To realize this, a methodology has to be elaborated and tested in multiple experiments.

5.1.2 Similarity and sediment mobility

Froude number

It was reasoned in chapter 2.5 that for the Froude condition it is more important that the flow remains subcritical and that it is near uniform [Kleinhans et al. 2010]. Table 5.2 provides Froude number of a range of typical values of velocity and water depth in the tilting tub. All values are below one so the flow in the tilting tub was always subcritical. In comparison, in natural systems Froude number generally falls in the range 0.05 to 0.2 (-). These values were based on flow depths and flow velocities falling in the ranges 2 - 50 m and 0.5 - 1.5 m/s. The typical experimental Froude numbers were 0.1 – 0.2 (-) for flow velocities in the range 0.05 - 0.1 m/s and flow depth in the range 1.0 - 2.5 cm. It is concluded that typical Froude numbers in experiment 28 (0.1 – 0.2) scale with those ones typical for natural systems (0.05 – 0.2).

Table 5.2 Froude similarity

water depth	flow velocity	Fr
cm	m/s	(-)
0.5	0.05	0.2
1	0.05	0.2
1.5	0.05	0.1
2	0.05	0.1
2.5	0.05	0.1
3	0.05	0.1
0.5	0.1	0.5
1	0.1	0.3
1.5	0.1	0.3
2	0.1	0.2
2.5	0.1	0.2
3	0.1	0.2
0.5	0.2	0.9
1	0.2	0.6
1.5	0.2	0.5
2	0.2	0.5
2.5	0.2	0.4
3	0.2	0.4
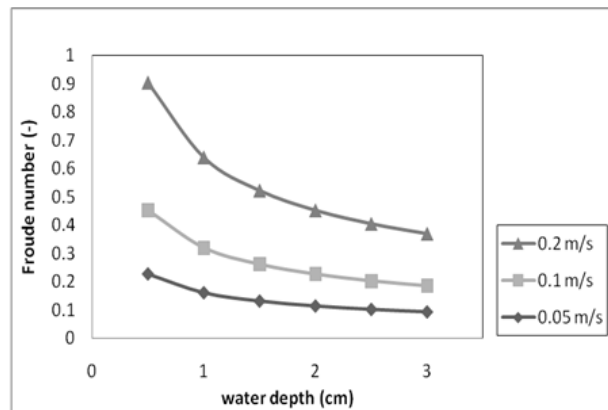
Sediment mobility

Particles start to move when the force that the fluid exerts on the particle is just larger than the force that keeps it in place (particle weight and the friction). To describe the initiation of motion a particle mobility parameter θ was introduced by Shields [Van Rijn 1993]. The particle mobility parameter θ depends on hydraulic conditions near the bed and the particle shape and position relative to other particles. The driving fluid forces depend strongly on the local near-bed velocities. They are described for by the bed shear stress (τ_b). To initiate motion, a bed shear stress is needed just larger than the critical bed-shear stress ($\tau_{b,cr}$). One can calculated the shear stress needed to initiate motion from sediment and water properties. Bonnefille (1963) and Yalin (1972) showed that the critical Shields parameter θ_{cr} can be calculated from the Shields curve (section 2.1.3) and the dimensionless particle parameter D_* [Van Rijn 1993]. The particle parameter D* reflects the influence of gravity, density and viscosity. Applying the formulations on the experimental properties gives a critical bed shear stress of 0.028 N/m^2 in table 5.3.

Table 5.3 Experimental properties and calculation of critical bed shear stress

ρ_w	(kg/m^3)	998.3	density of cold tap water	
ρ_s	(kg/m^3)	1042	density of light-weight grains	
s	(-)	1.04	relative density	ρ_s / ρ_w
D50	(m)	0.0021	median grain size	2.1 mm
D90	(m)	0.0028	90th percentile	2.8 mm
v	(m^2/s)	1.16E-06	kinematic viscosity coefficient of water	at 15°C

| g	(m/s^2)	9.81	gravity	
D*	(-)	14.39	dimensionless particle diameter	$D_* = [(s-1)g/v^2]^{1/3} d50$
θ_{cr}	(-)	0.0306	critical Shields parameter	$\theta_{cr} = 0.04 * D_*^{-0.1}$ *for $10 < D_* \leq 20$*
$\tau_{b,cr}$	(N/m^2)	0.028	critical shear stress	$\tau_{b,cr} = \theta_{cr} * ((\rho_s - \rho_w) gd_{50})$

So in order to initiate motion of light-weight grains a shear stress of 0.028 N/m² had to be exceeded. The actual shear stress that the flow exerted in experiment 28 follows from equation 2.1 ($\tau_b = \rho g u^2/C^2$). The Chezy coefficient (-) is given by:

$$C = 18 * \log (12*h / k_s) \quad \text{hydraulic rough conditions} \quad (5.1)$$

wherein k_s (m) is the bed roughness parameter and h the water depth (m). Bed roughness parameter k_s is divided in two roughness contributions. The first one being the particle roughness (k_s') and the second contribution is due to the bed forms (k_s''). Together they describe the actual bed roughness k_s. The experiments did not show emergence of ripples or dunes so the bed form contribution (k_s'') is assumed absent and $k_s' = k_s$. The particle roughness (k_s') follows from $k_s' = 3*d_{90}$ according to Van Rijn [1993]. The Chézy coefficient is also a function of water depth and the type of flow. In section it was reasoned that flow should by hydraulic rough in experiments. Table 5.4 provides the Chézy coefficient for 0.5 to 3 cm of water depth for hydraulic rough flow.

Table 5.4 Chezy coefficient assuming hydraulic rough flow

water depth	Chézy
cm	$m^{1/2}/s$
0.5	15.4
1	20.8
1.5	24.0
2	26.2
2.5	28.0
3	29.4
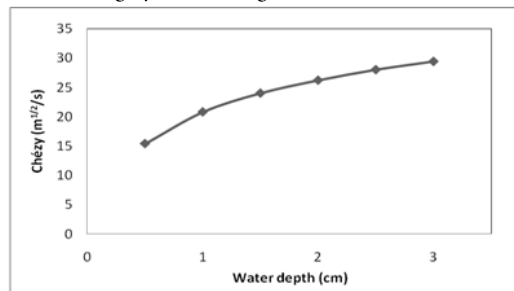
The bed shear stress in prototype systems is usually higher than in experiments. But sediment density of sand is higher than of light-weight sediment. The Shields number translates the two variables into a dimensionless parameter for experimental conditions and for prototype systems. Estimates of parameters in natural systems were based on example values of sediment and sea water properties and Chézy coefficients in Van Rijn [1993] and provided in table 5.5. It was calculated that to initiate motion of sand, a bed shear stress of 0.18 N/m² has to be exceeded. Table 5.6 compares the prototype conditions to experimental conditions for low flow conditions, moderate flow conditions and high flow conditions. Different Chézy values were applied for the flow conditions since roughness is usually not constant in space and time.

Table 5.5 Prototype properties and calculation of critical bed shear stress

ρ_w	(kg/m^3)	1030	density of cold tap water	
ρ_s	(kg/m^3)	2650	density of light-weight grains	
s	(-)	2.57	relative density	ρ_s / ρ_w
D50	(m)	0.0002	median grain size	0.2 mm
D90	(m)	0.0005	90th percentile	0.5 mm
v	(m^2/s)	1.31E-06	kinematic viscosity coefficient of water	at 15°C
g	(m/s^2)	9.81	gravity	
D*	(-)	4.17	dimensionless particle diameter	$D_* = [(s-1)g/v^2]^{1/3} d50$
θ_{cr}	(-)	0.056	critical Shields parameter	$\theta_{cr} = 0.04 * D_*^{-0.1}$ *for $10 < D_* \leq 20$*
$\tau_{b,cr}$	(N/m^2)	0.18	critical shear stress	$\tau_{b,cr} = \theta_{cr} * ((\rho_s - \rho_w) gd_{50})$

Table 5.6 Shields number for experimental conditions and prototype conditions

Typical experimental conditions				Typical prototype conditions				ratio of Shields numbers
Chezy	Velocity	Bed shear stress	Shields number	Chezy	Velocity	Bed shear stress	Shields number	
C in	U in m/s	τ_b in N/m^2	θ	C in m	U in m/s	τ_b in N/m^2	θ (-)	p/m (-)
20	**0.05**	0.061	0.068	40	0.5	1.53	0.473	7.0
25	**0.05**	0.039	0.044	50	0.5	0.979	0.303	7.0
30	**0.05**	0.027	0.030	60	0.5	0.68	0.210	7.0
20	**0.1**	0.245	0.272	40	0.8	3.917	1.210	4.4
25	**0.1**	0.157	0.174	50	0.8	2.507	0.774	4.4
30	**0.1**	0.109	0.121	60	0.8	1.741	0.538	4.4
20	**0.15**	0.551	0.612	40	1.1	7.406	2.288	3.7
25	**0.15**	0.353	0.392	50	1.1	4.74	1.464	3.7
30	**0.15**	0.245	0.272	60	1.1	3.292	1.017	3.7
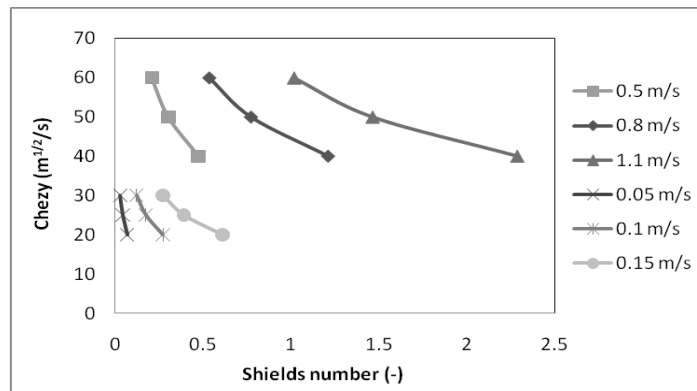
Dividing prototype Shields number by experimental Shields number gave a ratio of Shields number for the different flow conditions. It resulted in a ratio of 3.7 to 7.0. Stronger flow conditions were accompanied with a lower ratio of Shields numbers and may indicate closest similarity between prototype and experiment. Note that values of Chézy and velocity can be tuned in order to arrive at a particular value of the ratio of Shields numbers. In case of experimental velocity of 0.06 m/s and prototype velocity of 0.8 m/s as for previous method, the ratio of Shields numbers was 12.6. So scaling of sediment mobility indicated poor resemblance for those parameters. While from theory of wave motions it was concluded that those parameters scaled well.

Scale ratios
Different scale ratios were described by Stefanon et al. [2009] and reported in section 2.5.3. Table 5.7 below provides estimates of horizontal length scale L* and vertical length scale D* (average channel depth) of prototype and experiment.

Table 5.7 estimates of horizontal length scale L* and vertical length scale D*

	Beaufort Inlet	Ameland Inlet
L*$_p$ (m)	16000	25000
L*$_e$ (m)	2	2
D*$_p$ (m)	15	7
D*$_m$ (m)	0.025	0.025

Then scale ratios are calculated from the planimetric reduction scale λ_L and vertical reduction scale λ_D according to equation 2.15a-d. Table 5.8 provides the scale ratios of velocity, time and flow conductance and sediment. For comparison scale ratios from the theory of wave motions are given too.

Table 5.8 Scale ratios between experimental conditions and two prototype systems according to equation 2.15a-d

		Beaufort Inlet	Ameland Inlet
planimetric reduction scale	$\lambda_L = L^*_e / L^*_p$	1.3E-04	8.0E-05
vertical reduction scale	$\lambda_D = D^*_e / D^*_p$	1.7E-03	3.6E-04
scale ratio of velocity	$r_u = \lambda_D^{1/2}$	0.041	0.019
	$1/r_u$	24	53
scale ratio of time	$r_t = \lambda_L / r_u$	0.0031	0.0042
	$1/rt$	327	236
scale ratio of flow conductance	$r_c = \sqrt{(\lambda_L / \lambda_D)}$	0.27	0.47
	$1/r_c$	3.7	2.1
scale ratio of sediment	$r_{ds} = r_c / r_u$	7	25

Reynolds	*13*
Sq. tidal	*566*
$r_c = r_u r_{ds}$	*3.2*
Shields	*4*

Comparing the scale ratios from equation 2.15a-d with scale ratios previously found by the method of Reynolds (13 and 566) and from the Shields number (4) gives that the scale ratios of prototype Beaufort inlet resembled more than Ameland Inlet. The scale ratio of sediment for Beaufort (7) approached the value from scaling Shields numbers (4). Flow conductance (roughness contribution) compared well for the different methods (3.7 and 3.2). Scale ratio of time and scale ratio of velocity were about 50% lower than from applying Reynolds theory of wave motions. All methods show that sediment mobility is slightly too low in the experiments and friction too high. Both processes work together and should be tackled together. Nevertheless, factors of 3-4 were a great achievement for down-scaling sediment mobility and roughness contributions. Comparison of experimental velocities and time to prototype conditions indicate that solutions depended on the method. It does not necessarily indicate that the result of one method is better than the other. Deviations rather imply that an unequivocal method of up scaling results to prototype not yet exists. The scaling ratios of time found were 300 – 600 and of velocities 10 – 25. Multiplication of results from scale ratios provides a scaling factor in the vicinity of 7.500 for both methods (table 5.9). An upscaling factor 7.500 and experimental time of 143 hours in experiment 28 implies that experiment 28 covered 7.500 * 143 hours / 24 hours / 365.25 days = 68 prototype years.

Table 5.9 Comparison of scale ratios from two independent methods

	Reynolds [1887-1891]	Stefanon et al. [2009]
scale ratio of velocity	13	24
scale ratio of time	566	327
scale ratio of velocity * time	7358	7848

The most important parameter for defining scale ratios seem to be the flow velocity (u), the corresponding flow depth (d) and the sediment mobility (ds). None of the scaling parameters and equations given used bed slope (I), although the experimental method was based on a varying coordinate system resulting from tilting the experimental apparatus. The bed slope is considered an important factor in the experimental method. Most importantly, it generates the flow. Kleinhans et al. [2011, in review] calculated the effect of the change in bed slope due to tilting on sediment transport. They found that the effect was smaller than 3% on total transport. The absence of a slope parameter in scale ratios and the small effect (<3%) of the alternating slope on total transport allow us to make a direct comparison between experimental parameters and those of prototype systems.

5.2 Comparison of results to full-scale systems

This sub-chapter compares the experimental results to full-scale systems. First basic phenomena are discussed for. Then morphology of the ebb-tidal delta, flood-tidal delta and channel networks are compared to observations. Thereafter the evolution of Marsdiep Inlet is compared to experimental evolution. Last natural dynamic behaviour is compared to the experimental results.

5.2.1 Basic phenomena

This section compares and discusses basic phenomena in the experiments to nature. In experiment 26 – 29 sediment transport occurred both during the ebb- and flood phase. The alternation succeeded throughout the entire experiments. The dynamic state was manifested by migration of channels in the back-barrier and in the inlet which is prominent in full-scale systems. Likewise flood and ebb channels were clearly distinguished. Van Veen [1950] describes typical configuration of ebb and flood channels in his work. The comparison is made in figure 5.1 and figure 5.2. The typical emergence of a sill proves the alternation of sediment transport both during the ebb- and flood phase. Generally the duration of ebb transport (20 s) was slightly longer than the duration of flood transport (17 s) over a tidal cycle. It was a result of the channels draining pore water from the back-barrier at the time the bed slope was relatively steep due to tilting. Nevertheless the alternation of transport succeeded and resulted in a dynamic state of the system.

The plastic grains used in the experiments were coarse grains. The median grain size of the light-weight grains was 2.1 mm and the 90th percentile was 2.8 mm. Kleinhans et al. [2010] suggests the use of coarse grains to avoid smooth conditions. Likewise, ripples were absent for the experiments with light-weight plastic grains. Scour holes were observed. We refer to a scour hole when the bottom is visible such as in figure 5.8. When a scour hole arose the scour hole showed migration. After 5 to 50 tidal cycles the scour hole was usually filled up because of channel migration and erosion/deposition. After a certain period of time a scour hole returned at a certain place. It indicated cyclic behaviour. A scour hole was considered characteristic for the system since it was also filled up. They did not result from scale issues. Still flow over the bottom was undesirable and should be avoided. But it was not paid much attention because in nature the bottom may also consist of sediment layers with varying hardness.
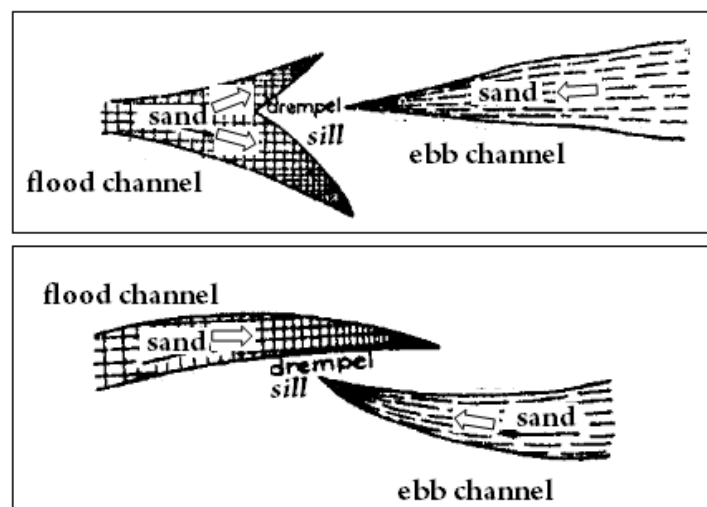

Figure 5.1 Sketch of the mutual " evasion" of flood and ebb channels by means of a forked tongue, reconstruction by author from Van Veen [1950].

Figure 5.2 Image of final configuration in experiment 28 at low water. The sketch represents the "evasion" of flood and ebb channels typical for tidal channels as in figure 5.1. It proves alternation of flood and ebb transport during experiment 28.

5.2.2 Morphology

In experiment 28 a tidal inlet system formed with an ebb-tidal delta, inlet channels and channel network in the back-barrier. In this section the typical morphology of the final configuration of experiment 28 is compared to full-scale systems.

Ebb-tidal delta

The ebb-tidal delta formed directly in front of the inlet in the sea basin. At flood the ebb-tidal delta was submerged while at ebb a large part lay above water (figure 5.3). The form of the ebb-tidal delta was a typical fan-shape with lobes at the sea side. Both the ebb and the flood flow occurred along the sides of the front delta where channels were observed near the barriers. Figure 5.4 shows the bathymetry of the ebb-tidal delta of Ameland inlet. Resemblance is seen in the fan-shape and the channel alongside the barrier in the upper part. A major difference is the inlet channel extending further into the ebb-tidal delta for Ameland inlet. The ebb-tidal delta in experiment 28 did not 'fold around' the inlet channel. Figure 5.5 shows another inlet along the Dutch Wadden Sea Coast with channels alongside both barrier islands. A delta front is located directly in front of the inlet. Resemblance with experiment 28 is better. In experiment 28 the sea margin of the delta showed lobes. While the margins in figure 5.4 and figure 5.5 show a smooth line. Such hooks resemble flood channels [Van Veen 1950] and might be of similar character as the lobes in the experimental ebb-tidal delta. Figure 5.6 is a photo of an inlet channel at the USA Atlantic Coast that extends far into the sea. It emphasizes that the experimental inlet channel should extend further into the ebb-tidal delta.

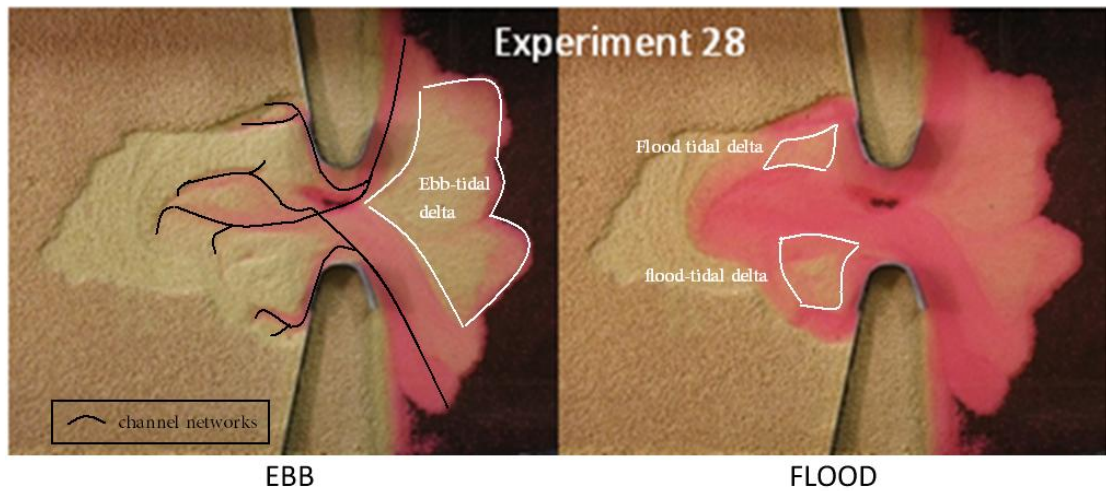Figure 5.3 Final configuration of experiment 28 at low water (left) and high water (right). The figure schematizes the ebb-tidal delta, flood-tidal deltas and channel networks.
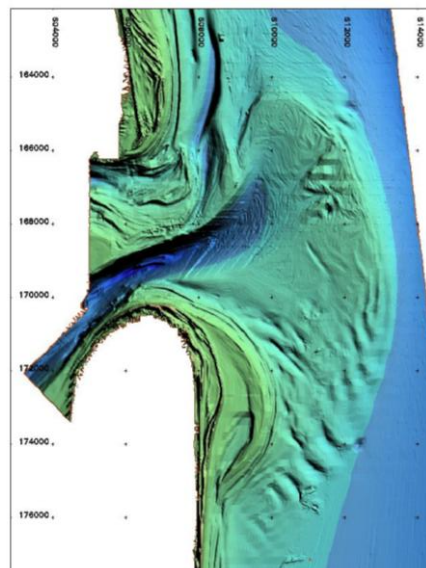

Figure 5.4 Ebb-tidal delta bathymetry from Ameland inlet survey 1996, RKZ Rijkswaterstaat KUST*2000.
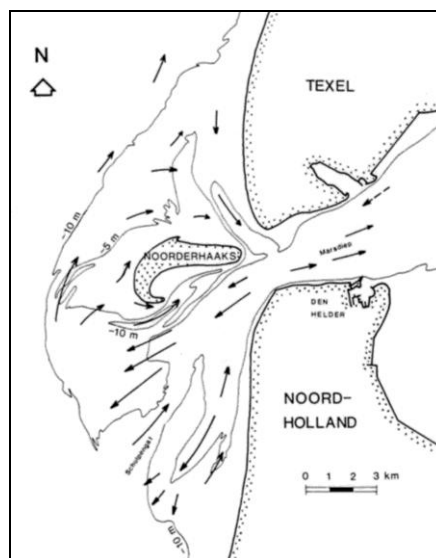

Figure 5.5 Contours of sand bodies and representation of net transport direction at Marsdiep Inlet, Dutch Wadden Sea Coast. By Sha, date unknown.

Figure 5.6 Photo of inlet channel that extends into the sea. Flood channels are presents alongside the barriers. Photo provided by M. van der Vegt. Source unknown.

Flood-tidal delta

At high water two shoals were observed in the back-barrier of figure 5.3. The shoals were considered to be flood-tidal deltas. These flood-tidal deltas did not show a specific form, their form was specified by the channels flowing around them. Figure 5.7 is a photo of a tidal inlet system near New York (USA) with channels near the inlet and shoals/flood tidal-deltas. At most tidal inlet systems at the US Atlantic Coast there is usually no main channel perpendicular to the inlet. The inlet channels divert into two channels alongside both barriers so there is one large flood-tidal delta. Smaller channels are present aside the flood-tidal delta. So resemblance with the two separate experimental flood-tidal deltas is not one to one here, but the nature of the system with channels around the delta is similar. The volume of the experimental flood-tidal was expected to be small since the volume is related to the effect of wind waves [Mayor-Mora 1977]. The effect of wind waves was absent in experiment 28. But at low water, the experimental flood-tidal delta seemed large. Note that the channel in the middle migrated north to south from the upper delta to the lower delta and back. The size of the flood-tidal deltas depended on the location of the middle channel. A part of the delta attached cyclically to the shoal. Figure 5.8 presents the Dutch Wadden Sea Coast. Resemblance with the experimental flood-tidal deltas is highest for the third inlet from the left, between Vlieland and Terschelling. The locations of the flood-tidal deltas agree.

Figure 5.7 Photo of Shinnecock inlet, New York, 1947. Photo from www.lishore.org/photos/ShinHist/470401.html.

Channel network

The channel network of the final configuration of experiment 28 was schematized in figure 5.3. The channels branched out into the back-barrier. A branching network is typical for tidal inlet systems. Figure 5.8 shows the bathymetry of the Western Wadden Sea. The third inlet shows a main channel through the inlet that branches out. Aside the barrier islands there are small channels. Close

resemblance is seen with experiment 28. Although number of branches from the main channel was smaller in experiment 28.
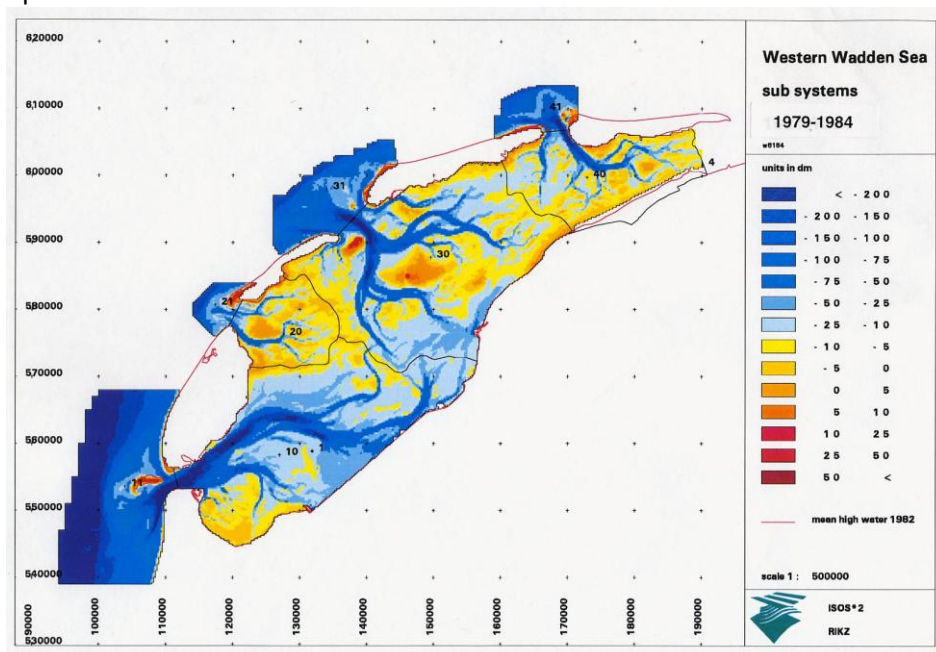
Figure 5.8 Bathymetry of Western Wadden Sea. From RIKZ, ISOS*2.
The islands are, left to right: Texel, Vlieland, Terschelling and Ameland.

The hierarchical analysis described in section 2.2.5 was applied on the final configuration of experiment 28 and experiment 29. The branching network of experiment 28 was one of order three (figure 5.9). The branching network of experiment 29, with higher water level, was one of order four (figure 5.10). Marani et al. [2003] emphasized the importance of the variable watershed area when concerning channel networks. The higher order of branching in experiment 29 might have been the result of the larger water volume and active area. Cleveringa and Oost [1999] found from applying Horton's method that tidal-channel systems in the Dutch Wadden Sea have three- to four- times branching networks. It is concluded that the experimental branching networks correlate with tidal inlet systems in the Dutch Wadden Sea.
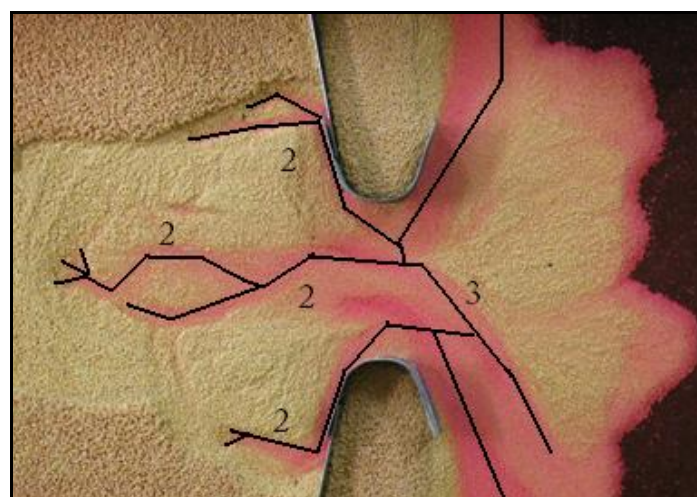
Figure 5.9 Experiment 28, photo 1673. According to Horton's hierarchical analysis the system is a three-times branching network.

Figure 5.10 Experiment 29, photo 1842. According to Horton's hierarchical analysis the system is a four-times branching network.

5.2.3 Comparison of experimental flow depth evolution to Marsdiep inlet

The channel depth at Marsdiep inlet increased linearly over a time span of 300 years (figure 2.6). Thereafter the increase was less strong and showed variability. Variability was deduced to result from human interference such as land reclamation from the 1700s. Maximum experimental inlet flow depth is presented in figure 5.11. During the first 60 hours of evolution the overall trend was a linear increase in maximum flow depth. The signal was slightly sinusoidal. After 60 hours the maximum flow depth remained more or less constant apart from a sinusoidal variability over 10 to 15 hours. In this period experimental morphology was developing. I observed resemblance between channel depth increase of Marsdiep Inlet (year 1400 – 1700) and of experiment 28 (5-60 hours). The absence of variability at Marsdiep inlet is plausible since there were little observations. After the year 1700 the signal consists of more observations and occurrence of variability. Experimental boundary conditions remained unchanged, still a variability in maximum channel flow depth was present. Experimental results support that at least some of the variability in channel depth after year 1750 may be attributed to forcing of the tide.

Figure 5.11 Maximum experimental inlet flow depth of experiment 28 at cross-section 686. The values were calculated from the moving average over 15 pixels in the cross-sections.

5.2.4 Cyclic behaviour and dynamic state

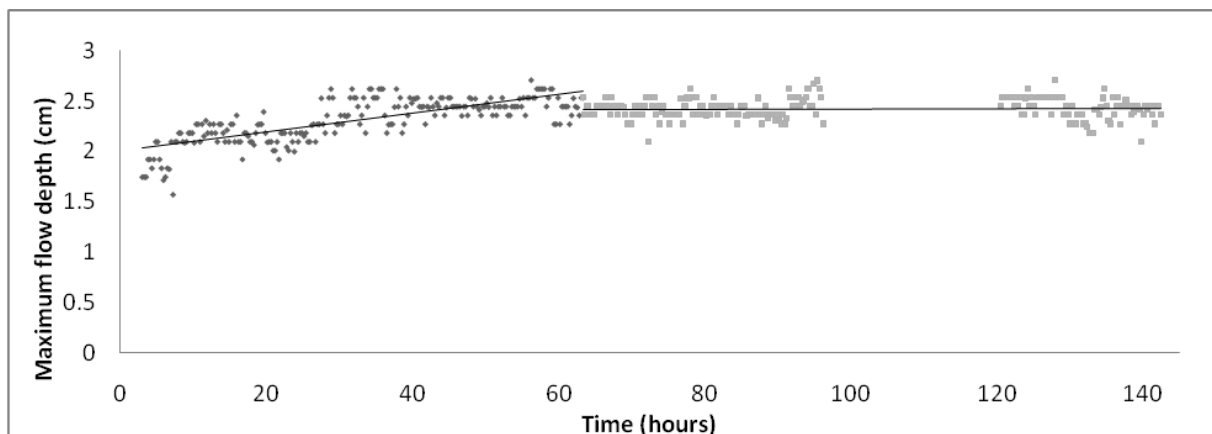Tidal inlet systems in nature show migration of bars, channels and shoals; change in number of inlet channels; stream takeover of channels in the back-barrier; abandonment of channels in the back-barrier [Oost 1995]. The experimental tidal inlet system showed migration of bars, channels and shoals in figure 4.13 – 5.16. The number of inlet channels switched between one and two (figure 4.13). In the evolutionary stage occurrence of three inlet channels occurred in figure 4.23. In the back-barrier separate ebb and flood channels existed (figure 5.2). Channels were dynamic in their morphology and abandonment and filling up of channels and subsequent emergence of new channels occurred. I recommend watching the movie of experiment 28 in slow-motion play to see the latter taking place. So cyclic behaviour and dynamic state of channels, shoals and bars present in full-scale systems was also observed for on the experimental scale.

Cyclic behaviour of switching between numbers of inlet channels occurred for Ameland Inlet [Oost 1995] in a period of approximately 50 years. Figure 4.13 of experiment 28 showed that experimental switching of number of inlet channels occurred on average in 2.5 hours. Comparison of 50 years (438300 hours / 12.33 hour = 35.540 tidal cycles) for full-scale system to 2.5 hours (9000 s / 79 s = 114 tidal cycles) on experimental scale results in a comparison factor of 35.539 / 114 = 312 (-). This comparison factor indicates that experimental inlet dynamics was speeded up by a factor 312. In the subchapter on scaling (section 6.1.2) a scale ratio of time for Ameland inlet was found of 1/236. The values of 312 and 236 show close resemblance between two unrelated approaches. The scale ratio of time incorporated depth and lengths of experiment and full-scale system. But sediment mobility was scaled at 25 meaning that the sediment was not mobile enough. The scale rules did not incorporate the effect of a tilting sediment bed. The occurrence of experimental cyclic behaviour associates with all parameters and indicates that experimental sediment mobility was appropriate. It is thus suggested that the net effect of tilting is such that it more or less negates the scale effects predicted from scale rules.

5.3   Comparison of results to models

Modelling efforts were done by Maarten van der Vegt of U.U. to model the hydrodynamics in the experimental apparatus. Such a model has to incorporate a changing coordinate system. But incorporation of a changing coordinate system in time is not embedded in regular software and programming languages. So development of a model that covers the experimental conditions has proven to be difficult. Still, the experimental results resemble processes modelled in depth-averaged schemes. The experimental apparatus solely introduced a tidal current without undertow and wave asymmetry. Fresh water was used so density currents were not present. Meandering rivers with a width-depth ratio of approximately 25 show strong spiral flow effects due to their morphology. An experimental channel of 2.5 cm would be equivalent to 0.1 cm depth when ignoring the increased roughness in low water depths. This channel would have to show considerable spiral flow in the curves. To compensate for the increased roughness effect in experiments it is expected that the equivalent water depth would have to be slightly deeper to have similar spiral flow effects. Low width to depth ratios of experimental channels suggested that the water depth was relatively high. Therefore curvature-induced secondary flows were thought to be of significant influence. So the experimental hydrodynamic processes simulated indicate that depth-averaged model schemes that consider spiral flow effects would compare best with experimental results.

5.4   Comparison of results to lab experiments

Experiments are usually time consuming. Stefanon et al. [2009] performed an analogue experiment. They applied the general method of a wave signal to generate flow and needed 30 to 60 days to complete a single experiment. Use was made of light-weight sediment with a density of 1041 kg/m^3. Inlet width was 20 cm which is similar to our experiment (23 cm). Flow depth in the experiments was similar (about 2 cm), we also used a light weight sediment (density 1055 kg/m^3). In contrast, our experiments took 5 to 10 days. The back-barrier areas in experiment 28 and 29 were about a factor

two to three smaller than the back-barrier in Stefanon et al. their experiments. The quick evolution of experiment 28 indicated that sediment mobility was high in our experiments. The tidal inlet system being considerably smaller probably indicated that hydrodynamics (velocities) were less strong. Hydrodynamics being less strong and sediment being more dynamic is counterintuitive. But it is considered a plausible effect of tilting the basin since other conditions were similar. Stefanon et al. [2009] formed typical morphology but dynamic behaviour was absent. Higher sediment mobility in our experiments was thus the key for dynamic behaviour to occur in experiments. Other experimental constraints in prior experiments were the emergence of large scours and ripples. These were absent in experiment 28. It is concluded that the novel method of generating flow by tilting works well. The novel method proofs to be an innovation in the field of tidal experimental research that avoids previous experimental constrains such as ebb-dominance. Besides, the short experimental time allows doing many experiments in a short range of time.

Mayor-Mora [1977] provided data on experimental tidal prism – cross sectional area relationships. Figure 3.4 and 3.5 provided that high water volume and channel area in experiment 28 remained about constant after 70 hours. Channel area was about 40 cm^2 and high water volume about 3.5L. High water volume minus low water volume represented tidal prism. Low water volume could not be calculated but is estimated to approximate 0.5L. The conversion of S.I. units to U.S. customary units for square meter and cubic meter is given by Van Rijn [1993]:

        cubic feet (ft3)   0.02837 m3

        square feet (ft2)   0.093 m2.

Table 5.10 converges the S.I. units to U.S. units. Values for channel area and tidal prism of about 12.5% higher and lower were   also calculated to incorporate an uncertainty level.

Table 5.10 Conversion of S.I. units to U.S. units for channel area and tidal prism in experiment 28

channel area				tidal prism		
cm2	m2	ft2		L	m3	ft3
35	0.0035	0.038		3.5	0.0035	0.12
40	0.004	0.043		3	0.003	0.11
45	0.0045	0.048		2.5	0.0025	0.088

The channel area – tidal prism relationship for experiments by Mayor-Mora [1977] is given in figure 5.12. The results from experiment 28 were incorporated in the graph. Tidal prism and channel area of experiment 28 were lower. Mayor-Mora [1977] calculated the power relation of different combinations of channel area- tidal prism found in their experiments. Present results approximate the power-relation found by Mayor-Mora [1977]. So despite the use of different grains and a different method to generate flow the experimental results show consistency. Experiments predict an inlet area an order of magnitude higher than the 95-percent confidence limit of extrapolated field data [Mayor-Mora, 1977]. Mayor Mora [1977] suggested that the inlet area versus prism relationship may not be a power-relation for the entire range of conditions from experiments to prototype or that scale effects are important. They described that possible scale effect in their experiments was the use of typical size quartz sand which did not scale with prototype barrier sediment conditions. But our results were consistent with founding's of Mayor-Mora [1977] while we scaled sediment by the use of light-weight grains. It is thus suggested that the inlet area versus prism relationship is not a power-relation for the entire range of conditions from experiments to prototype. The experimental inlet area found is higher than suggested by the power-relation of Mayor Mora [1977] in figure 5.12. This might be explained by bed effects at low flow depths and demonstrates a coupling with frictional effects for the lower conditions. More research on this subject is recommended.
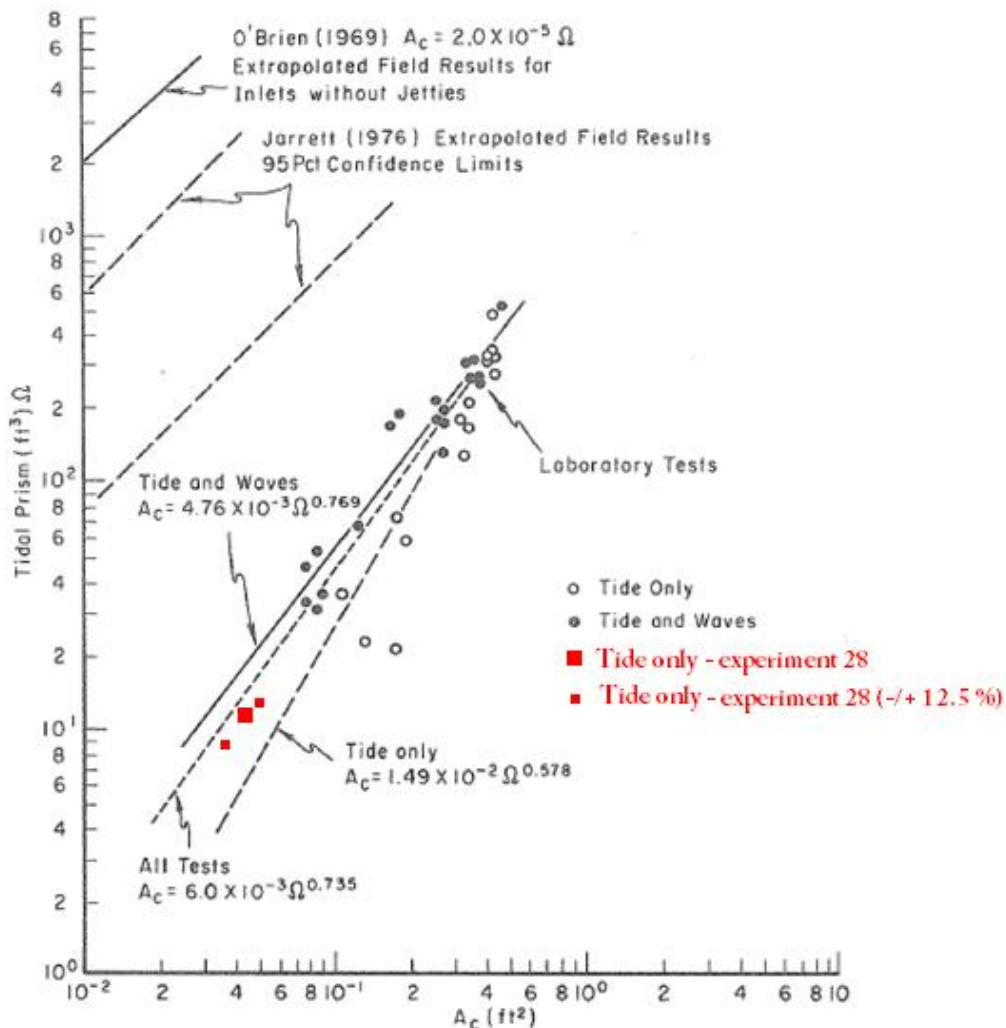
Figure 5.12 Tidal prism, Ω, and cross-sectional area, A, on log-log paper measured experimentally in experiments by Mayor-Mora [1977]. A best-fit regression analysis shows that logarithms of prism and area are linearly related. Channel area and tidal prism of experiment 28 were incorporated.

5.5   Translation to the physical system

This section discusses important issues in full-scale systems such as sea level rise and storms. What do experimental results teach us about their effects?

The tidally averaged forcing that generated flow in the experiments was constant and extreme events did not occur. From this it is concluded that cyclic behaviour and dynamic state of a tidal inlet system resulted solely from alternation of ebb and flood flow. Phenomena such as the occurrence of storms and different tidal constituent were absent in the experiments and thus not essential for cyclic behaviour to occur. Boundary conditions such as geology, dominant direction of wind waves and the forcing tide usually vary at different stretches of the coastlines around the world. Also, present-day tidal inlet systems are subject to human interference such as land reclamation, construction of groins and dredging. It is thus difficult to define equilibrium state when dynamic behaviour occurs simultaneously and the systems are prone to human interference. The experimental results showed that when high water volume and channel area were about constant, morphology still changed and the ebb-tidal delta grew. The sediment deposited on the ebb-tidal delta was from new captured areas. Since sediment level was higher than mean sea level, the ebb-tidal delta could continue to grow while high water volume was about constant. In such a case, defining equilibrium state from a constant tidal prism – channel area relation would have been incorrect.

Sea level rise is a much debated concern. Knowledge on the resulting behaviour of the physical system is important for e.g. safety issues. The effect of a sea level rise on an existing tidal inlet system was studied in experiment 29. The results indicated that for a constricted inlet width, high water volume and back-barrier area increased. Also the number of channels in the back-barrier increased. The inlet channel depth increased consequently with a rise in mean water level. The dynamic state of the system persisted. Considering the Dutch Wadden Sea, growth of the back-barrier would imply that parts of the provinces of Friesland, Groningen and Noord-Holland along the Wadden Sea would be eroded when unprotected by i.e. dikes. The experiment considered a single tidal inlet system. While the Dutch Wadden Sea consists of a series of tidal inlet systems. Growth of the watersheds would imply that the Wadden Sea would be too small to cover growth of all the separate inlet systems. The experiment suggests that in a completely natural situation without human interference the number of tidal inlet systems in the area might decrease as a result of sea level rise. But in the present situation the islands are populated and the present coastline should remain, by Dutch law, as it is. Growth of the back-barrier should thus be avoided. Experimental results indicated that important variables describing tidal inlet morphology were tidal inlet width, the inlet being constricted, tilt amplitude (representing tidal wave height), mean water level and sediment level. Of these variables tidal inlet width is probably the only variable that can be secured by e.g. constructing groins. To avoid growth of the back-barrier from sea level rise experimental experience suggests that inlet width should be decreased. Also the relation between mean water depth, sediment level, inlet width and tidal system area can be defined. The latter is important for determining the required inlet width for different prognoses of sea level rise. The experimental apparatus allows to test such an intervention or relative effect of parameters and study unforeseen effects.

Note that these experimental findings should not be translated 1:1 to natural systems. Sediment supply from the continental shelf is a major driver of morphological evolution, especially when concerning the effect of sea level rise. This process was not incorporated in the experiment.

5.6 Recommendations for further research

The morphology of the experiments compared rather well with observation. Furthermore dynamic equilibrium state in an experimental tidal basin was a great achievement. Still recommendations are provided here to achieve certain aspects observed for in nature such as folding of the ebb-tidal delta around inlet channel and simulate sediment rearrangement on shoals and in channels.

The folding of the ebb-tidal delta around the inlet channel was not present in experiment 28 and experiment 29. It is recommended to increase the amplitude of tilting to 70 mm/min to increase the strength of the ebb-flow. The tidal inlet systems along the US Atlantic Coast usually have a flood-tidal delta in front of the inlet with main channels flowing around. The experiments show a main channel in the middle of the back-barrier. The arising of this channel is likely a result of tilting. The tilt encourages water to flow perpendicular to the pivot point since the tilt is highest there (figure 3.9). Whether it is possible for a flood tidal delta to form in front of the inlet remains questionable. It is recommended to test whether a flood-tidal delta will form in a deeper basin. Hubbard et al. [1979] described wind waves to be the major factor in formation of large lobate deltas, in particular flood-tidal deltas. Experiments with simulation of wind waves may provide insight on its effect on morphology and if it the relation also holds on the experimental scale. Higher sediment cohesion might also have potential to divert the relatively strong flow around the flood-tidal delta. System dynamics was desired although it seemed that the channels were extremely dynamic. In order to secure meandering, bars should not erode too fast so that erosion in the back-barrier area is focused at a specific bank location for long enough time [Kleinhans et al. 2008]. Higher cohesion of the light-weight sediment may be achieved by addition of smaller fractions of plastic grains. It can also enable sediment rearrangement. The channel network showed a branching pattern. The number of main channels in the back-barrier (about three) in experiment 28 was comparable to observations. But the number of branches from the main channels was lower than for natural systems. A certain discharge

is needed for a channel to form [Rinaldo et al. 1999]. A higher tidal prism will thus promote a higher number of channels and branches and occurred in experiment 29. To validate the discharge – channel number relation, evolution from plane bed should be simulated with a higher water level (of about 3.2 cm). A last recommendation is to consider sediment availability in combination with sediment level. A higher sediment level in experiment 28 gave a more dynamic system. Also higher water level in experiment 29 promoted dynamics. But in experiment 29 scour holes were significant at the last stage of sea level rise. A combination of higher water level (3.5 cm) and higher sediment level (5.5 cm) is recommended. Also the experiment should be run longer to ensure dynamic equilibrium state and simultaneous cyclic and dynamic behaviour. The variable inlet width is likely to have a significant effect on morphology. Inlet width of 23 cm in experiment 28 and 29 was determined from experimental experience. The inlet was a very dynamic part of the system. Experimental observations suggest further research on the effect of inlet width on morphology and on inlet dynamics.

Chapter 6: Conclusions

We succeeded in creating a dynamic tidal inlet system from plane bed by applying a novel method to generate flow. The tide was generated by vertically tilting the set-up, instead of pumping water in and out. In our experiments sediment transport occurred both during the ebb phase as well as during the flood phase. Morphology emerged that resembled nature with the existence of an ebb-tidal delta, channel network and inlet channel(s). So the principle of tilting the bed rather than changing water levels to reproduce the typical morphology of tidal flow works. In addition, the use of light-weight grains, non-erodible barriers, a start perturbation and an initial sediment basin level considerably higher than mean sea level were required initial conditions to produce a dynamic tidal inlet system.

Channels formed through backward erosion and started to bifurcate and migrate after retreating from the basin margin. Formation of new channels from bifurcations occurred with abandonment and subsequent filling up of former channels. Resemblance with natural cyclic behaviour such as the number of inlet channels existed and typical ebb- and flood channels separated by sills were present. The parameters that were most sensitive to the equilibrium morphology were sediment bed level, average water level, inlet width and tidal amplitude. Low average water level with respect to the sediment bed caused long sharply curved channels, caused by backward erosion. These channels had few branches and persisted on the irregularly shaped ebb-tidal delta. Higher average water levels increased migration rates, number of branches and a regularly shaped ebb-tidal delta formed. Inlet width and tidal amplitude most importantly affected the shape and extent of the back-barrier basin and ebb-tidal delta since they determined strength of flow. The effect to a rise in sea level on equilibrium morphology was a wider and longer back-barrier basin with more channels, a deeper inlet channel and the ebb-tidal delta built up in the vertical. The experimental set-up allows investigating estuaries, shore-parallel tidal currents, and so.

From applying scale rules it was found that experimental sediment mobility was low. But the scaling rules did not incorporate the effect of a tilting sediment bed. The time scale of experimental cyclic behaviour more or less agreed with the scale ratio of time. It is thus suggested that the net effect of tilting was such that it more or less counterbalanced low sediment mobility predicted from scaling rules. In addition, our experiments suggest that the inlet area versus tidal prism relationship does not hold for the entire range of conditions rather than resulting from scale issues.

In nature constant tidal prism – channel area usually define equilibrium state. The experimental tidal prism and channel area were constant while the ebb-tidal delta and tidal area still expanded. It indicated that the subject of defining equilibrium state is not straightforward. Meanwhile our experiments showed morphological equilibrium state when the back-barrier area remained equally large and the ebb-tidal delta did not expand anymore. This equilibrium state coincided with migration of bars, channels and shoals and was defined to be a dynamic equilibrium state.

References

Cayocca, F. 2001. Long-term morphological modelling of a tidal inlet: the Archachon Basin, France. Coastal Engineering 42 (2001) 115- 142.

Chang, H.H., 1979. Geometry of rivers in regime. Journal of the Hydraulics Division, Vol. 105, No. 6, June 1979, pp 691 - 706

Dastgheib, A., Wang, Z.B., de Ronde, J., Roelvink, J.A., 2008. Modelling of mega-scale equilibrium condition of tidal basins in the western Dutch wadden sea using a process-based model. Copedec VII, 2008, Dubai, UAE. Paper No: D-08.

Davis Jr, R.A. and FitzGerald D.M., 2004. Beaches and coasts. Blackwell science Ltd, UK. Page 200-217.

De Swart, H.E. and Zimmerman, J.T.F., 2009. Morphodynamics of tidal inlet systems. Review article. Annual review of fluid mechanics, 2009. 41:203-29.

Dieckmann, R., Osterthun, M., Partenscky, H.W., 1988. A comparison between German and North American tidal inlets. Coastal engineering, Chapter 199.

Dissanayake, D.M.P.K., Roelvink, J.A., Van der Wegen, M., 2008. Effect of sea level rise on inlet morphology. Copedec VII, 2008, Dubai, UAE. Paper No: D-12. From http://www.delftcluster.nl/website/files/files_org/AIO/conferencedubai.pdf

Dissanayake, D.M.P.K., Roelvink, J.A., Van der Wegen, M., 2009. Modelled channel patterns in a schematized tidal inlet . Coastal Engineering, Volume 56, Issues 11-12, November-December 2009, Pages 1069-1083.

Geleynse, N., Storms, J.E.A., Walstra D-J. R., Jagers H.R.A., Wang, Z.B. and Stive M.J.F., 2010. Controls on river delta formation; insights from numerical modelling. Earth and Planetary Science Letters 302 (2011) 217–226

Hayes, M.O., 1980. General morphology and sediment patterns in tidal inlets, *Sediment.Geol.,* 26:139- 156.

Hoyal , D. C. J. D. and Sheets, B.A., 2009. Morphodynamic evolution of experimental cohesive deltas. Journal of geophysical research, volume 114. F02009, doi:10.1029/2007JF000882.

Hubbard, D.K., Oertel, G. and Nummedal D., 1979. The role of waves and tidal currents in the development of tidal-inlet sedimentary structures and sand body geometry: examples from North Carolina, South Carolina and Georgia. Journal of sedimentary petrology, Volume 49, no. 4. Page 1073-1092.

Kleinhans, M.G., Schuurman, F., Bakx, W. and Markies, H., 2008. Meandering channel dynamics in highly cohesive sediment on an intertidal mud flat in the Westerschelde estuary, the Netherlands. Geomorphology 105 (2009) 261–276

Kleinhans, M.G., van Dijk, W.M., van de Lageweg, W.I., Hoendervoogt, R., Markies, H. and Schuurman, F., 2010. From nature to lab: scaling self-formed meandering and braided rivers. *International Conference on Fluvial Hydraulics RIVERFLOW, Braunschweig, Germany, Sept 2010.*

Lanzoni, S. and G. Seminara, 2002. Long-term evolution and morphodynamic equilibrium of tidal channels. J. of Geophys. Res. 107(C1): 3001-3013

Marani, M., Lanzoni, S., Belluco, E., D'Alpaos, A., Defina, A., Rinaldo, A., 2003. On the drainage density of tidal networks. Water Resources Research 39 (2), 105–113.

Mayor-Mora, R.E., 1977. Laboratory Investigation of Tidal Inlets on Sandy Coasts. GITI REPORT 11, U.S. Army Coastal Engineering Research Centre.

Oost, A.P., 1995. Dynamics and sedimentary development of the Dutch Wadden Sea with emphasis on the Frisian inlet. Published PhD thesis, Universiteit Utrecht, 455 pp.

Perillo, G.M.E., 1995. Geomorphology and sedimentology of estuaries. Development in sedimentology 53,Elsevier Science Publishers B.V., Amsterdam. ISBN: 0-444-88170-0

Powell, M.A., Thieke, R.J. and Mehta, A.J., 2006. Morphodynamic relationships for ebb and flood delta volumes at Florida's tidal entrances. Ocean Dynamics 56: 295–307 DOI 10.1007/s10236-006-0064-3

Reynolds, O., 1887-1891. Papers on mechanical and physical subjects. University of California. Volume II, chapter 55, page 326-335.

Rinaldo, A., Fagherazzi, S., Lanzoni, S., Marani, M. and Dietrich W.E., 1999. Tidal networks 3. Landscape-forming discharges and studies in empirical geomorphic relationships. Dipartimento di Ingegneria Idraulica, Marittima e Geotecnica, Universita´ di Padova, Padua, Italy

Stefanon, L., Carniello, L., D'Alpaos, A. and Lanzoni, S., 2010. Experimental analysis of tidal network growth and development, *Continental Shelf Research,* 30:950–962.

Tambroni, N., Bolla Pittaluga, M., Seminara, G., 2005. Laboratory observations of the morphodynamic evolution of tidal channels and tidal inlets. *J. Geophys. Res.* 110:F04009

Valeria, G., Christof, R.A., Giovanni, S., 2007. Tidal meanders and tidal deltas: Laboratory observations. Department of Civil and Environmental Engineering, University of Genoa, Italy. IAHR conference proceedings. http://www.dicat.unige.it/flubio/fellowspapers/Garotta_Venice_IAHR07_final.pdf

Van der Vegt, M., 2006. Modelling the dynamics of barrier coasts and ebb-tidal deltas. Doctoral thesis at Utrecht University.

Van der Wegen, M. and J. A. Roelvink, 2008. Long-term morphodynamic evolution of a tidal embayment using a two-dimensional, process-based model,

Van der Wegen, M., Wang, Z.B., Savenije, H.H.G. and Roelvink J.A., 2008b. Long-term morphodynamic evolution and energy dissipation in a coastal plane, tidal embayment. Journal of Geophysical research, volume 113, F03001, doi:10.1029/2007JF000898.

Van Dijk, M., 2009. Autocyclic behaviour of alluvial and deltaic systems. Geologica Ultraiectina, No. 306. Faculty of geosciences, Utrecht University.

Van Dijk, W.M., van de Lageweg, W.I., Hoendervoogt, R. and Kleinhans, M.G., 2010. Incipient meandering and self-formed floodplanes in experiments. River Flow 2010 conference proceedings - Dittrich, Koll, Aberle & Geisenhainer (eds)

Van Rijn, L.C., 1993 – Principles of sediment transport in rivers, estuaries and coastal seas. Aqua Publications. ISBN 90-800356-2-9

Van Veen, J., 1950. Reprinted in 2001. Eb- en vloedschaar systemen in de Nederlands getijwateren. Tijdschrift Koninklijk Nederlandsch Aardrijkskundig genootschap. Vol. 67. Pagina 303-325.